DOE/NASA/0161-7
NASA CR-165191

CELL MODULE AND FUEL CONDITIONER

6TH QUARTERLY REPORT: JANUARY-MARCH, 1981

D.Q. Hoover, Jr.
Westinghouse R&D Center
Westinghouse Electric Corporation
Pittsburgh, PA. 15235

April, 1981

Prepared for
NATIONAL AERONAUTICS AND SPACE ADMINISTRATION
Lewis Research Center
Under Contract DEN 3-161

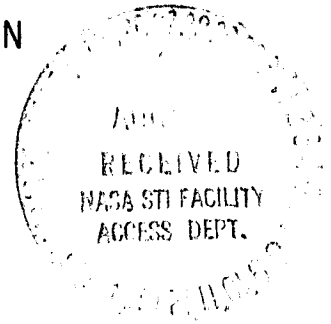

for
U.S. DEPARTMENT OF ENERGY
Energy Technology
Division of Fossil Fuel Utilization
Under Interagency Agreement DE-AI-01-80ET17088

D17-59

DOE/NASA/0161-7
NASA CR-165191

CELL MODULE & FUEL CONDITIONER DEVELOPMENT

6TH QUARTERLY REPORT: JANUARY-MARCH, 1981

D.Q. Hoover, Jr.
Westinghouse R&D Center
Westinghouse Electric Corporation

April, 1981

Prepared for
NATIONAL AERONAUTICS AND SPACE ADMINISTRATION
Lewis Research Center
Under Contract DEN 3-161

for
U.S. DEPARTMENT OF ENERGY
Energy Technology
Division of Fossil Fuel Utilization

TABLE OF CONTENTS

TABLE OF CONTENTS (continued)

1. INTRODUCTION

This report is for the second Phase of a six Phase program to develop commercially viable on-site integrated energy systems (OS/IES) using phosphoric acid fuel cell (PAFC) modules to convert fuel to electricity. Phase II is a planned two year effort to develop appropriate fuel cell module and fuel conditioner conceptual designs. The fuel cell module development effort comprises three coordinated tasks:

Task 1: Design of Large Cell Stacks

Task 2: Stack Fabrication

Task 3: Stack Testing

The "Fuel Conditioner Subsystem Development" task is the fourth technical task of this effort. Provision for "Management, Reporting and Documentation" is included as a fifth task.

The work accomplished during this reporting period is described at the subtask level in the following section.

II. TECHNICAL PROGRESS

TASK 1: DESIGN OF LARGE CELL STACKS

1.1 Detailed Analytical Model

Development of the detailed analytical model for the MK-2 (Z bipolar plate) is continuing.

The lumped parameter model was used in analyzing the data obtained in the OS/IES loop tests of stacks 561 and 562. This data analysis provides new values of the cell parameters (e.g., catalyst utilization, resistance, temperature sensitivity) used to calculate local performance in the detailed analytical model.

1.2 Stack Design

The detailed description of the design of the stacks being built and tested is in the document "Phosphoric Acid Fuel Cell Materials - Fabrication and Assembly Procedures." This document is being edited and revised and was expanded this quarter to include descriptions of 563 and 564. The current version (at the end of this quarter) of this document was forwarded to the NASA Project Manager for his review.

1.3 Full Scale Module Design

An anaylsis of the compressive load distribution between the cell active area (anode-matrix-cathode composite) and the inactive area (shims and seals) is in progress.

Polyphenylene Sulfide (Ryton, Phillips Petroleum Company) is a leading candidate for the manifold material. Fabricators and custom molders have been contacted to determine in what sizes the material can be molded. Discussions with materials specialists at Westinghouse have disclosed no corrosion or fabrication problems thus far.

TASK 2: STACK FABRICATION

During this quarter, fabrication of stacks 560 (a five-cell, MK-2 design), 561 (a 23-cell, MK-1 design) and 562 (a 23-cell, MK-2 design) was completed, fabrication of components for 563 (a 23-cell, MK-1 design) continued and fabrication of components for 564 (a 23-cell, MK-2 design) was initiated. All stacks are nominally 1200 cm^2 (31 x 43.5 cm prior to heat-treatment) and include:

- heat-treated bipolar and bipolar/cooling plates
- Mat-1 matrices
- rolled electrodes with catalyst loadings of 0.3 mg/cm^2 and 0.5 mg/cm^2 on the anode and cathode, respectively
- a modified version of acid management scheme 2
- Teflon shims

Stacks 560, 561 and 562 were wet assembled with ~48 cc of 100% phosphoric acid per cell added to the matrix and electrodes with additional acid in the reservoir of each bipolar plate. Prior to pre-testing, additional acid was added via the fill tube. The net absorbed by each stack was determined by collecting the acid which came out of the drain tube and subtracting from the amount added.

A more detailed description of the component fabrication and stack assembly procedures was supplied to the NASA Project Manager in a separate document "Phosphoric Acid Fuel Cell Materials - Fabrication and Assembly Procedures."

A plan to develop a five-cell module assembly was evolved during this period.

2.1 Methods and Approach

As a result of discussions and meetings, a decision to develop a five-cell module technology was made during this quarter. Basically the concept is that the cooling plate halves (if not bonded together)

form convenient holders and separation planes to define the modules. The advantages of this concept are that the modules can be pretested before they are placed in a stack and that, after assembly, individual modules with prematurely failed cells can be replaced. The success of the concept depends on:

1) a means of sealing the edges of the cooling plate halves without bonding them together while retaining low contact resistance

2) a means of removing modules from the stack without adversely affecting the other cells and modules in the stack.

A plan for the development of these modules, describing some of the methods to be investigated, was submitted separately to the NASA Project Manager. Fabrication of components for four test modules will be fabricated and tests will be initiated in the next quarter.

2.2 Simulated Stack Fabrication

Stack 560 was assembled this quarter. Improvements over the previous five-cell, MK-2 stack (558) included:

- Thinner bipolar plates (0.30 cm vs 0.43)
- Thicker end plates (0.56 cm vs 0.43) to facilitate sealing to the manifold frame
- Reduced thickness of the shim in the area between the acid reservoir and the active area of the cell to provide better acid feed to the cell.

During assembly, 0.5 cc were added to the acid reservoir of each cell and the stack absorbed 4 cc/cell of the acid added via the fill tube prior to pretesting.

2.3 Short Stack Fabrication

Assembly of stacks 561 and 562 was completed this quarter. During assembly, 0.5 cc and 2 cc were added to the acid reservoirs of these stacks, respectively. The net absorption of acid added prior to pretesting was 1 and 2.6 cc/cell, respectively.

The electrodes, matrices, bipolar plates and blanks for the bipolar/cooling plates for stack 563 were fabricated during the previous quarter. The treed cooling patterns were machined in the bipolar/cooling plates and these were leak tested during this quarter. The heat treatment of the bipolar and bipolar/cooling plates was in progress at the end of this quarter.

Approval to begin component fabrication for stack 564 was given by the NASA Project Manager during this quarter. The thick ($\sim$0.56 cm) end and bipolar/cooling plate halves were molded and leak tested.

TASK 2. STACK TESTING

During this period, testing of stack 560 (a 5-cell MK-2 design) was initiated and it is currently being operated continuously, OS/IES loop testing of stack 561 (a 23-cell MK-1 design) was initiated and completed and pretesting of stack 562 (a 23-cell MK-2 design) was carried out and OS/IES loop testing of 562 is in progress.

3.2 Simulated Stacks

The primary objectives of the stack 560 tests are to:

- Establish the performance and endurance of the MK-2 design with heat-treated plates and Mat-1 matrices.
- Test acid management scheme 2, including the modified shim design described in the procedures document.

Testing of stack 560 has proceeded according to the test plan. The following tests were carried out:

- OCV (stable and transient) test
- pressure drop vs flow on both anode and cathode
- effect of both anode and cathode flows on stack performance
- effects of varying anode gas composition
- polarization with varying anode and cathode gas compositions.

The stack is now being operated continuously to obtain endurance data.

Polarization characteristics of stack 560 measured after 100 hrs operation are shown in Figure 1, some results of stack performance tests are summarized in Table I and the performance of individual cells are given for several operating conditions and after various operating times in Table II. The oxygen gains (60 to 70 mV/cell) and high steady state OCVs ($\sim$0.9 V/cell) indicated that all cells were performing satisfactorily. The hydrogen gain of 10 mV between 75% and 100% H_2 (dry basis) is in good agreement with theory.

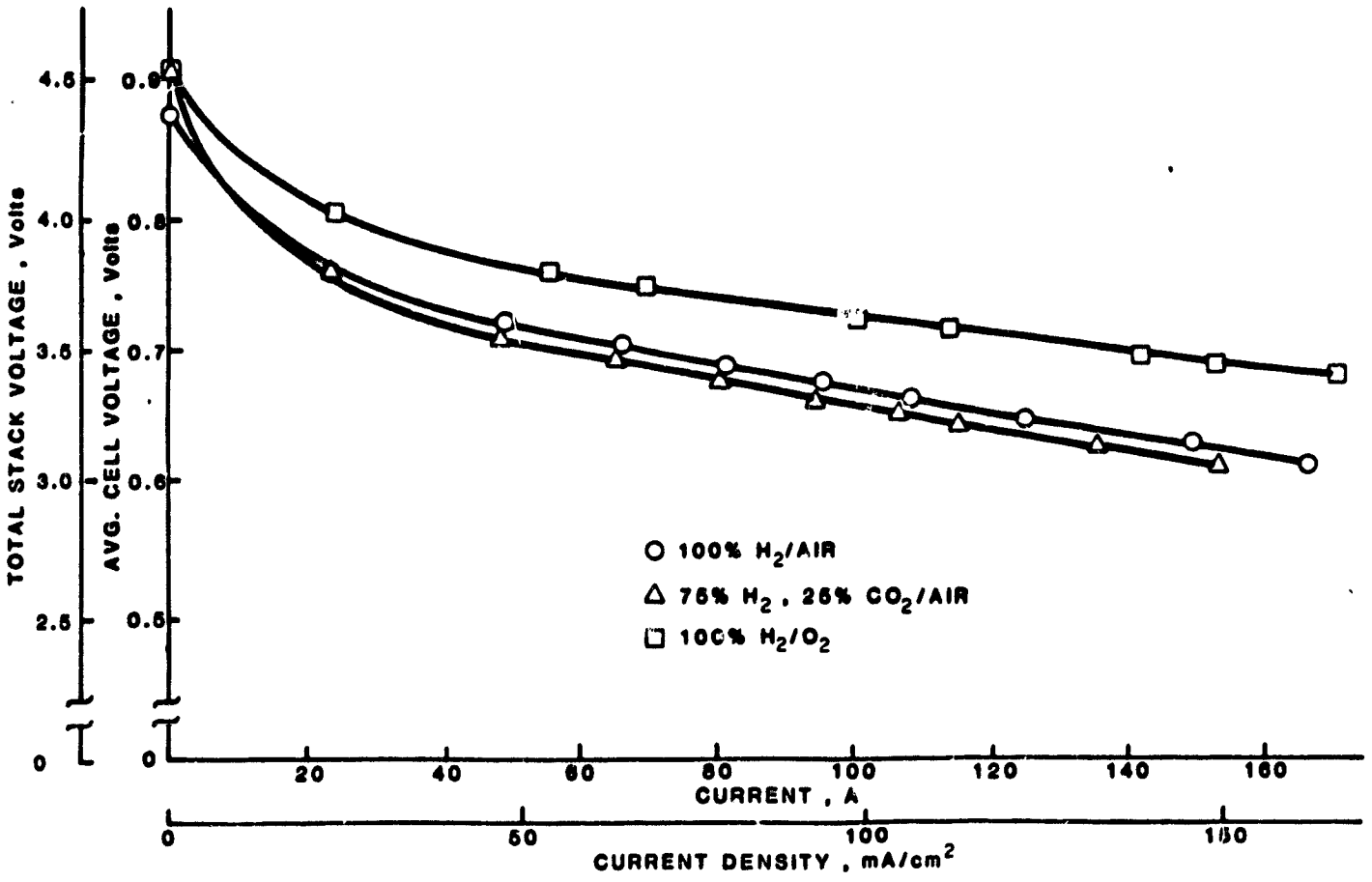

FIGURE 1. POLARIZATION OF STACK 560

TABLE I PERFORMANCE CHARACTERISTICS OF STACK 560 AT DIFFERENT REACTANT COMPOSITIONS

CONDITIONS	PERFORMANCE, volts/cell		
	H_2/O_2	H_2/Air	75% H_2, 25% CO_2/Air
OCV	0.91	0.87	0.91
100 mA/cm² (102A)	0.72	0.66	0.65
150 mA/cm² (153A)	0.69	0.62	0.61

TABLE II. BASELINE PERFORMANCE OF STACK 560 (at 177°C)*

CELL NO.	PARAMETERS	PERFORMANCE, Volts/Cell					
		@ OCV	@ 150 mA/cm²				@ 100 mA/cm²
			100% H_2		75% H_2, 25% CO_2		100% H_2
	Length of Operation, hrs	7	40	400	12	400	412
	Air Flow Stoich	-	4.7	2.0	4.8	2.0	2.9
1		0.883	0.628	0.629	0.613	0.610	0.661
2		0.954	0.623	0.604	0.611	0.602	0.653
3		0.928	0.629	0.615	0.619	0.612	0.659
4		0.933	0.633	0.634	0.621	0.620	0.667
5		0.923	0.627	0.627	0.616	0.613	0.662
	Avg. Cell Voltage, Volts	0.924	0.628	0.622	0.616	0.611	0.660
	H_2 Util.,%	-	82	82	82	81	80
	Load, amps	0	153	152	152	150	100

* ΔT, stack: 10 to 20°C

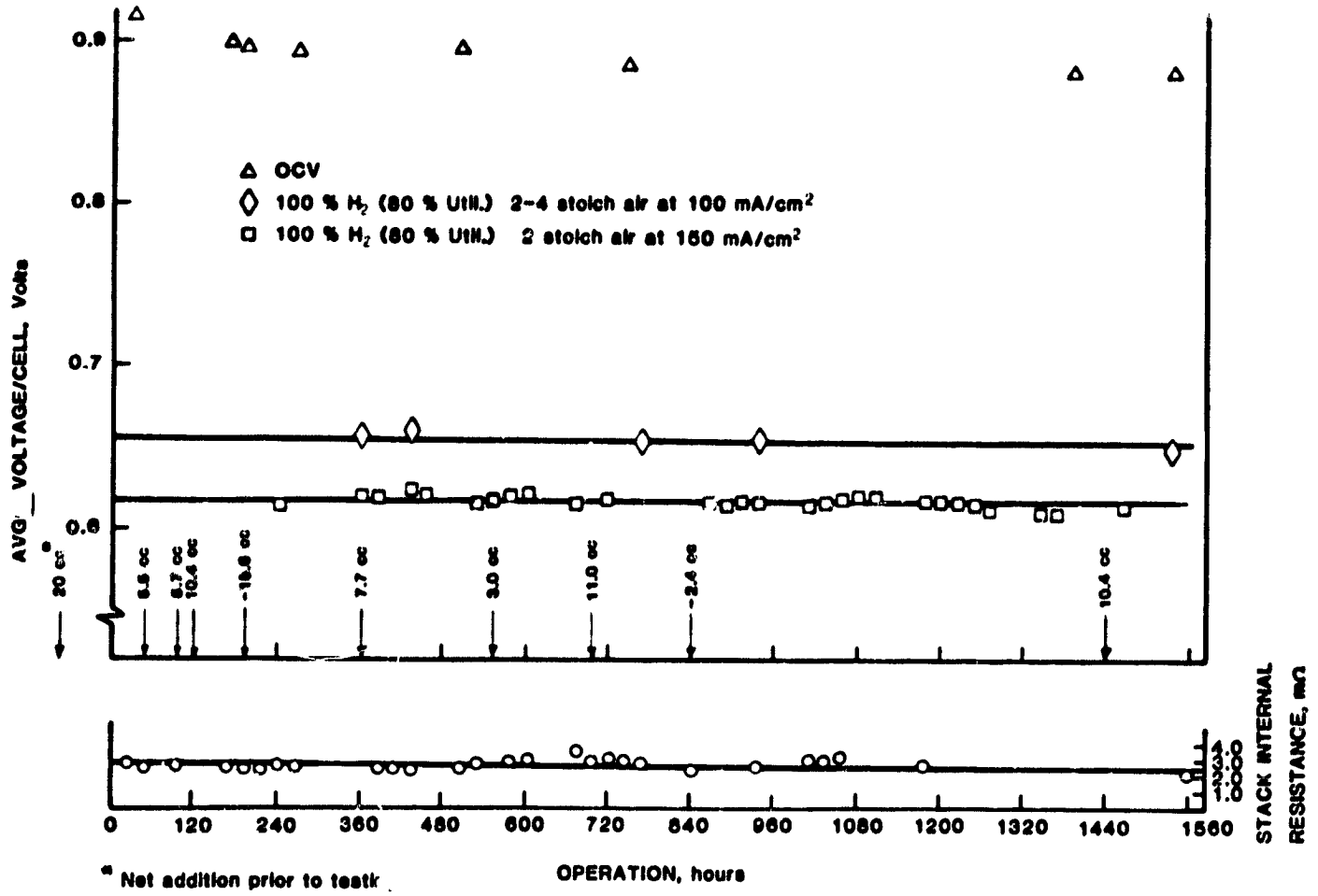

FIGURE 2. LIFEGRAPH OF STACK 560

TABLE III. INITIAL OCV TEST (STABLE & TRANSIENT) FOR STACK 560

CELL NO.	AIR ON H_2 ON	AIR OFF H_2 ON	AIR OFF H_2 ON (1 MINUTE)	AIR ON H_2 OFF	AIR ON H_2 OFF (1 MINUTE)	AIR OFF H_2 OFF	AIR OFF H_2 OFF (1 MINUTE)
1	.895	.867	.840	.864	.854	.861	.833
2	.940	.919	.914	.912	.898	.911	.909
3	.928	.901	.895	.897	.885	.895	.888
4	.928	.907	.899	.902	.884	.901	.894
5	.915	.892	.883	.885	.874	.884	.876
AVG.	.921	.897	.886	.892	.879	.890	.880

Figure 2 shows the OCV, stack resistance and performance at ∿150 mA/cm^2 and ∿175°C during 1560 hours of operation. There was no performance decrease while the resistance decreased slightly.

The transient OCV data for individual cells of stack 560 taken during the first three hours of testing are shown in Table II. These tests are used as diagnostic tools to determine the need for acid additions or other adjustments. The slow decay of voltage during transient tests indicate that there is no crossover of reactants.

The air and fuel side pressure drops of stack 560 were measured and are plotted in Figures 3 and 4. As indicated by the comparison with 558 in Table IV., they are generally higher than for a similar stack with non-heat treated plates. The higher values for 560 are apparently due to the reduction in channel flow areas that occur during heat treatment.

TABLE IV. PRESSURE DROP COMPARISON

PARAMETERS	STACK 558	STACK 560
Flow, lpm	57 (4 stoich)	57 (4 stoich)
Δp, cm H_2O	9.4	14.7

The effect of anode and cathode gas flow rates were measured and are shown in Figures 5 and 6. The effect of air flow is small above ∿40 lpm (2.9 stoich) for either H_2 or 75% H_2, 25% CO_2 fuel. As shown in Figure 5, performance is insensitive to fuel utilization at values below 82% for 100% H_2 and ∿66% for fuel diluted with 25% CO_2 (dry basis).

The effect of varying anode gas composition for 2 and 4.8 stoich air flows are shown in Table V. The effect of 25 vol% CO_2 in the fuel is ∿15 mV which is close to the theoretical value of 12 mV. The effects of 1 and 3% CO are ∿10 and 19 mV respectively at 175°C.

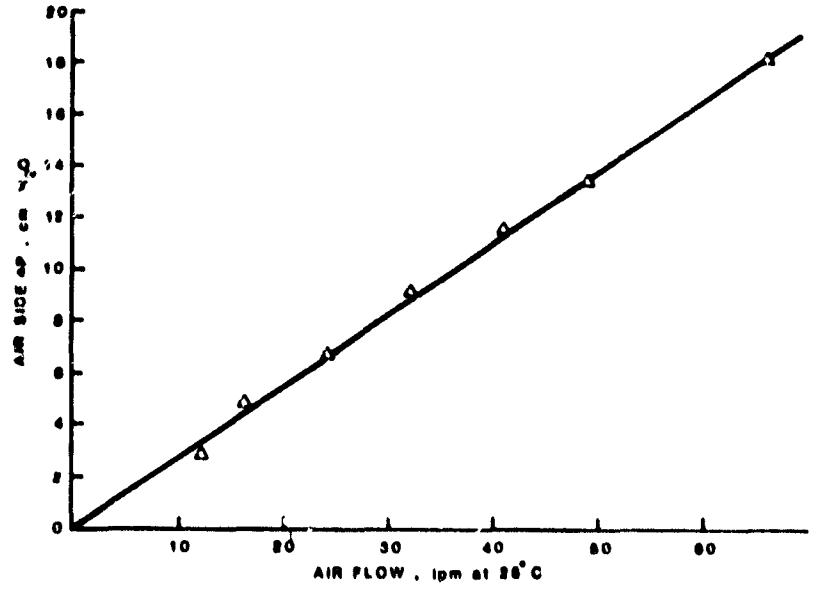

FIGURE 3. AIR FLOW vs PRESSURE DROP, STACK 560

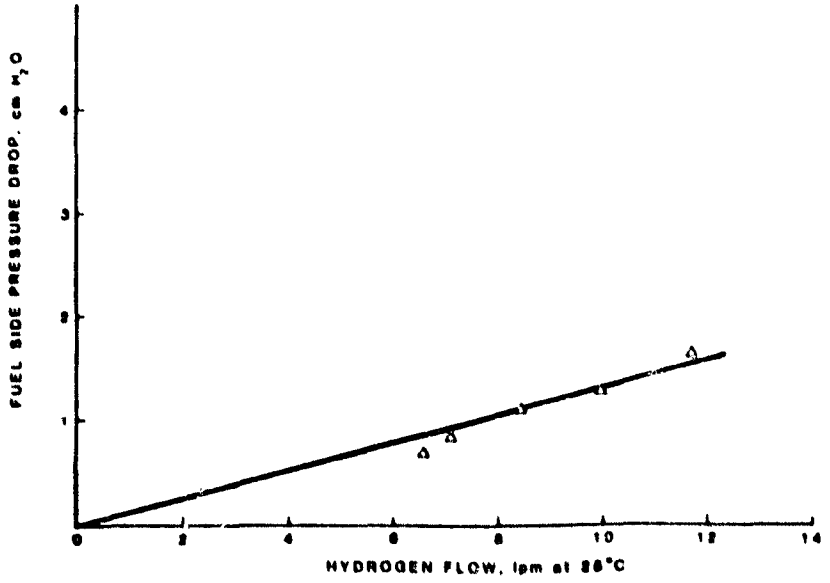

FIGURE 4. HYDROGEN FLOW vs PRESSURE DROP, STACK 560

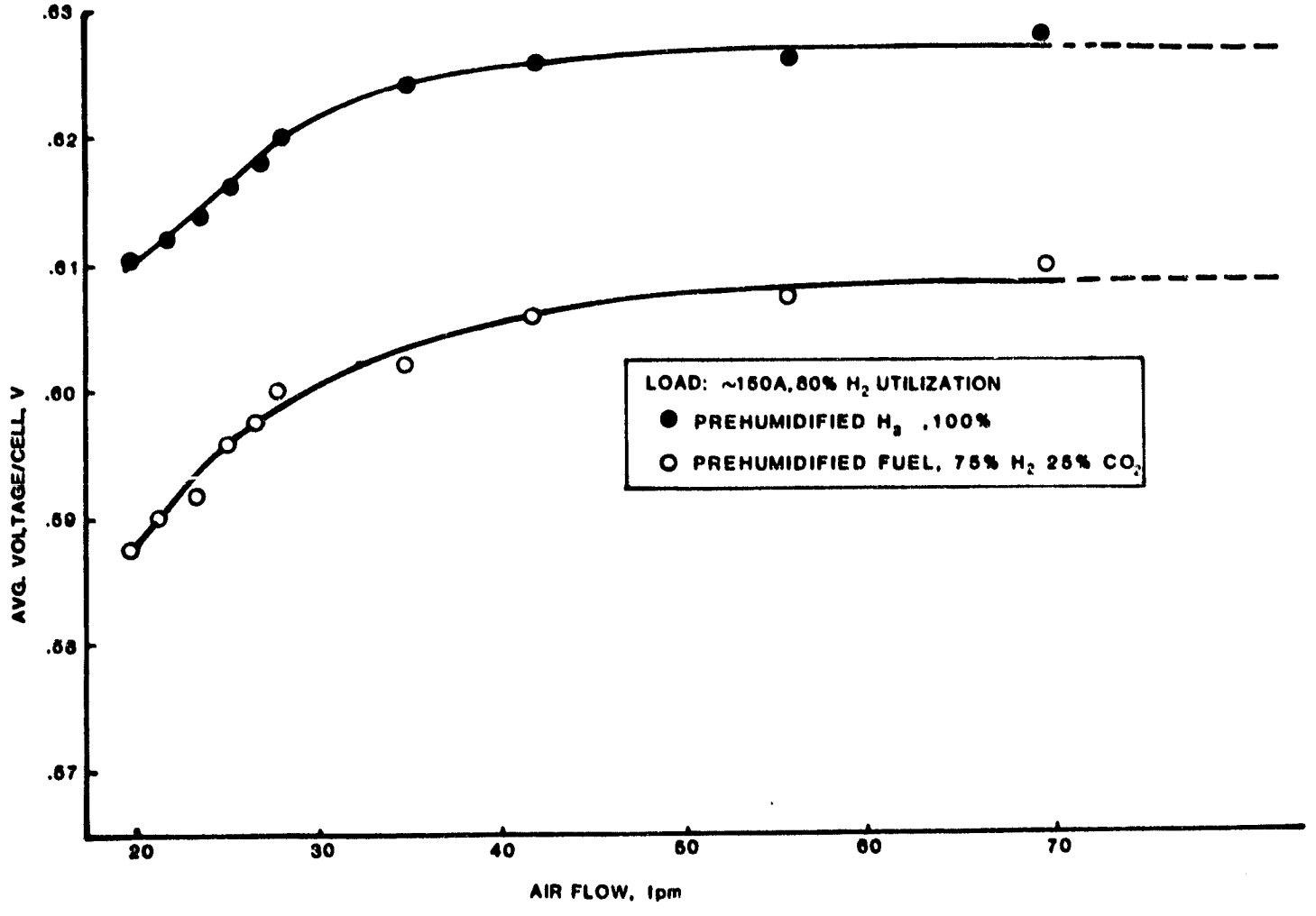

FIGURE 5. EFFECT OF AIR FLOW RATE ON PERFORMANCE, STACK 560

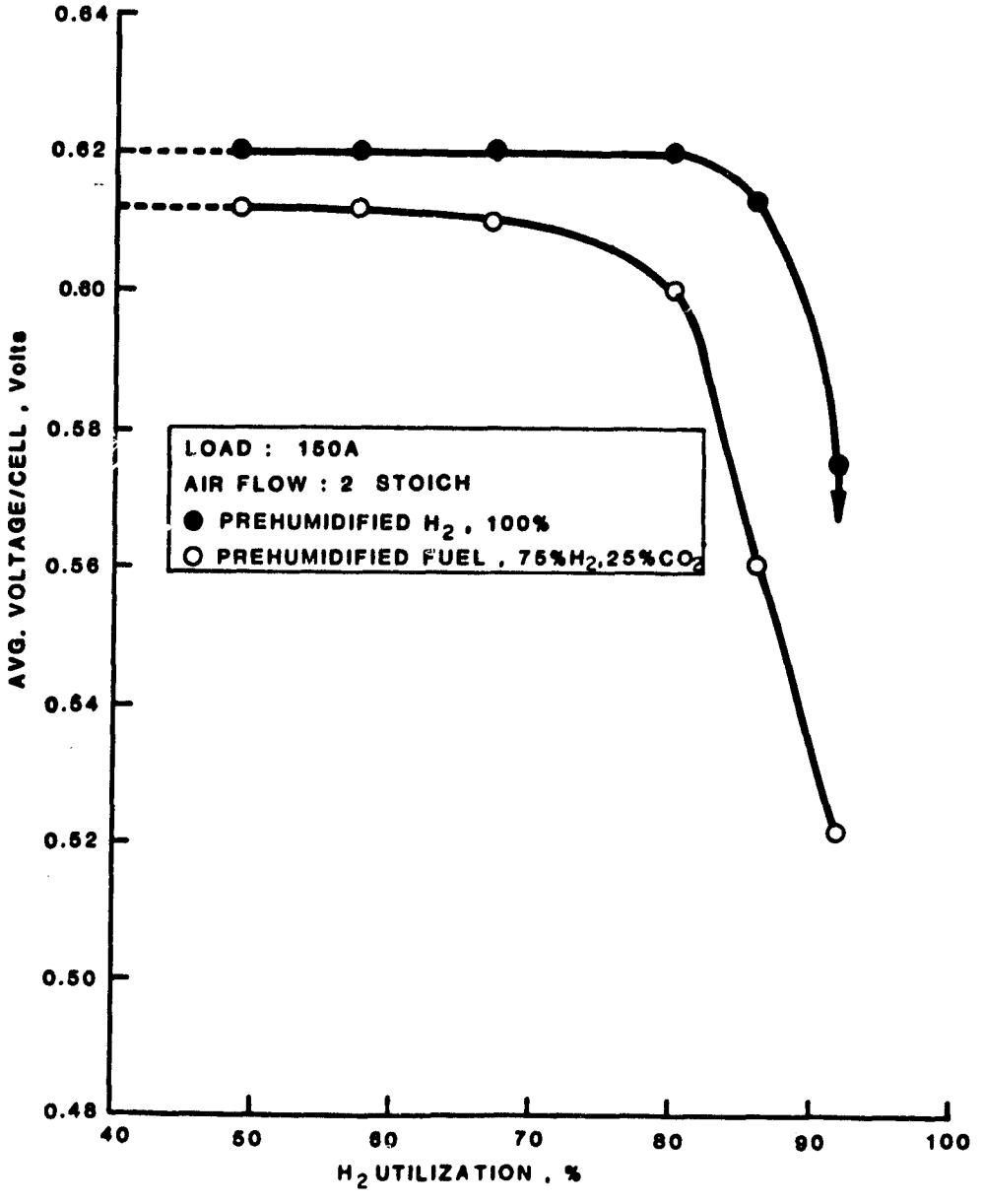

FIGURE 6. EFFECT OF H_2 UTILIZATION ON STACK PERFORMANCE, STACK 560

TABLE V. THE EFFECT ON PERFORMANCE OF VARYING ANODE GAS COMPOSITION
(No. of hrs. in OPERATION: 500)

ANODE GAS COMPOSITION, Vol%			PERFORMANCE, Volts	
H_2	CO_2	CO	@ ∿4.8 ST AIR	@ ∿2.0 ST AIR
100	0	0	0.622	0.618
75	25	0	0.608	0.602
75	24	1	0.596	0.594
75	22	3	0.588	0.584

3.3 Short Stack Testing

During this report period, short stacks 561 (23-cell, MK-1) and 562 (23-cell, MK-2), were tested. The test program for each comprised a relatively short period (∿30 hrs) of pretesting to verify the integrity of stack assembly and the electrochemical performance of the cells (OCV and polarization) and a more extended series of tests in the OS/IES loop. The OS/IES loop tests provide data on performance of the treed cooling plate design, the effect of the separated cooling plate concept (Z bipolar plates) and data on the effects of various operating parameters (e.g., temperature level, current density, CO in fuel). The information obtained in the OS/IES loop tests is then used to verify (and if necessary to modify) the computer models which in turn guide the design of subsequent stacks.

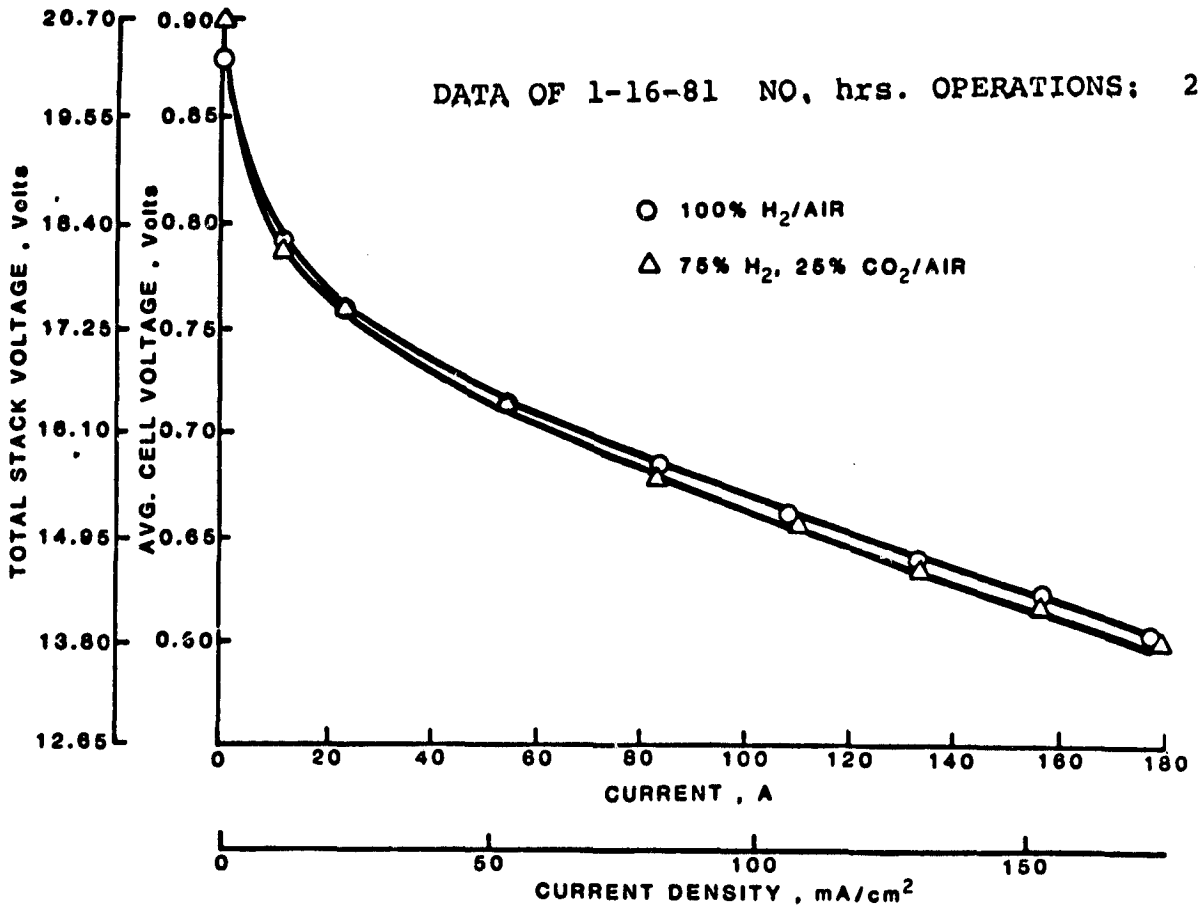

FIGURE 7. POLARIZATION OF STACK 561

3.3.1 Pretesting

Stack 561

Pretesting of the 23 cell stacks 561 (MK-1) and 562 (MK-2) was successfully completed during this period. The results are described in detail below.

The polarization data taken during pretesting of stack 561 are plotted in Figure 7 for two different fuels and summarized for typical points in Table VI. The effect of 25% CO_2 in the fuel is ~12 mV/cell. The initial steady state and transient OCV's indicated that all cells were functioning properly. The stack OCV and performance at 150 mA/cm^2 remained constant during the 24 hours of pretest operation.

TABLE VI. PERFORMANCE CHARACTERISTICS OF STACK 561 AT TWO REACTANT COMPOSITIONS AFTER 20 HRS.

CONDITIONS	PERFORMANCE, volts/cell	
	H_2/Air	75% H_2, 25 CO_2/Air
OCV	0.88	0.90
100 mA/cm^2 (102A)	0.67	0.66
150 mA/cm^2 (153A)	0.63	0.62

The pressure drop-air flow rate characteristics of stack 561 was measured and the results are plotted in Figure 8.

The effect of hydrogen utilization on stack performance at 150 mA/cm^2 and 175°C with humidified hydrogen and a combined cathode process plus cooling gas mass flow rate equal to 26.6 stoichs of air

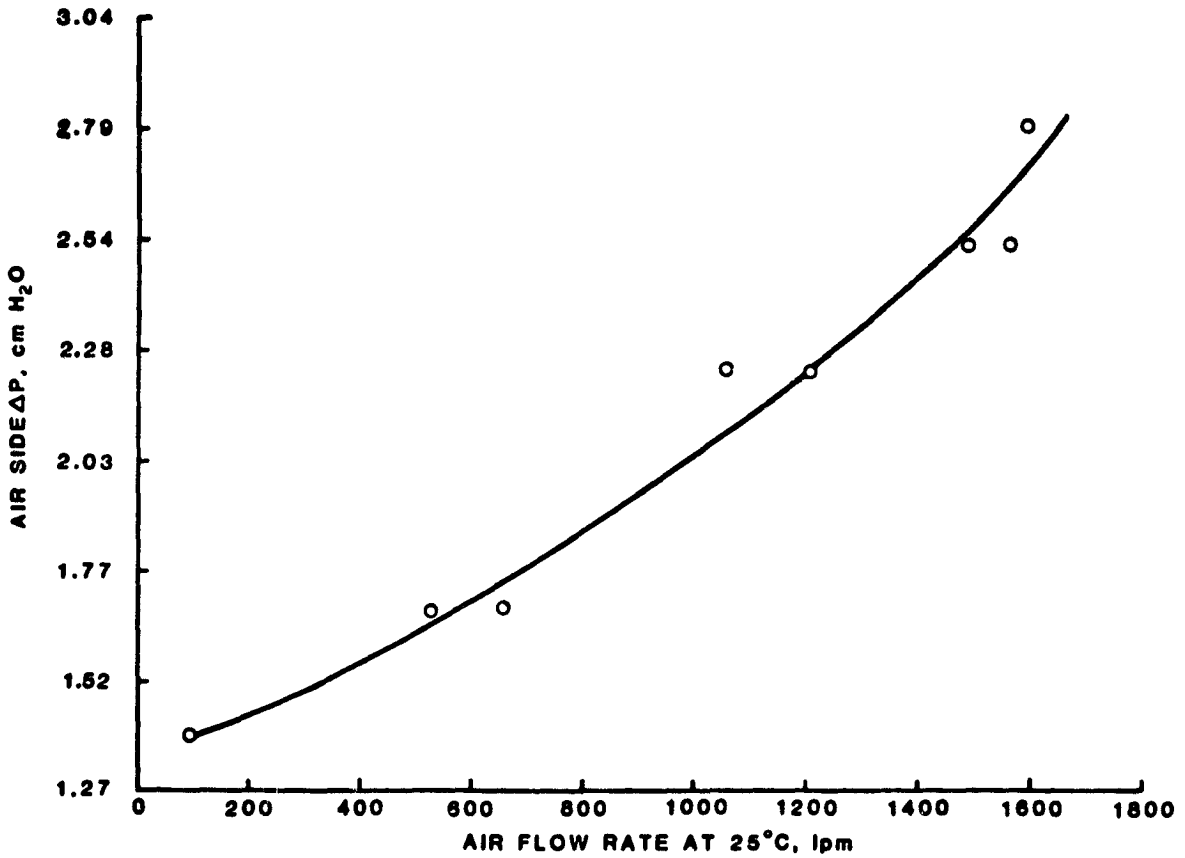

FIGURE 8. AIR FLOW RATE vs PRESSURE DROP, STACK 561

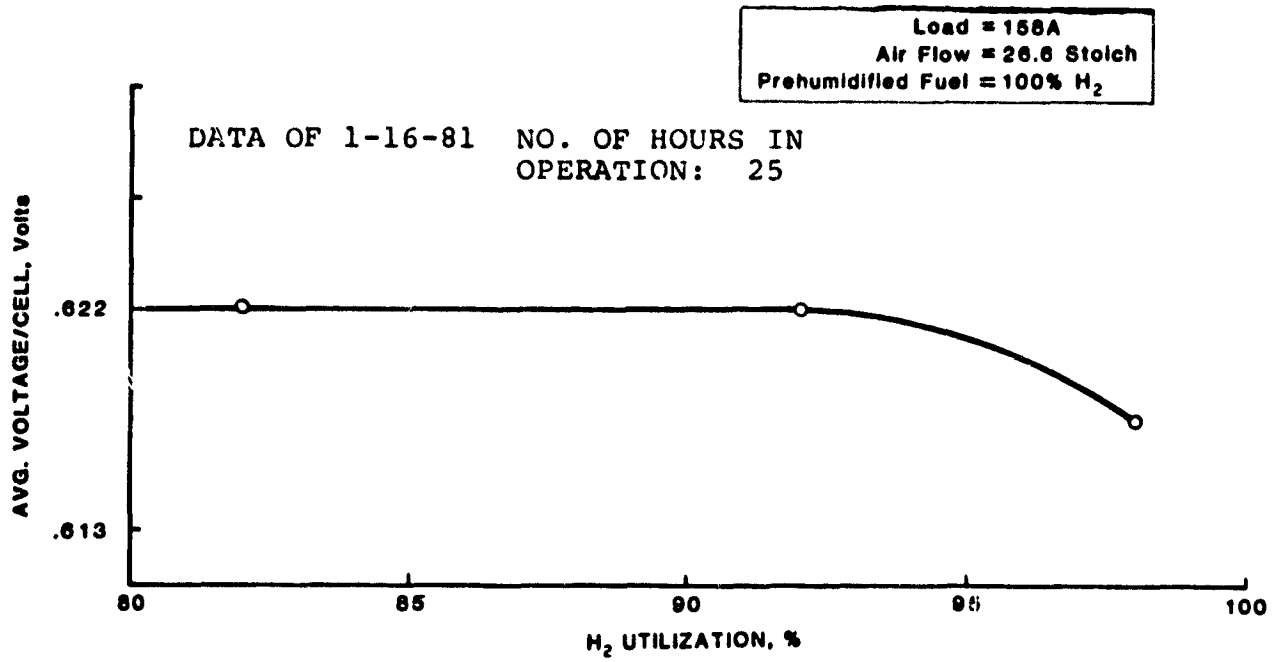

FIGURE 9. EFFECT OF H_2 UTILIZATION ON STACK PERFORMANCE, STACK 561

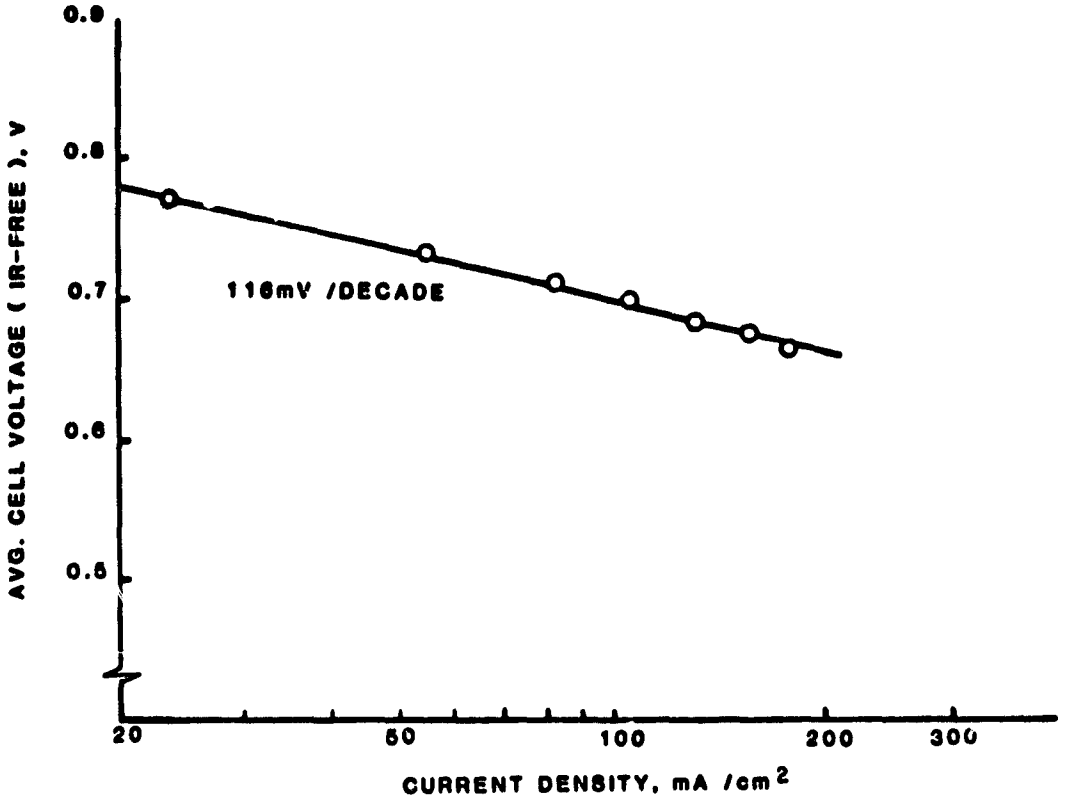

FIGURE 10. IR-FREE VOLTAGE vs CURRENT DENSITY, STACK 561

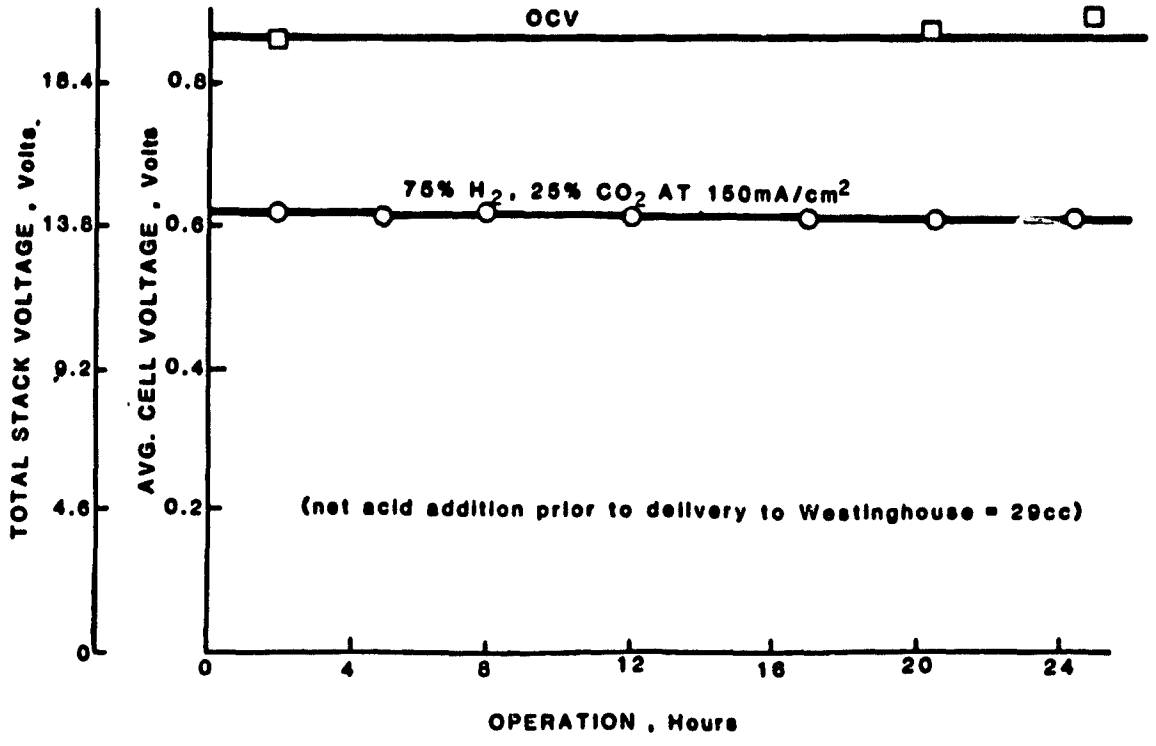

FIGURE 11. LIFEGRAPH OF STACK 561

flow is plotted in Figure 9. The performance is insensitive to utilization for values below 92% which indicated that the fuel inlet manifold was gas tight and there was no reactant crossover.

Figure 10 is a plot of the polarization data for stack 561 on an IR-free basis.

Figure 11 is a lifegraph for stack 561 for the pretest period. It shows that the average cell voltage at 150 mA/cm^2 with 75% H_2. 25% CO_2 was steady at 0.62 volts/cell during the 25 hour period. Net acid addition during the pretest period was 29 cc ($\sim$1.3 cc/cell).

Stack 562

Stack 562 was pre-tested for 27 hours over a 5-day period with steady and reproducible performance. The following tests were performed:

- OCV test (stable and transient)
- polarization characteristics with varying anode gas composition
- fuel flow rate vs pressure drop
- process air flow rate vs pressure drop
- effect of hydrogen flow rate on performance
- effect of air flow rate on performance

The individual cell performances for two current densities and two fuel compositions are tabulated in Table VIII. The initial steady state and transient open circuit voltages for the cells indicated that the matrices and electrodes were sufficiently wetted with acid prior to the start of pre-testing and that all cells were functioning properly. The transient voltage drops for all cells were 23 mV or less after one minute. The value specified in the testing procedure submitted to the NASA Project Manager was 150 mV. The OCV and performance at 150 mA/cm^2 on two fuels were constant through the 27 hour test period as shown in Figure 12.

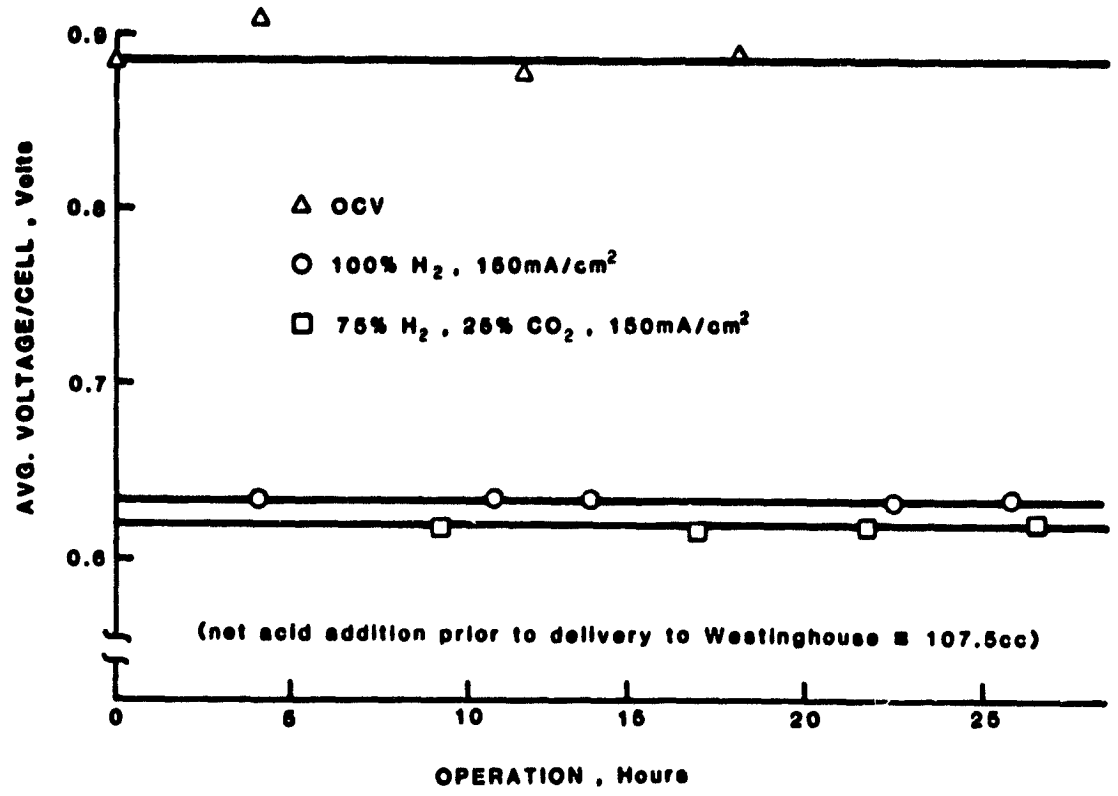

FIGURE 12. LIFEGRAPH OF STACK 562

TABLE VIII BASELINE PERFORMANCE OF STACK 562

	~100 mA/cm²		~150 mA/cm²	
Cell No.	100% H_2	75% H_2 25% CO	100% H_2	75% H_2 25% CO_2
1	.666	.652	.636	.624
2	.667	.657	.639	.626
3	.661	.650	.630	.618
4	.670	.662	.641	.632
5	.654	.640	.620	.611
6	.669	.660	.639	.630
7	.665	.656	.635	.626
8	.670	.660	.640	.630
9	.669	.656	.636	.625
10	.661	.637	.678	.610
11	.670	.640	.640	.618
12	.647	.622	.607	.589
13	.664	.649	.631	.618
14	.659	.647	.624	.612
15	.661	.648	.624	.618
16	.667	.656	.638	.629
17	.663	.653	.631	.621
18	.670	.660	.639	.630
19	.666	.657	.634	.626
20	.668	.660	.639	.632
21	.669	.660	.641	.632
22	.658	.648	.630	.620
23	.666	.653	.635	.625
Average Cell Voltage	.664	.651	.633	.621
Load, amps	100	98	151	148
% H_2 Util.	78.5	77.0	79.1	77.5
No. Stoich Process Air	2.5	2.6	2.3	2.5
No. Stoich Cooling Air	31.7	32.3	25.9	26.4
Date	3/16/81	3/16/81	3/17/81	3/17/81
Time	3:39	4:00	11:03	11:43
No. Hours Operation	23.5	23.75	25.75	26.5

The polarization data for humidified H_2 and 75% H_2 and 25% CO_2 are plotted in Figure 13. The performance on H_2/CO_2 showed a drop of ~12 mV/cell at 150 mA/cm^2 compared to the performance on H_2. This is in close agreement with the theoretical prediction of 12 mV/cell.

The process air and fuel pressure drop-flow rate characteristics of stack 562 are plotted in Figures 14 and 15 respectively. The pressure drops for a given flow rate are higher than for stack 561 due to the reduced flow area of the Z bipolar plates but this is a minor effect on the fuel side and the air side volumetric flow rate for a given operating condition is much smaller on the air side since only the required process gas flows through these passages.

The effects of hydrogen and air flow on stack performance for the two fuels are plotted in Figures 16 and 17 respectively. The flow rates are given in terms of utilization of fuel and stoichs of air as well as volume and these provide a means of correlating the pressure drops of Figures 14 and 15 with stack operation.

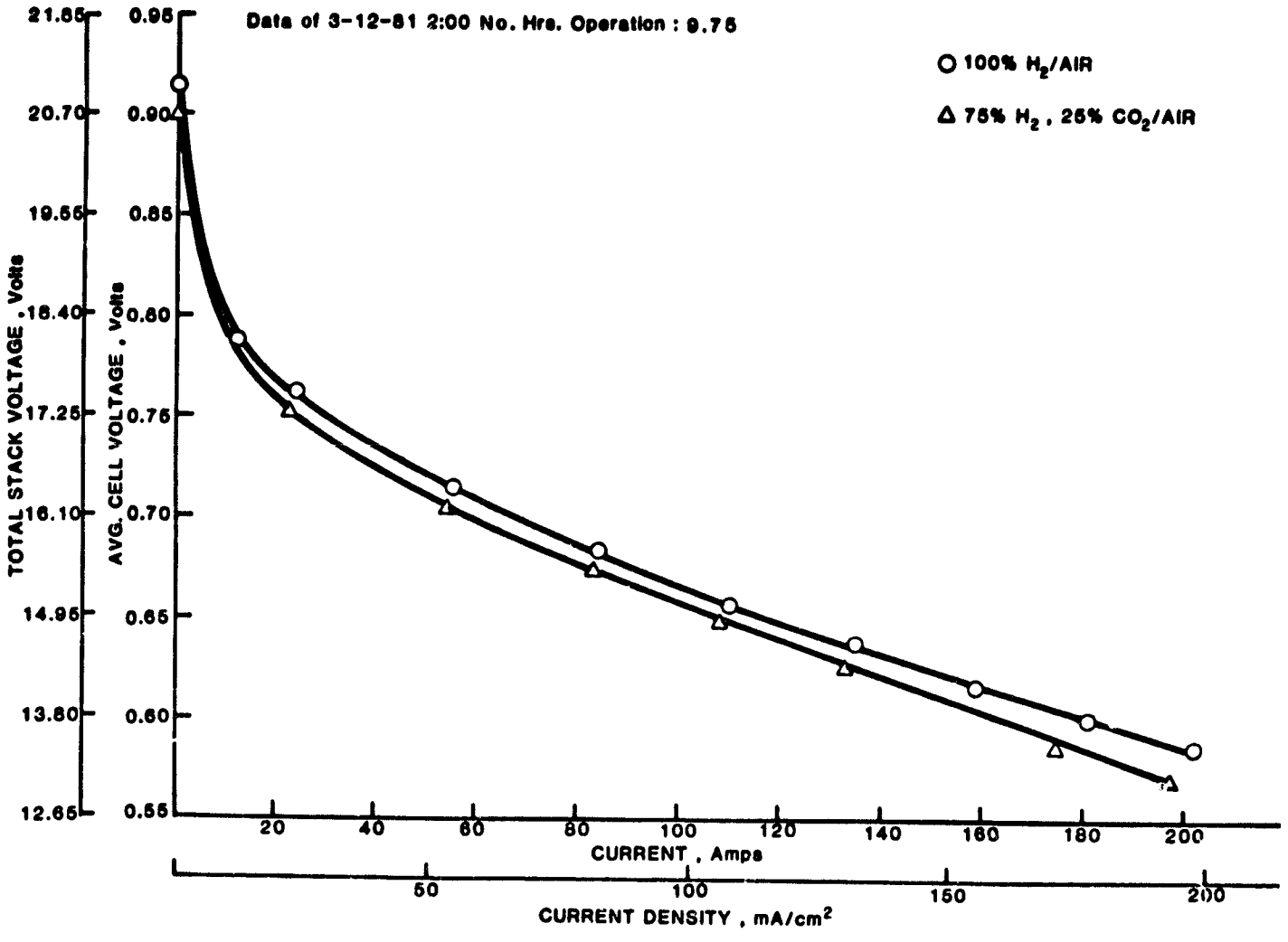

FIGURE 13. STACK 562 POLARIZATION CHARACTERISTICS

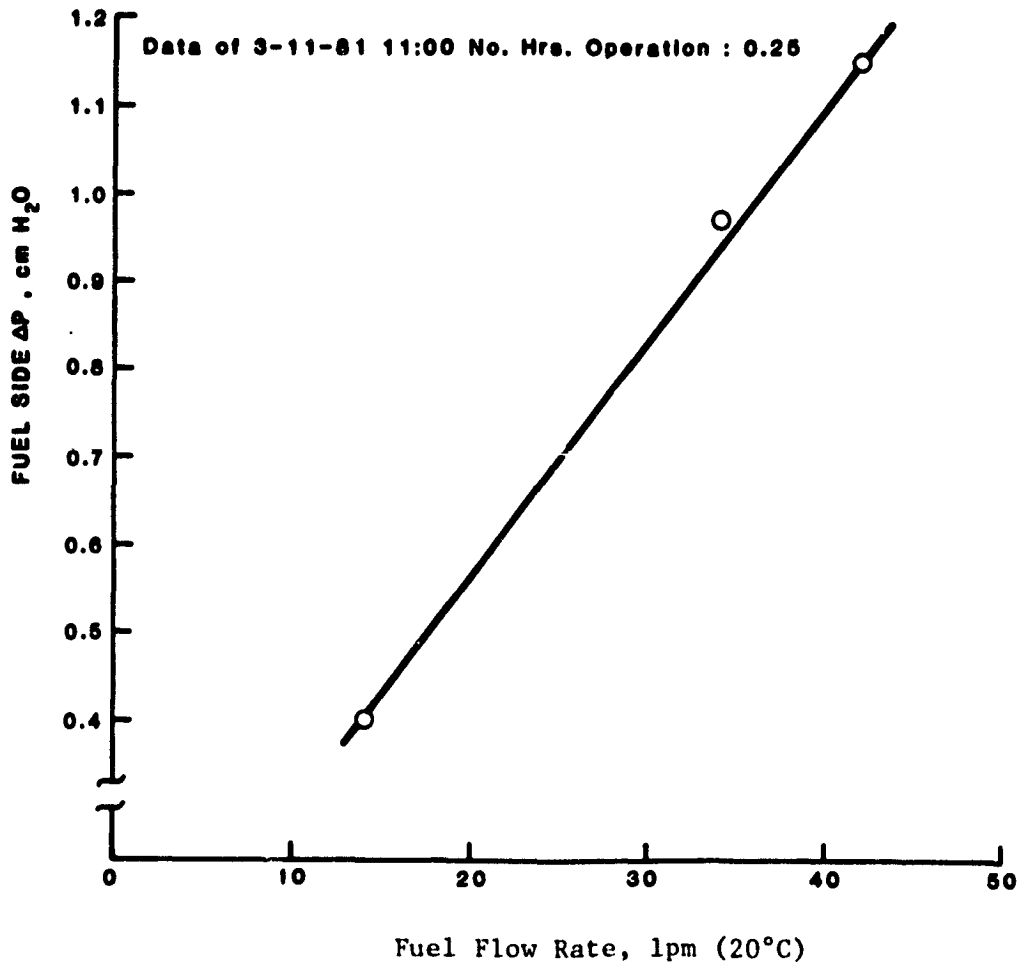

FIGURE 14. FUEL FLOW RATE vs PRESSURE DROP, STACK 562

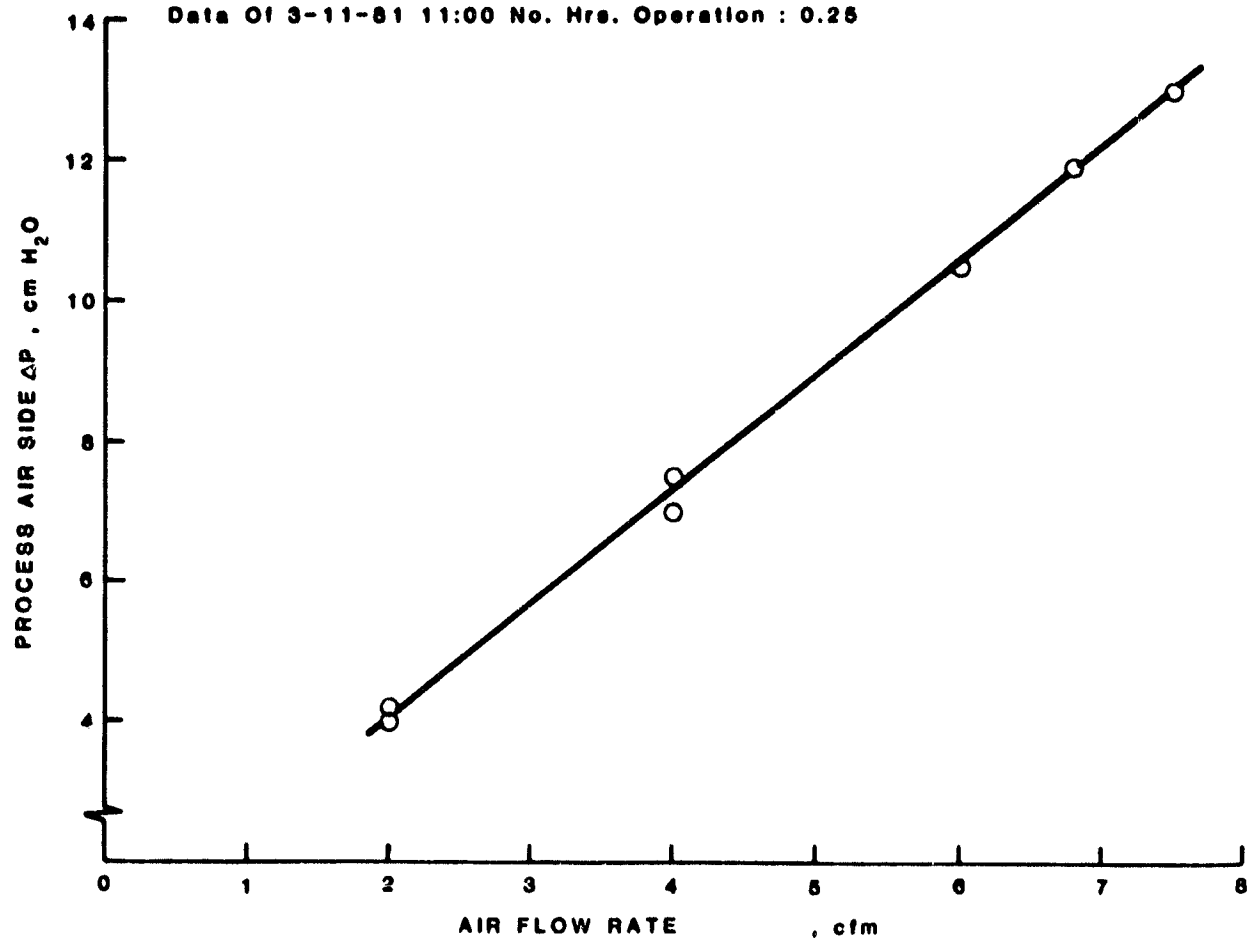

FIGURE 15. PROCESS AIR FLOW RATE vs PRESSURE DROP, STACK 562

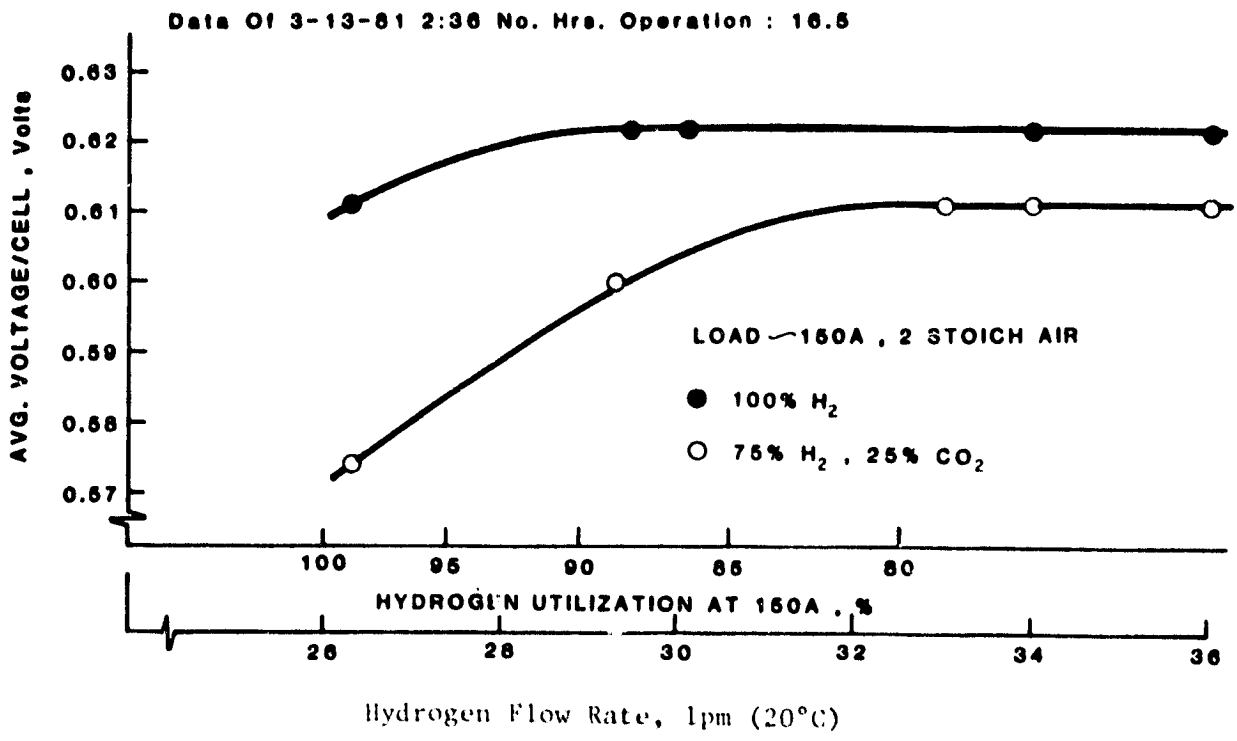

FIGURE 16. EFFECT OF HYDROGEN FLOW RATE ON STACK PERFORMANCE, STACK 562

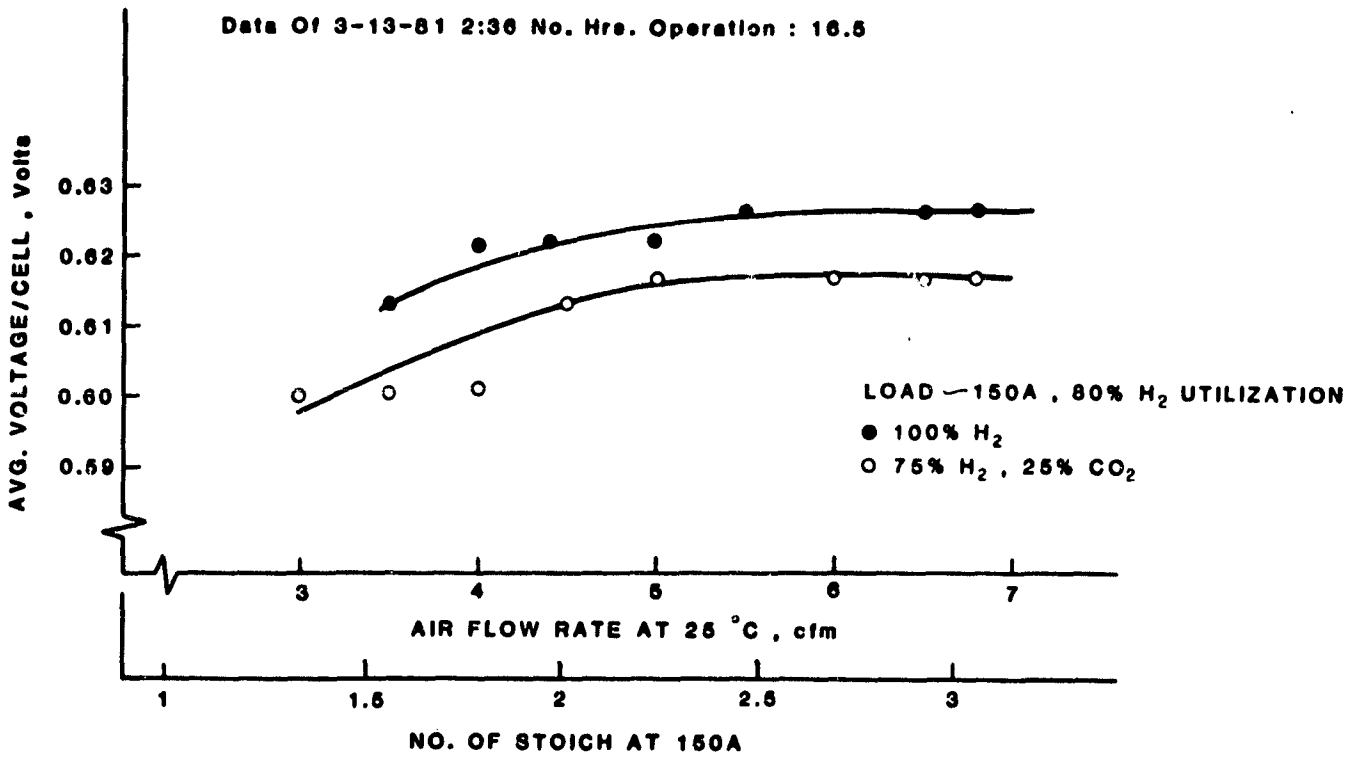

FIGURE 17. EFFECT OF AIR FLOW RATE ON PERFORMANCE, STACK 562

3.3.2 OS/IES Loop Testing

During this reporting period, Stack 561 was installed, tested and removed from the OS/IES loop and Stack 562 was installed and testing initiated.

The objectives of the OS/IES loop tests are to:

1. Verify the ability of the treed cooling channels to achieve cell temperature differentials substantially smaller ($\sim$1/2) than that of the cooling gas temperature rise over a wide range of operating conditions.

2. Test modifications of cooling channel distributions (by blocking selected channels) to guide the design of cooling channel distributions for subsequent stacks.

3. Verify the improvement in cell performance that is expected from the MK-2 (Z pattern) design.

4. Acquire data on the effects of various operating parameters (e.g., fuel utilization, temperature level, fuel CO content) on cell performance, temperature distribution and stream pressure drops for verification and/or modification of the equations used in the lumped parameter and detailed analytical model computer programs. These programs are then used in the design analysis and tradeoff studies of subsequent stacks.

In accordance with the above objectives, Stack 561 was operated at 62 distinct steady state conditions which are described, along with the results and discussion, below. The tests run to date on Stack 562 are also described below and a plan for the continuation of tests during the next quarter was submitted to the NASA Project Manager.

Stack 561

Stack 561 was tested at a total of 62 steady state conditions during this period. The performance remained stable with no apparent decay during the test period. Excellent temperature uniformity was

obtained for current densities of 58 to 195 mA/cm^2. Test results and test conditions, including results of one pretest as No. 1, are summarized in Table X and discussed in detail below.

Stack 561 is a 23-cell MK-1 stack with heat treated bipolar plates and Mat-1 matrix. The four cooling plates are located after cells 4, 9, 14 and 19. The cooling channel spacing was 1.3 cm and 1.4 cm at the hydrogen inlet and exit edges of the plates, respectively. Four rows of six thermocouples equally spaced along the air flow direction were installed in the hydrogen channels. Thermocouple row 11 was located 5 cm from the hydrogen inlet edge of the stack in cell 11 (numbered from the bottom up); row 12 was located along the stack centerline in cell 12; row 13 was located 5 cm from the hydrogen exit edge of the stack in cell 13; and row 17 was located along the centerline of the stack in cell 17. Cell 12 is the center cell of the stack and is located midway between the middle two cooling plates.

The average temperature of the stack, as given in Table X and on the figures, was obtained by averaging the temperatures of rows 11, 12 and 13. The peak to average temperature differential (gradient) is an important parameter since stack performance is primarily dependent on the average while stack life should be primarily affected by the peak. The value given in Table X is obtained by subtracting the average temperature from the maximum temperature indicated by any thermocouple in rows 11, 12 or 13.

Test Conditions

The data in Table X includes inlet temperatures of fuel and air streams, fuel utilization, makeup air flow rate in stoichs, total air flow rate through the stack, air side pressure drop, and dry fuel composition. In all tests, the dry fuel mixture was humidified by bubbling through room temperature water before heating to the indicated inlet temperature.

TABLE X - SUMMARY OF TEST CONDITIONS AND TEST RESULTS FOR STACK 561

TABLE X-SUMMARY OF TEST CONDITIONS AND TEST RESULTS FOR STACK 561

Test	Current Density, mA/cm^2	Average Volts/Cell V	Average Temperature °C	Peak to Average Temperature Difference °C	Fuel Utilization	H_2 Inlet Mole Fraction (Dry)	CO_2 Inlet Mole Fraction (Dry)	CO Inlet Mole Fraction (Dry)	Fuel Inlet Temperature, °C	Makeup Air Stoichs	Loop Flow Rate (Makeup + Recirculation), g/sec	Inlet Air Temperature, °C	Air Temperature Rise °C	Air Pressure Drop, in.H_2O
1	152	.613	177	9.4	.82	.75	.25	0	103	13.3		128	41	
2	158	.586	182	11.9	.72	.75	.25	0	75	8.2	3.0	123	46	1.46
3	101	.647	175	5.6	.66	.75	.25	0	110	9.0	3.4	151	13	1.61
4	98	.630	175	7.8	.75	.75	.25	0	114	9.3	3.5	150	12	1.61
5	100	.647	175	5.4	.66	.75	.25	0	112	9.1		150	13	1.61
6	107	.591	181	9.3	.49	.75	.25	0	71	6.0	2.5	124	66	1.17
7	107	.620	179	8.2	.66	.75	.25	0	120	5.9	2.2	123	69	.89
8	107	.619	186	8.6	.66	.75	.25	0	122	6.0	2.0	122	56	.76
9	156	.588	175	10.7	.64	.83	.17	0	115	6.2	3.6	113	53	1.69
10	156	.578	175	10.5	.64	.83	.17	0	114	3.9	3.7	113	52	1.75
11	198	.566	175	11.8	.59	.89	.11	0	108	4.1	4.78	113	52	3.08
12	107	.635	176	7.7	.51	.80	.20	0	120	6.0	7.9	117	54	.72
13	107	.628	178	7.5	.50	.80	.20	0	120	6.0	1.9	116	56	.73
14	107	.588	181	6.1	.51	.80	.20	0	119	2.0	1.9	115	58	.73
15	156	.570	181	9.5	.55	.85	.15	0	113	3.8	3.6	99	56	1.60
16	198	.564	159	12.3	.58	.93	.07	0	109	4.1	4.85	96	56	2.64
17	107	.609	161	5.8	.51	.80	.20	0	116	6.0	1.9	96	58	.72
18	107	.621	181	9.1	.64	.76	.24	0	122	5.9	2.1	123	53	.81
19	155	.589	177	9.1	.66	.83	.17	0	115	10.9	3.6	115	56	1.71
20	155	.590	179	8.9	.66	.83	.17	0	116	7.2	3.6	116	56	1.72
21	155	.537	182	6.5	.66	.83	.17	0	118	2.1	3.5	113	58	1.71
22	155	.531	166	9.3	.66	.83	.17	0	119	2.1	5.22	114	47	2.82
23	156	.582	178	10.0	.63	.83	.17	0	113	6.1	3.6	116	56	1.70
24	156	.575	179	9.6	.63	.83	.17	0	113	6.0	3.6	116	55	1.69
25	198	.552	178	11.7	.61	.86	.14	0	107	6.1	4.78	114	56	2.58
26	107	.578	176	6.3				0	119		2.4	119	50	1.01
27	198	.498	179	10.6				0	111		5.00	112	55	2.74
28	107	.619	179	9.8				0	116			114	60	.76
29	200	.556	175	14.1				0	102			115	50	2.99
30	107	.621	181	7.3	.77	.76	.24	0	124	5.9	2.3	122	57	.98
31	156	.585	180	9.3	.74	.76	.24	0	113	6.1	3.7	118	57	1.75
32	198	.560	178	12.4	.74	.75	.25	0	108	3.9	5.06	114	56	2.71
33	156	.563	178	9.0	.72	.76	.24	0	111	3.1	3.7	115	56	1.76
34	156	.532	180	7.9	.72	.76	.24	0	112	2.1	3.7	113	60	1.74
35	107	.614	178	6.5	.74	.77	.23	0	126	6.0	2.4	120	56	.98
36	107	.576	174	5.2	.74	.77	.23	0	124	1.9	2.8	120	51	1.19
37	107	.585	151	6.8	.73	.77	.23	0	122	6.1	2.6	95	56	1.20
38	107	.536	155	6.5	.73	.77	.23	0	122	1.6	2.7	97	58	1.13
39	156	.509	163	12.1	.68	.77	.23	0	110	2.1	3.6	97	62	1.70
40	156	.561	156	9.4	.70	.75	.25	0	77	6.0	3.83	89	57	1.76
41	156	.552	162	9.8	.70	.75	.25	0	73	6.0	3.83	99	55	1.77
42	156	.563	170	9.8	.70	.75	.25	0	87	6.0	3.83	108	56	1.80
43	156	.572	178	9.6	.70	.75	.25	0	90	6.0	3.81	117	53	1.82
44	156	.565	171	10.5	.70	.75	.25	0	95	6.0	3.83	107	56	1.83
45	199	.499	156	13.9	.70	.75	.25	0	33	3.9	4.85	86	59	2.51
46	199	.513	166	13.4	.70	.75	.25	0	35	3.9	4.85	95	59	2.58
47	199	.526	172	13.2	.70	.75	.25	0	41	3.9	4.81	104	57	2.56
48	199	.535	180	13.0	.70	.75	.25	0	41	3.9	4.77	114	56	2.59
49	199	.525	172	13.1	.70	.75	.25	0	41	3.9	4.81	103	58	2.56
50	199	.507	173	14.6	.71	.74	.24	.016	100	3.9	4.81	103	60	2.56
51	199	.501	173	15.2	.70	.73	.23	.026	100	3.9	4.81	103	61	2.56
52	199	.483	175	16.3	.70	.72	.24	.040	100	3.9	4.81	103	63	2.56
53	108	.580	151	7.3	.69	.75	.25	0	107	4.4	2.6	92	55	1.03
54	108	.529	158	7.4	.69	.75	.25	0	115	4.3	2.6	102	52	1.04
55	107	.599	166	7.2	.68	.75	.25	0	120	4.4	2.6	112	50	1.07
56	107	.609	169	7.3	.68	.75	.25	0	107	3.9	2.4	122	52	.99
57	107	.604	172	7.4	.68	.75	.25	0	108	3.9	2.4	112	56	.98
58	99	.635	170	6.1	.70	.75	.25	0	120	6.0	1.5	97	52	.62
59	99	.638	152	5.5	.70	.75	.25	0	120	6.0	1.5	105	45	.67
60	99	.643	158	5.2	.70	.75	.25	0	120	6.0	1.5	115	60	.67
61	99	.655	170	5.2	.70	.75	.25	0	120	6.0	1.5	130	36	.68
62	99	.663	180	5.2	.70	.75	.25	0	120	6.0	1.5	142	38	.69

The first OS/IES loop tests (2 to 5) were conducted without insulation on the stack for comparison with pretest data and to observe the cell sensitivity to fuel utilization. These early tests were run by increasing hydrogen flow until a sharp drop in voltage of the stack (or a cell) was observed. They indicated a high sensitivity to hydrogen flow but, after test No. 29, a leak in the fuel supply line downstream of the metering devices was discovered and repaired. Thus the actual rate of fuel flow to the stack for tests 2 through 29 was less than indicated (and hydrogen utilization greater) by an unknown amount.

Tests 6 to 18 were performed with the stack insulated and using the cooling plates as designed and described in detail in a separate document. Temperature distributions of tests 7, 8, 9, 10 and 18, which are representative operating conditions, showed that the average temperature at the hydrogen inlet edge of the stack (row 11) was 10°C higher than that of the exit edge (row 13). Two cooling channels (25 and 29 from the inlet edge) per cooling plate near the hydrogen exit edge (2 and 6 from the exit edge) were blocked to improve temperature uniformity. All remaining tests (numbers higher than 29) were made with this modified cooling plate configuration.

In tests 6 through 29, stack performance was measured as a function of X (makeup air flow) for a series of current densities. The series at 2 stoich makeup was not completed because cells 12 and 14 produced low voltages (high sensitivity to oxygen utilization) at 2 stoich makeup.

After repairing the fuel leak mentioned above, tests 30 to 36 were run to measure the effect of air makeup on performance with a known fuel flow. Comparison of test 31 with test 9 indicates that approximately 14% ((.74-.64)/.74)of the fuel had been leaking. Tests 37 to 39 were run to determine the effect of makeup air on performance at lower average temperature.

The remaining tests (40 through 62) were made to determine the effect of average temperature on performance. Seventy percent fuel utilization and 49 stoich makeup air were used for these tests. The

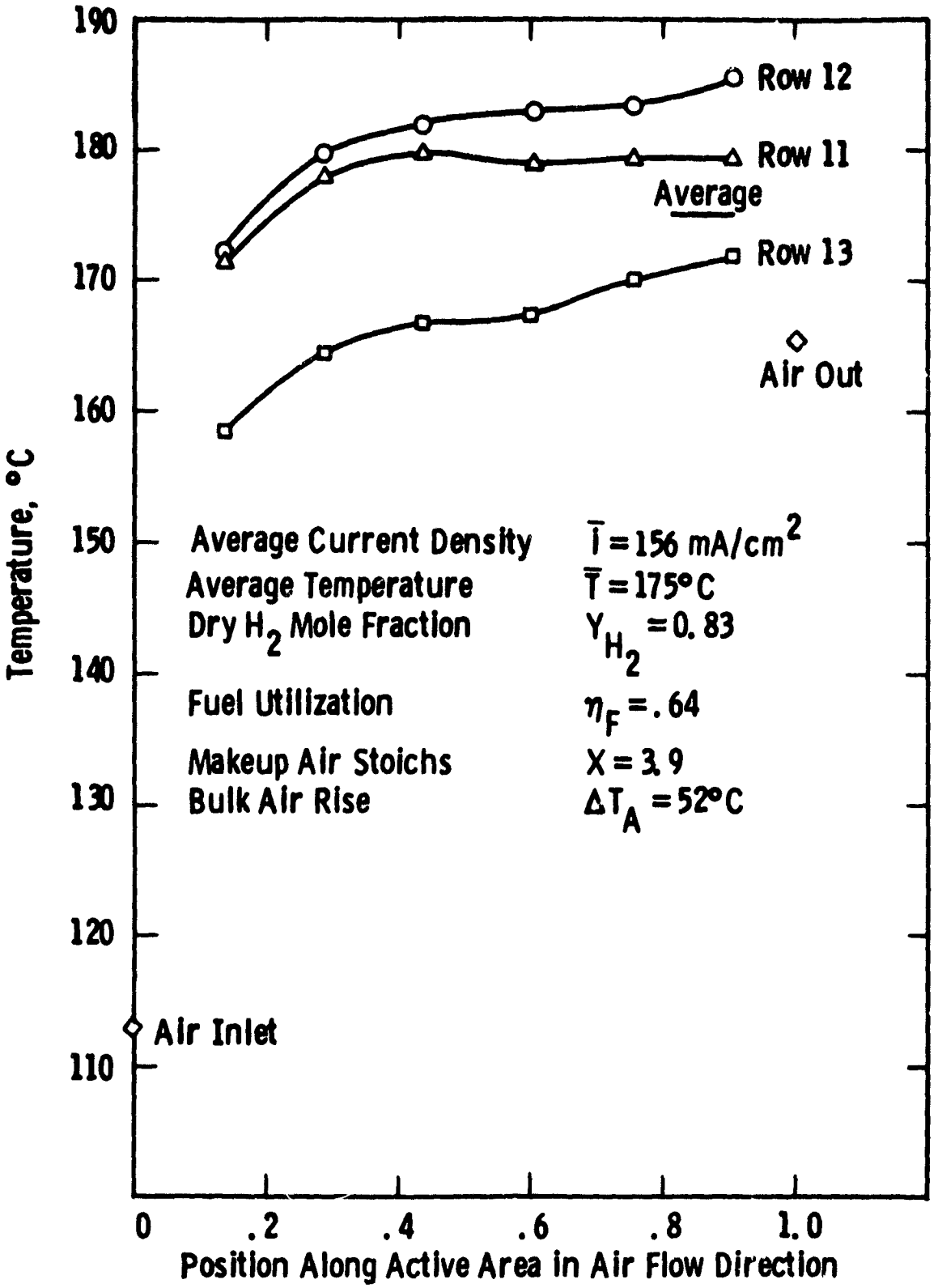

Fig. 18 — Temperature distribution for stack 561 with all cooling channels open - Test 10

procedure was to start with low inlet air temperature at a fixed current until steady state operation with an average stack temperature near 150°C was achieved. The air inlet temperature was then raised in steps to obtain steady state performance for stack temperatures between 150 and 180°C. A final point for each current was obtained by lowering air inlet temperature to duplicate data and show that the performance was independent of whether the point was reached by raising or lowering the temperature. This series also included the effect of CO from 0 to 4 percent at 195 mA/cm^2 in tests 49 through 52.

Discussion of Results

Temperature Distribution

The effect of changing the cooling distribution (by blocking cooling channels 25 and 29 in the cooling plates) on temperature distribution are shown in Figures 18 and 19 and the effect on performance for the two tests (10 and 43) are given in Table X. With the blocked channels the average temperature near the exit edge (row 13) was 8.1°C higher than that of the inlet edge while it was 11.4°C lower with all channels open. The difference between rows 11 and 13 was ≤5°C in more than three fourths of the tests with 28 cooling channels per plate. The peak to average gradient was reduced from 10.5°C to 9.6°C by the modification.

Figures 19, 20 and 21 show temperature distributions for nominal 4, 2 and 6 stoich makeup at the same current density for 28 cooling channels per cooling plate. They indicate a trend toward a more uniform temperature as the makeup air flow is reduced from 6 to 2 stoichs. This is due to the fact that the reduced O_2 concentrations near the air exit reduce the reaction rates and the heat generation, resulting in a reduced temperature level.

Figures 19, 22, and 23 show temperature distributions at 155, 107 and 195 mA/cm^2 for 4 stoich makeup and 70 percent fuel utilization. The distribution remains remarkably similar over the range of current densities.

Curve 727856-A

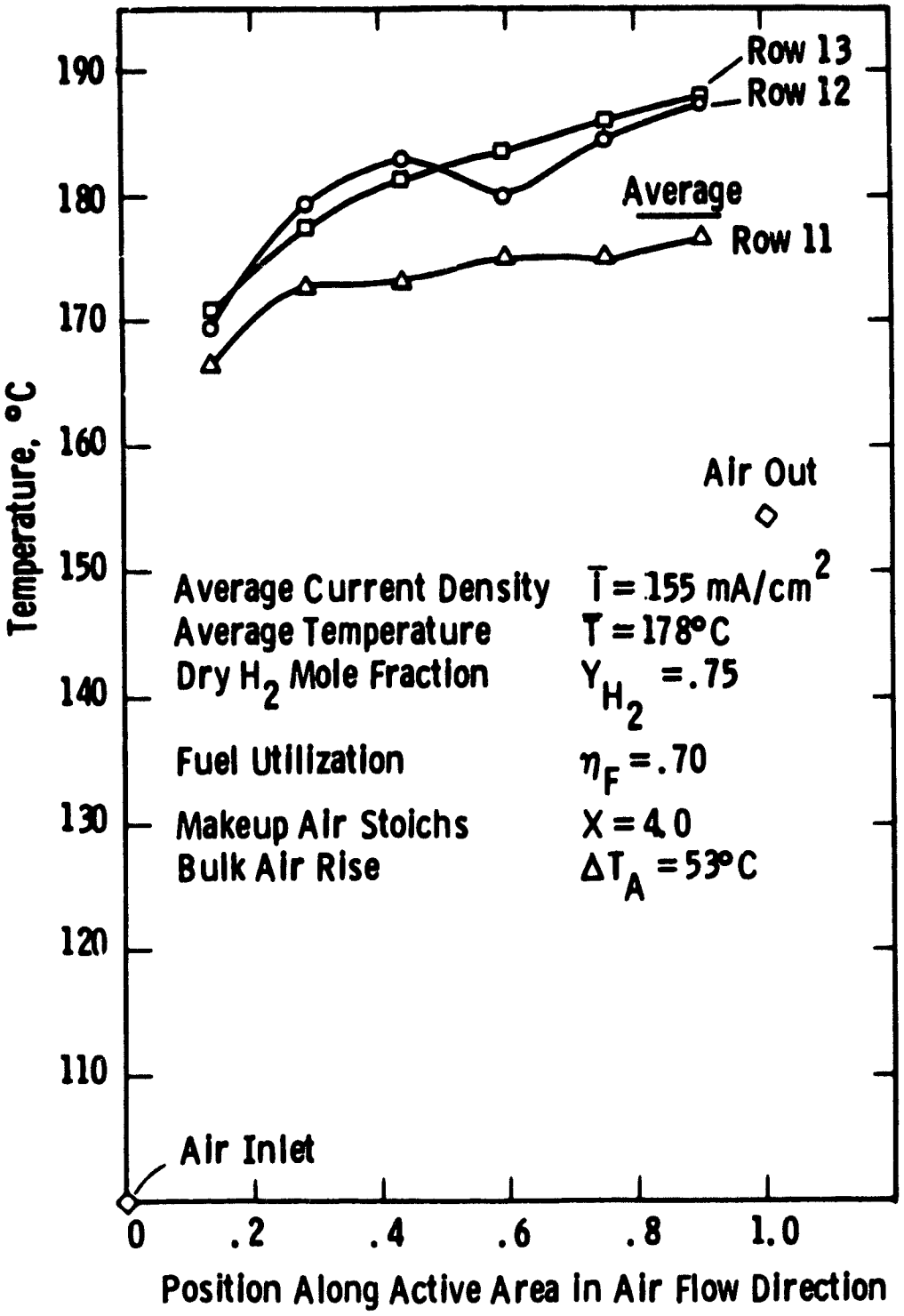

Fig. 19 — Temperature distribution for stack 561 with modified cooling plate Geometry - Test 43

Curve 727855-A

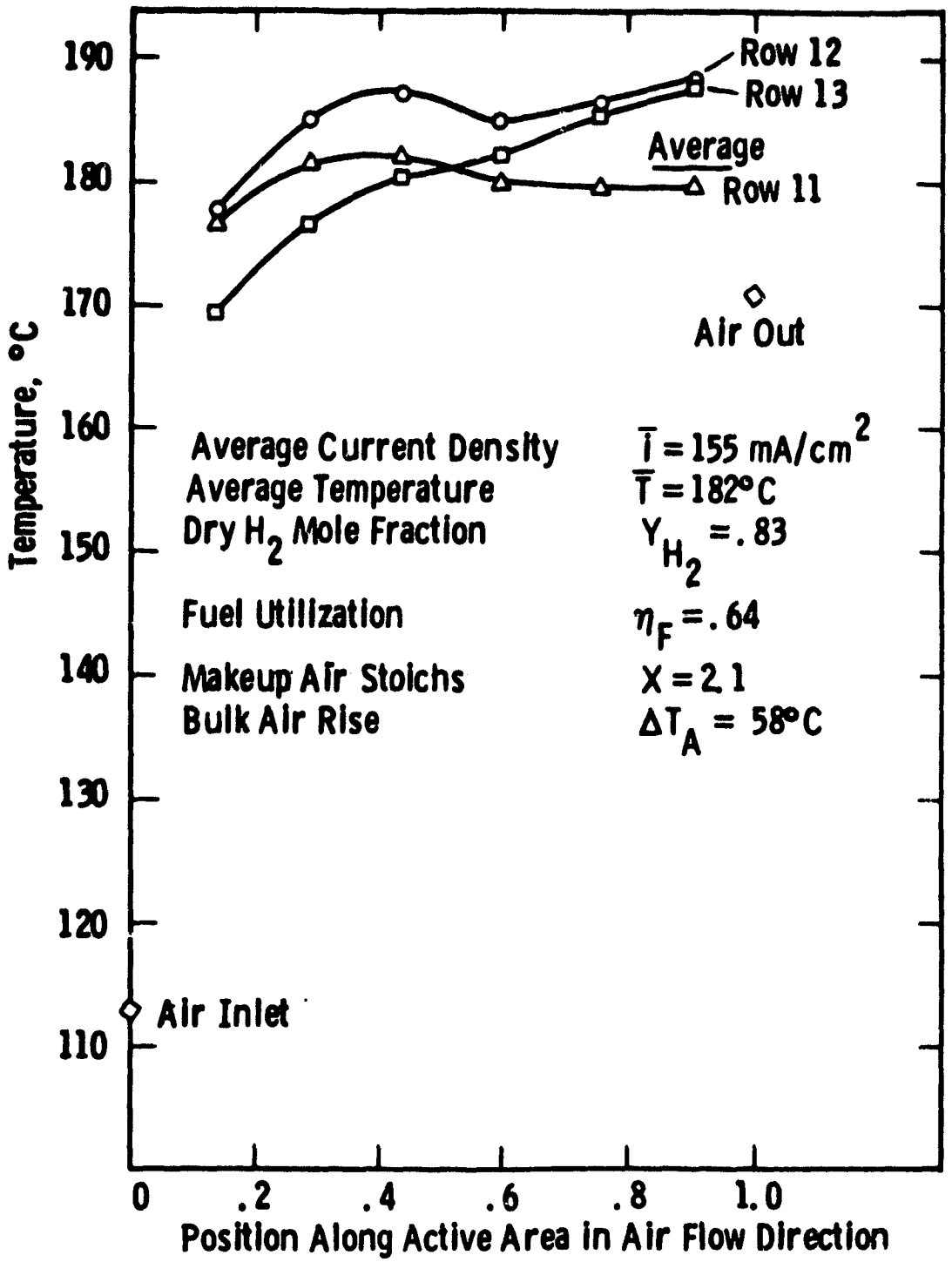

Fig. 20—Temperature distribution for stack 561 with modified cooling plate Geometry-Test 21

Curve 727857-A

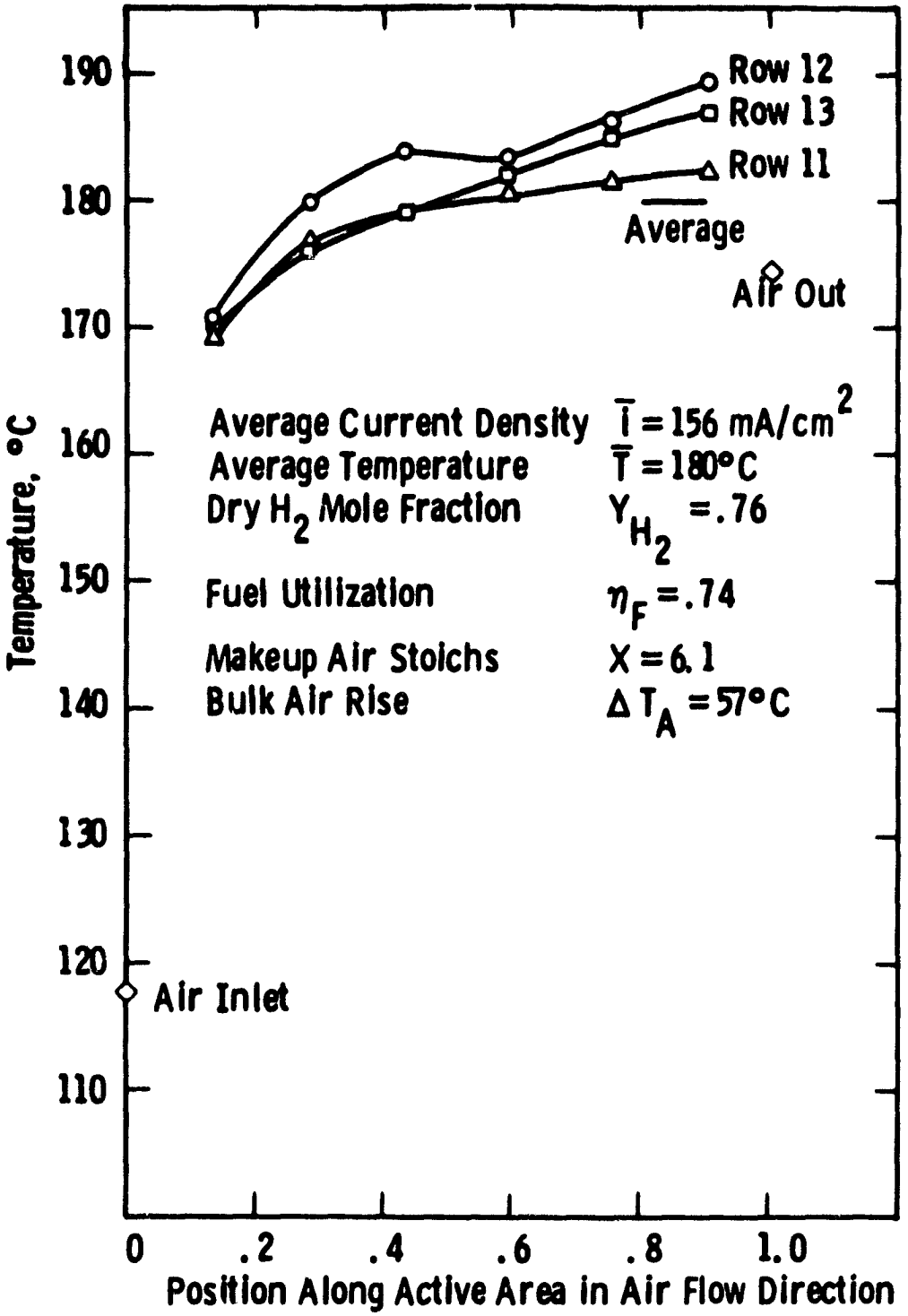

Fig. 21– Temperature distribution for stack 561 with modified cooling plate Geometry - Test 31

Curve 727874-A

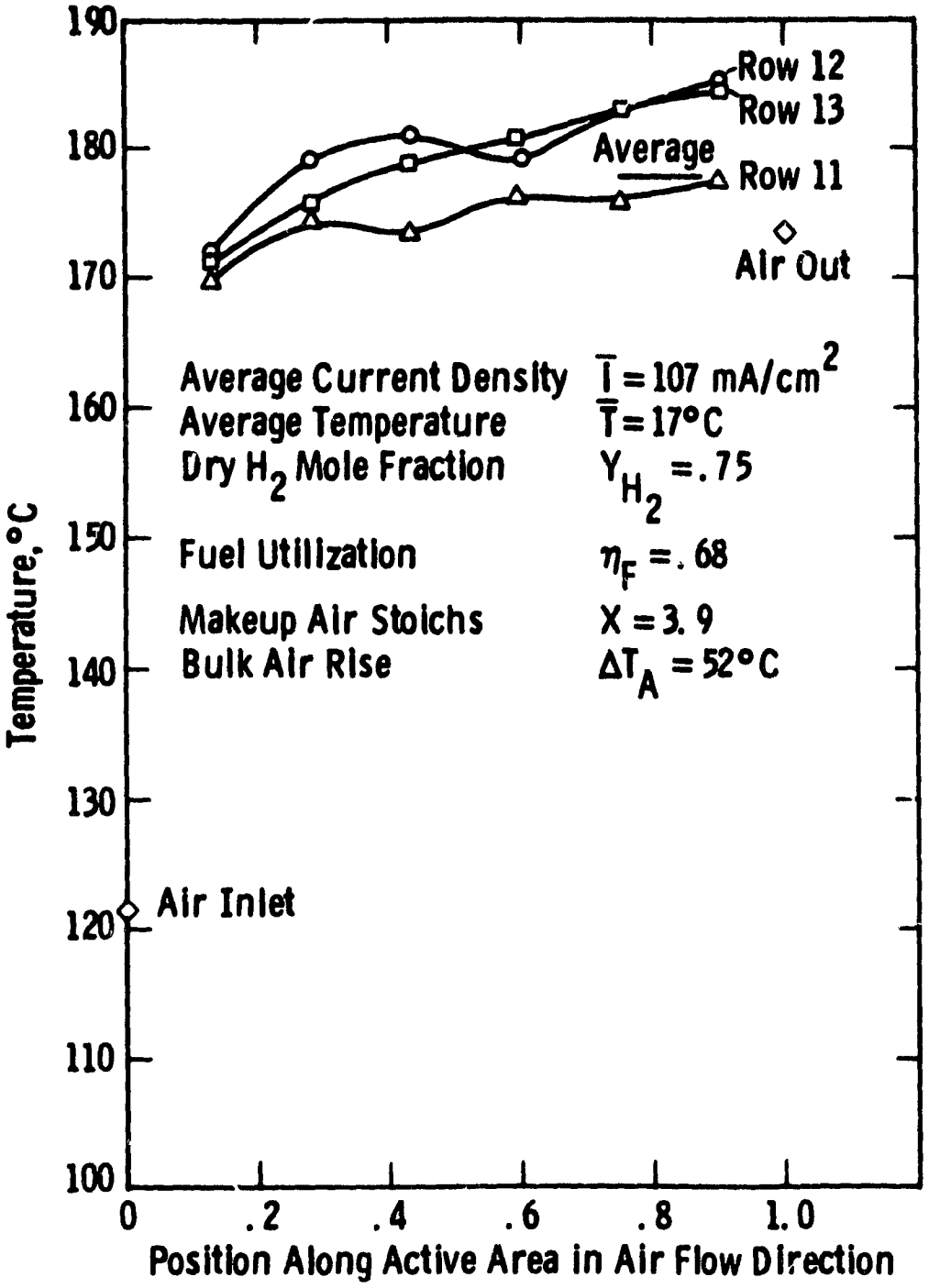

Fig. 22—Temperature distribution for stack 561 with all cooling channels open - Test 56

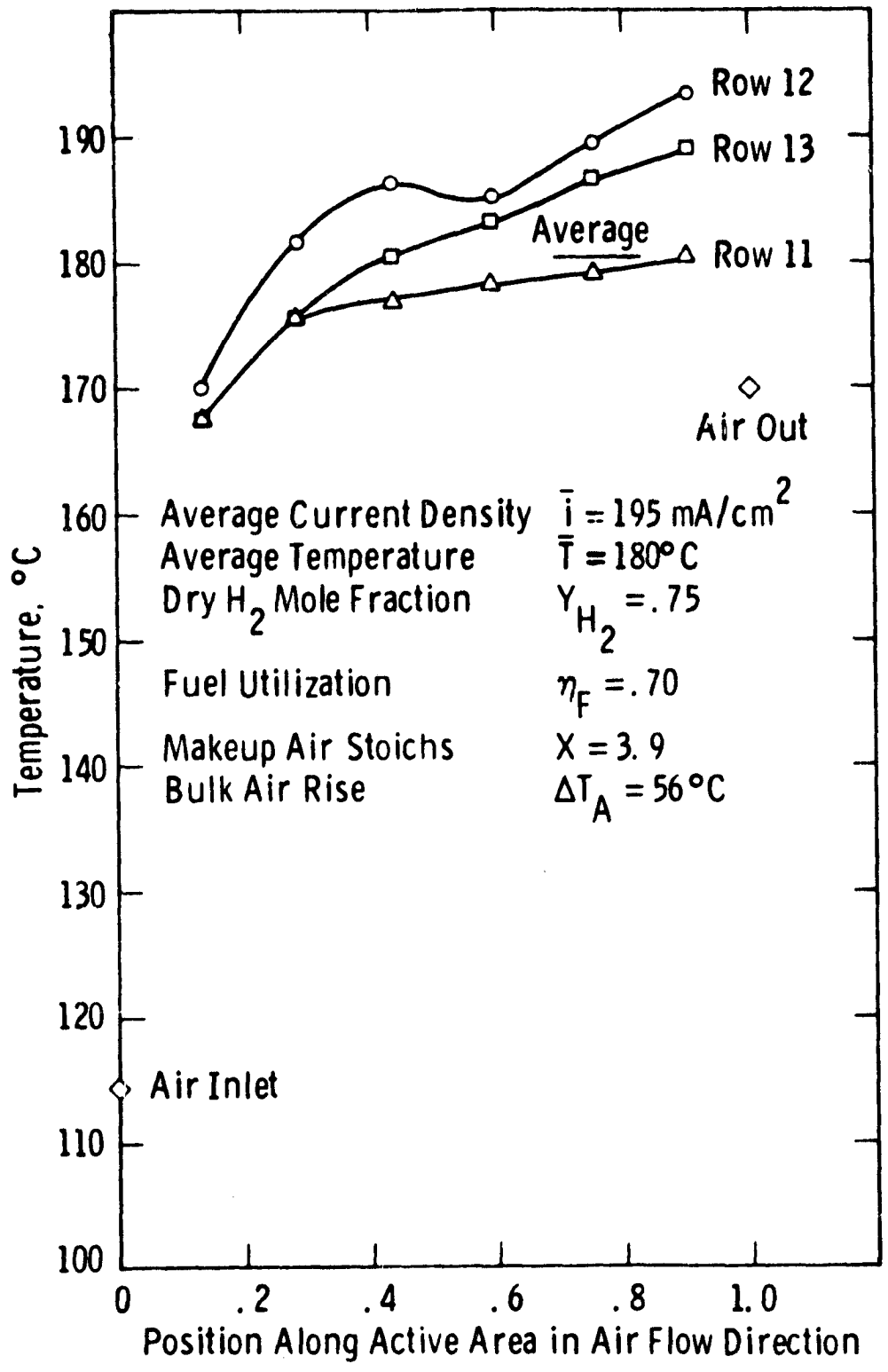

Fig. 23—Temperature distribution for stack 561 with all cooling channels open - Test 48

Figure 24 shows the effect of 4% CO on the temperature distribution when compared to Figure 23. For 4% CO, row 13 was 22.7°C below row 11 but the peak to average gradient was still only 16.3°C at a measured average air rise of 62.9°C. At 1.6% CO, row 13 was 5°C below row 11. It was concluded that a design with 28 cooling channels spaced to approximate the plugged configuration will give satisfactory temperature distribution over the range of current densities up to 200 mA/cm^2 for fuels with up to 4% CO. No tests were made with CO in the fuel with 30 cooling channels. However, due to the sensitivity of performance with CO to temperature level, it appears clear that the additional cooling at the hydrogen exit edge would result in low current densities there and a much greater spread in the temperature distribution.

Figure 25 is a comparison of the measured temperature distribution with those predicted by the detailed analytical model for the test conditions. Numbers on the left of the figure enclosed in parentheses are calculated temperatures in °C including air in and out. Numbers on the right are the temperatures measured in test 31. The theory predicts a slightly higher temperature at the air leading edge and underpredicts the maximum temperature by about 5°C. The average cell temperature is 180°C for both test and calculation. The test configuration has higher cooling channel density near the hydrogen inlet and lower density near the outlet than the idealized channel distribution used for the calculation. Considering the complex interaction among temperature levels, reaction rates, reactant depletions, current densities, heat generation rates and reactant distributions and that only temperatures can be measured directly; the agreement between calculated and measured temperatures is very good.

Figure 26 shows the calculated current density corresponding to the calculated temperature distribution in Figure 25. The current density is a maximum for any fuel stream at the inlet and decays with distance along the channel. Current density first increases along an air stream due to increased temperature and then decreases as the effect of O_2 depletion becomes significant. The measured temperature distribution

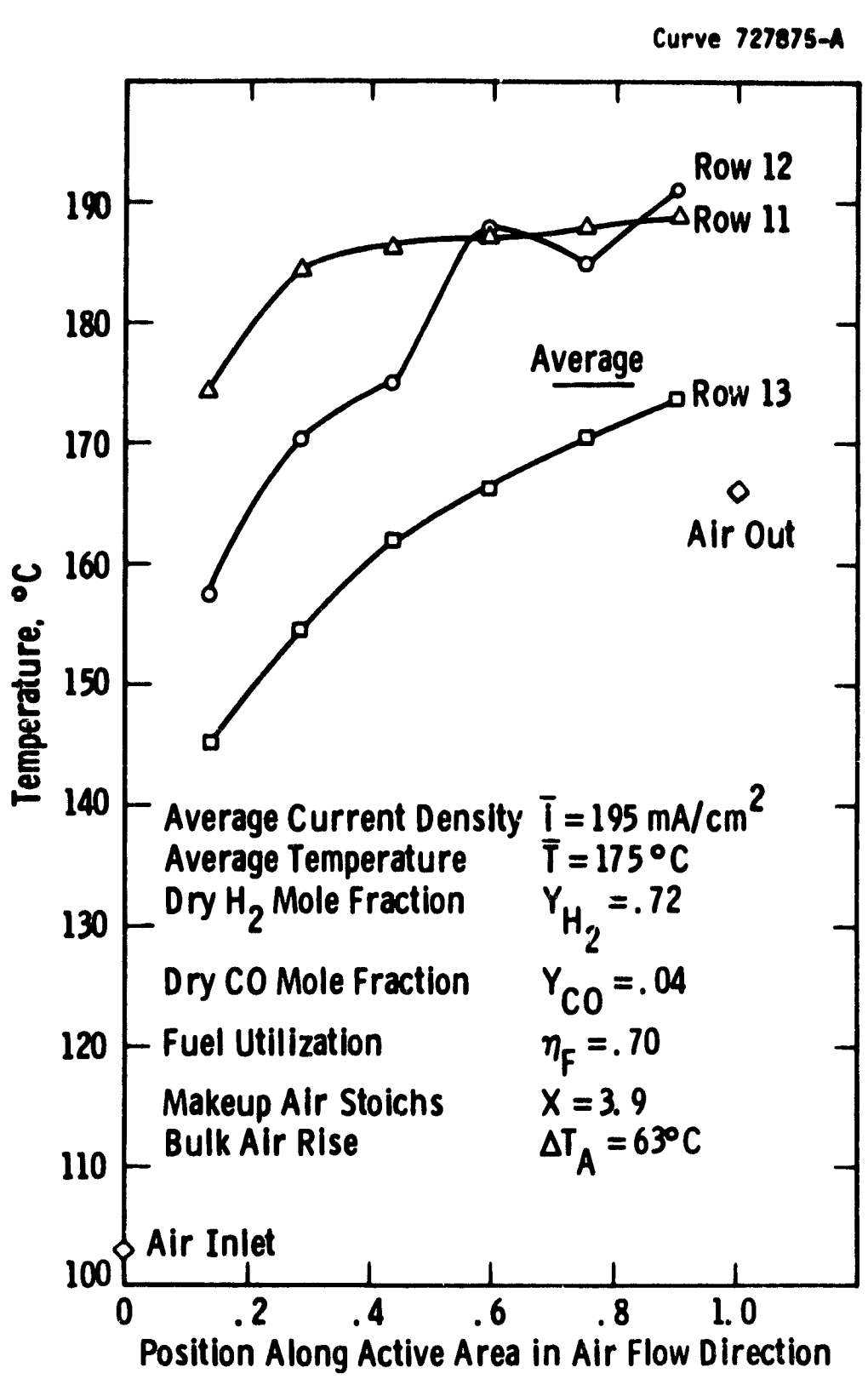

Fig. 24—Temperature distribution of stack 561 with modified cooling plate geometry and 4% CO in fuel-Test 52

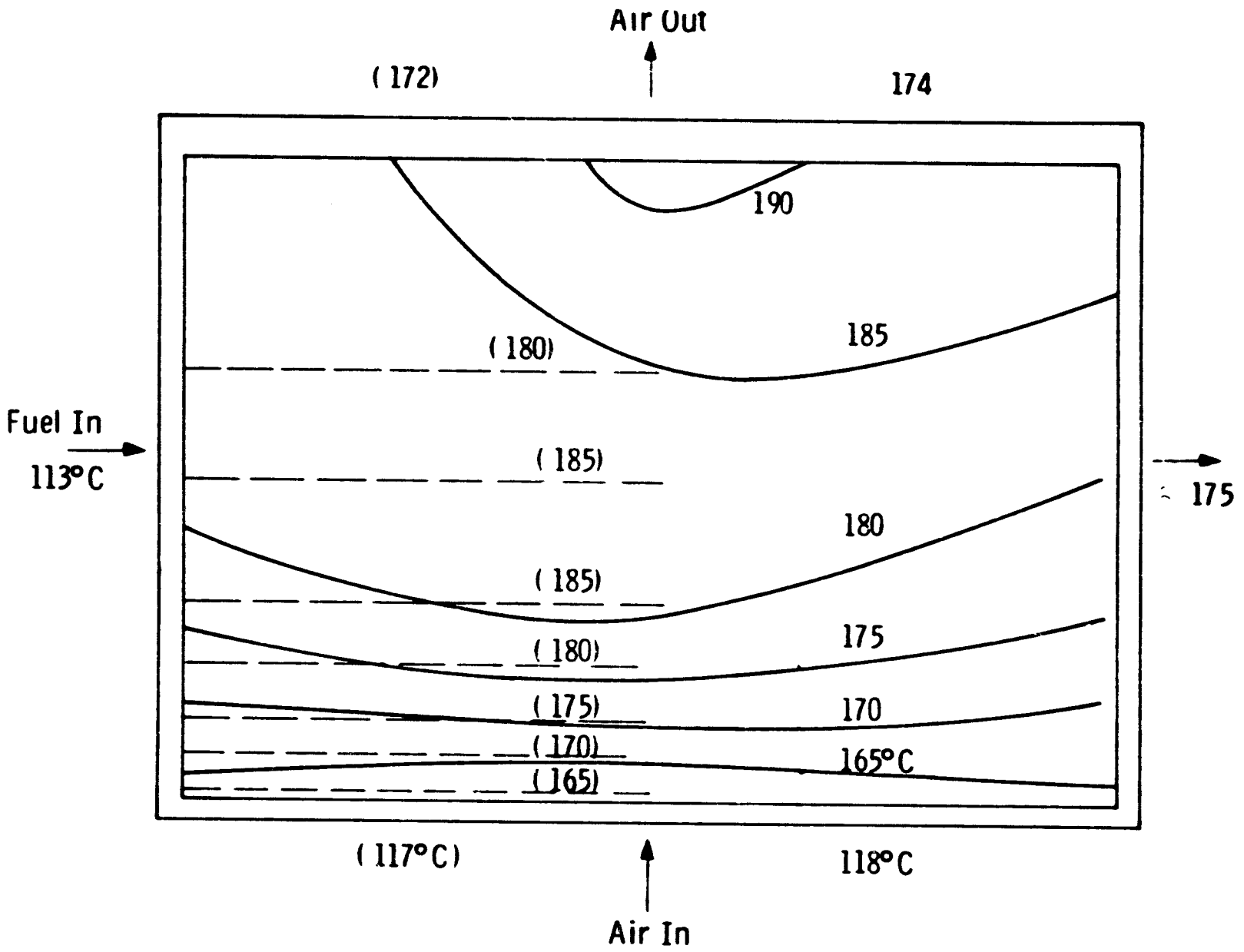

Fig. 25—Temperature distribution in stack 561-Test 31 compared to predicted values from analytical model in parenthesis

Curve 727861-A

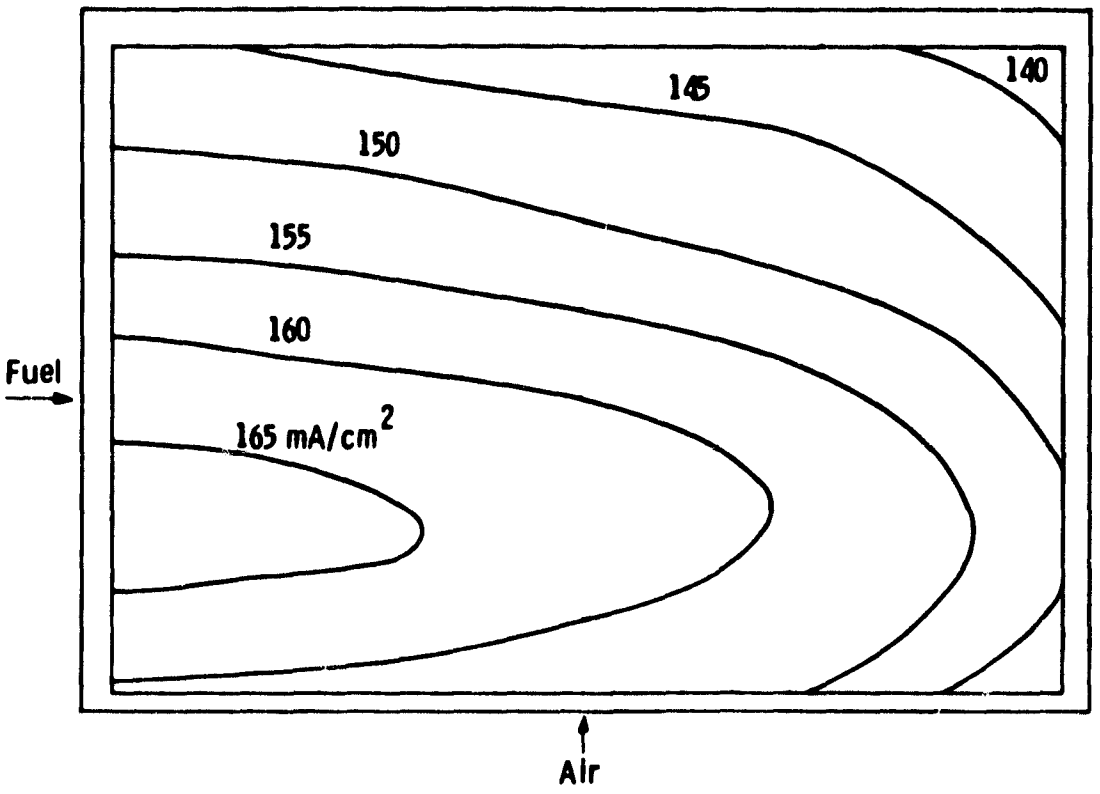

Fig. 26 – Current density calculated for stack 561 with conditions of Test 31

(Figure 25) indicates that current density varies more sharply in the fuel flow direction than predicted by the present analysis. It is believed that this is due to the fact that water vapor is transferred to the fuel stream. This is consistent with the high observed dewpoint of the anode exhaust stream. The analysis assumed that all water produced is removed by the process air stream. In the future, the analytical model will be extended to include the effect of vapor transfer to the fuel stream.

Effect of Makeup Air Flow

The makeup air flow rate (stoichs) is an important system parameter since it determines the oxygen and water mole fractions in the recirculated and exhaust streams. Low makeup and vent flows make it easier to recover water from and reduce heat lost in the vent stream but lower output voltage (or cell efficiency). Figure 27 shows polarization curves for 2, 3, 4 and 6 stoich makeup for similar temperatures and fuel utilizations. The measured change between 6 and 4 stoichs is about 10 mV compared to a calculated 6 mV. The measured change between 4 and 2 stoichs is about 40 mV compared to a calculated 25 mV. Thus stack 561 is about 1.6 times more sensitive to makeup flow than predicted by theory. This increased sensitivity would be predicted if the process flow is actually lower than the predicted flow split for the channel design. Pressure drop data presented in a later section suggests this possibility but the evidence is not conclusive.

The Effect of Temperature on Performance

Figure 28 presents the average cell voltage as a function of average stack temperature for 4 current densities. The flow rates for fuel and air were held constant for each current and the stack temperature was varied by changing the inlet air temperature. Fuel utilization, fuel composition and makeup stoichs were held constant for all current densities. The values of 4 stoich makeup and 70% fuel utilization were chosen to avoid the sensitivity observed at 2 stoich makeup or higher

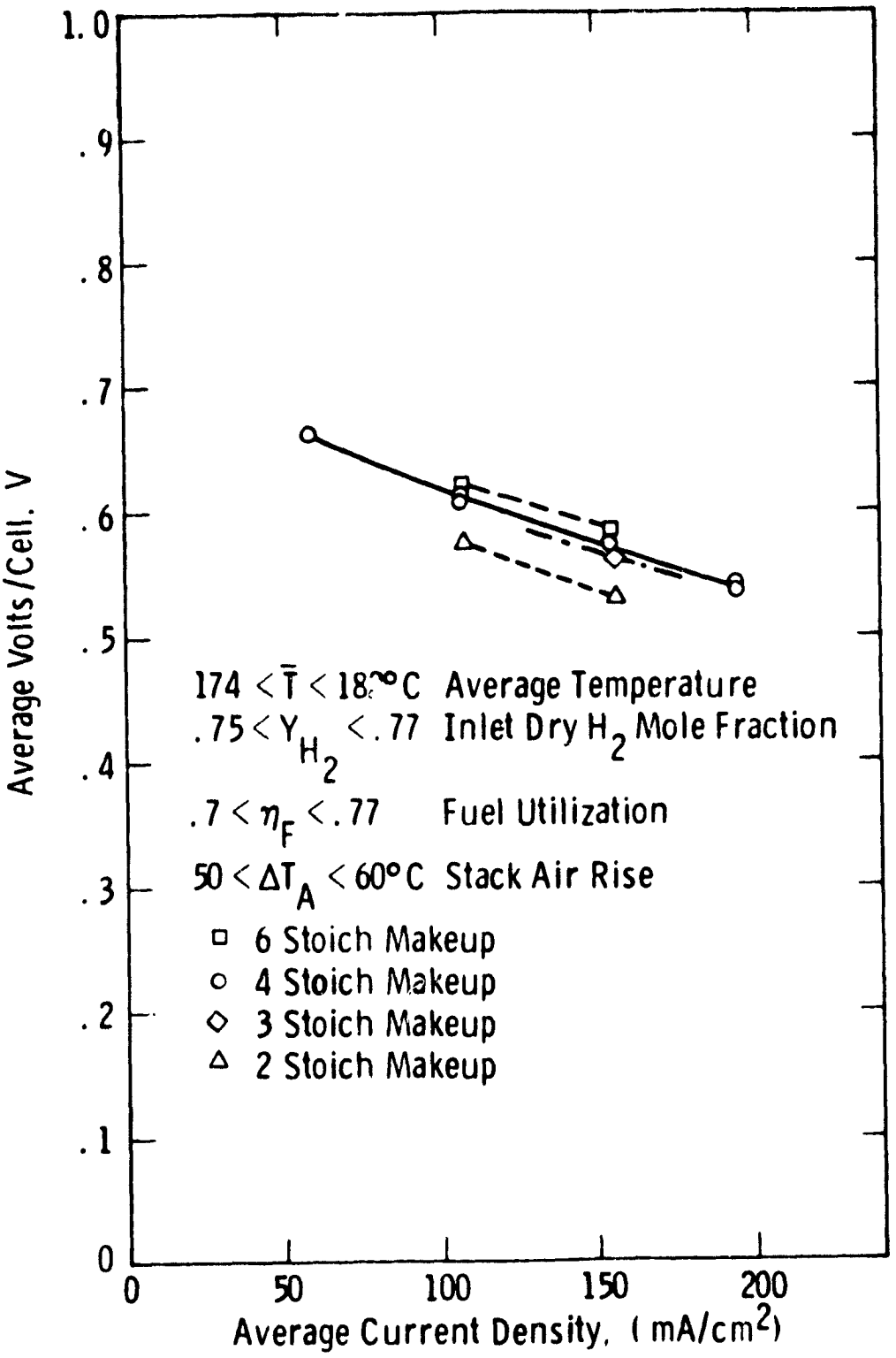

Fig. 27—Polarization data for stack 561 at various makeup air flow rates

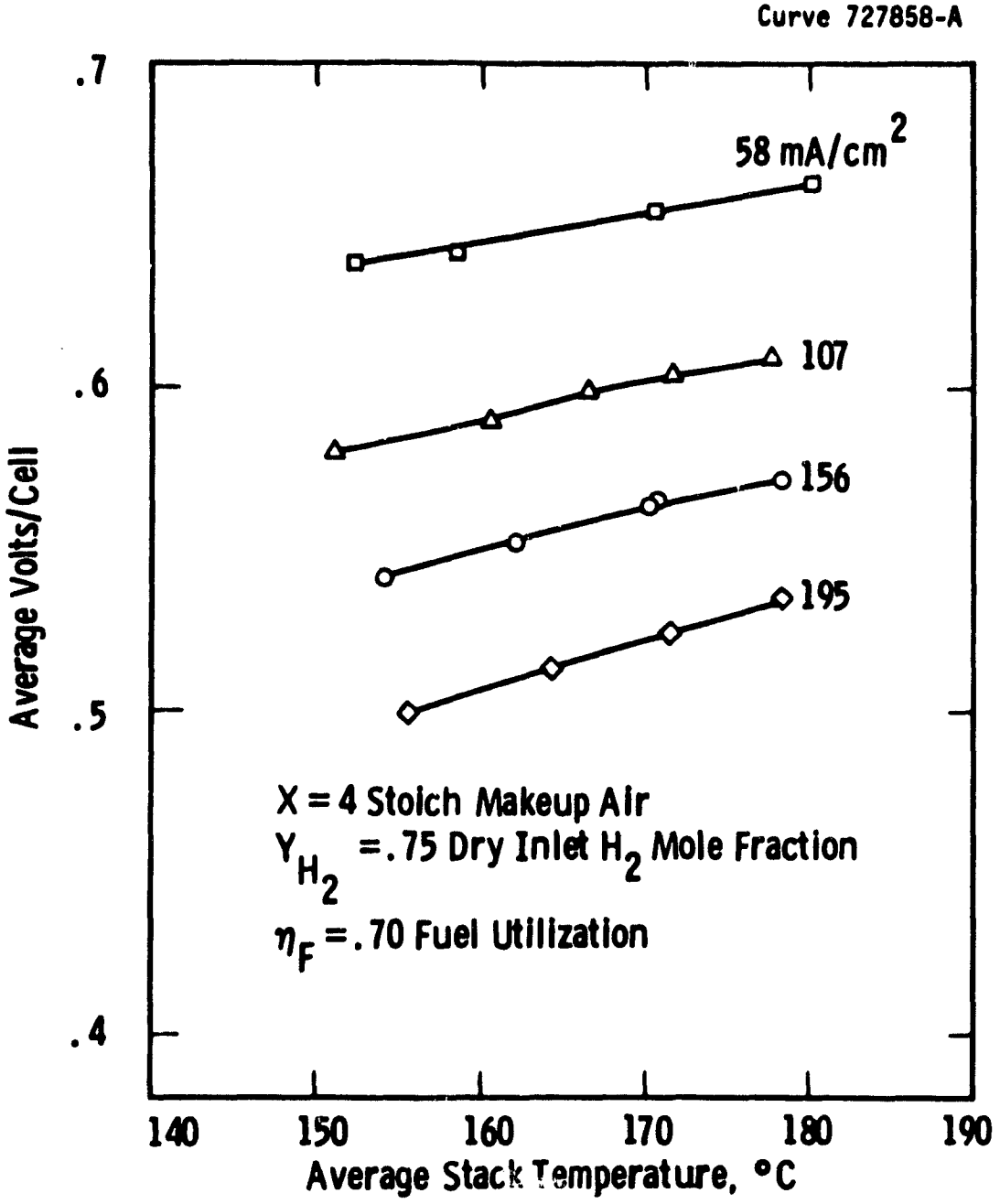

Fig. 28 – Performance of stack 561 as a function of temperature

utilizations. The temperature sensitivity under these conditions ranges from 0.94 mV/°C at 58 mA/cm^2 to 1.47 mV/°C at 195 mA/cm^2. Reference 1 states that this sensitivity is 1.15 mV/°C for phosphoric acid fuel cells. The sensitivity at 107 and 155 mA/cm^2 was within 0.05 mV/°C of this value.

The data in Figure 28 was used to plot the polarization curves in Figure 29 as a function of average stack temperature. Data points are omitted since values are interpolated from tests in Figure 28.

Effect of CO on Performance

The effect of CO in the fuel on cell voltage with 28 cooling channels per plate was obtained at two current densities. The tests at 107 mA/cm^2 with an average temperature of 179°C showed a voltage loss of approximately 1.74 mV/cell per percent CO for CO concentrations up to 5.5% of the dry fuel. The tests at 195 mA/cm^2 with an average temperature of 174°C showed a voltage loss of 12.6 mV/cell per percent CO for up to 4% CO. These results indicate higher sensitivity of the CO effect to current density and/or temperature than previous data. Reference 1 lists sensitivity to CO as 6.14 mV per percent CO at 177°C but with a higher anode catalyst loading (0.35 vs 0.3 mg/cm^2).

Pressure Drop

The data for the air side pressure drop across the fuel cell stack is plotted in Figure 30. Different symbols were used for the earlier and latter tests to determine whether any change had occurred due to blockage by acid or creep of matrix and electrodes into the process channels. There does not appear to be any significant difference between the data. The solid line and the circled points define the pressure drop predicted by the analytical model based on cooling channel pressure drop coefficients measured during Phase I and laminar flow theory for the process channels. The effective process channel dimensions were assumed to be 0.0724 cm x 0.1327 cm which would be equivalent to 0.030 in. x 0.055 in. (0.76 cm x 0.14 cm) before heat treatment. The process flow fraction (λ) predicted by the analysis is 0.132 at 155 mA/cm^2.

Curve 727860-A

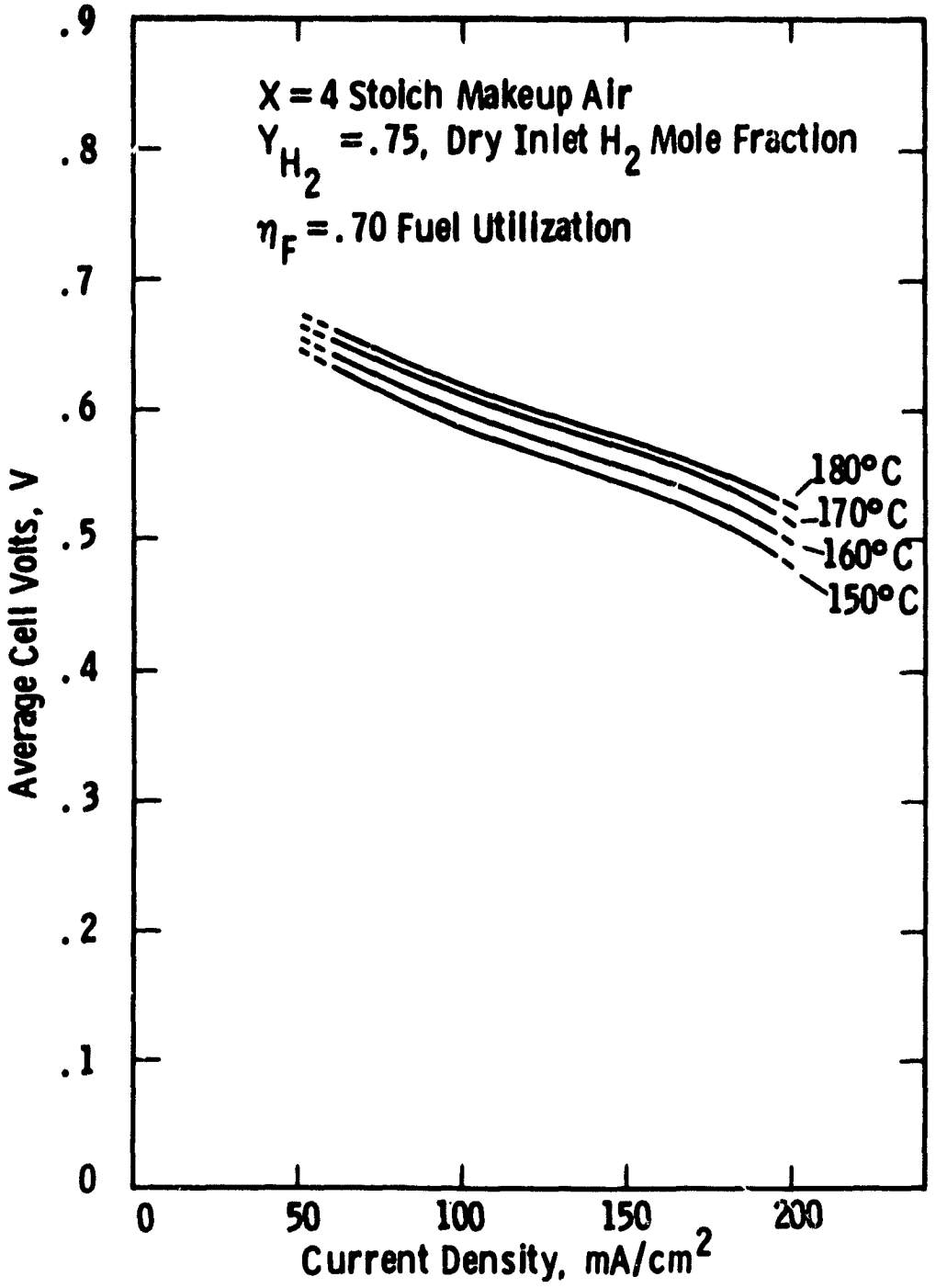

Fig. 29 — Polarization curves for stack 561 at various temperatures

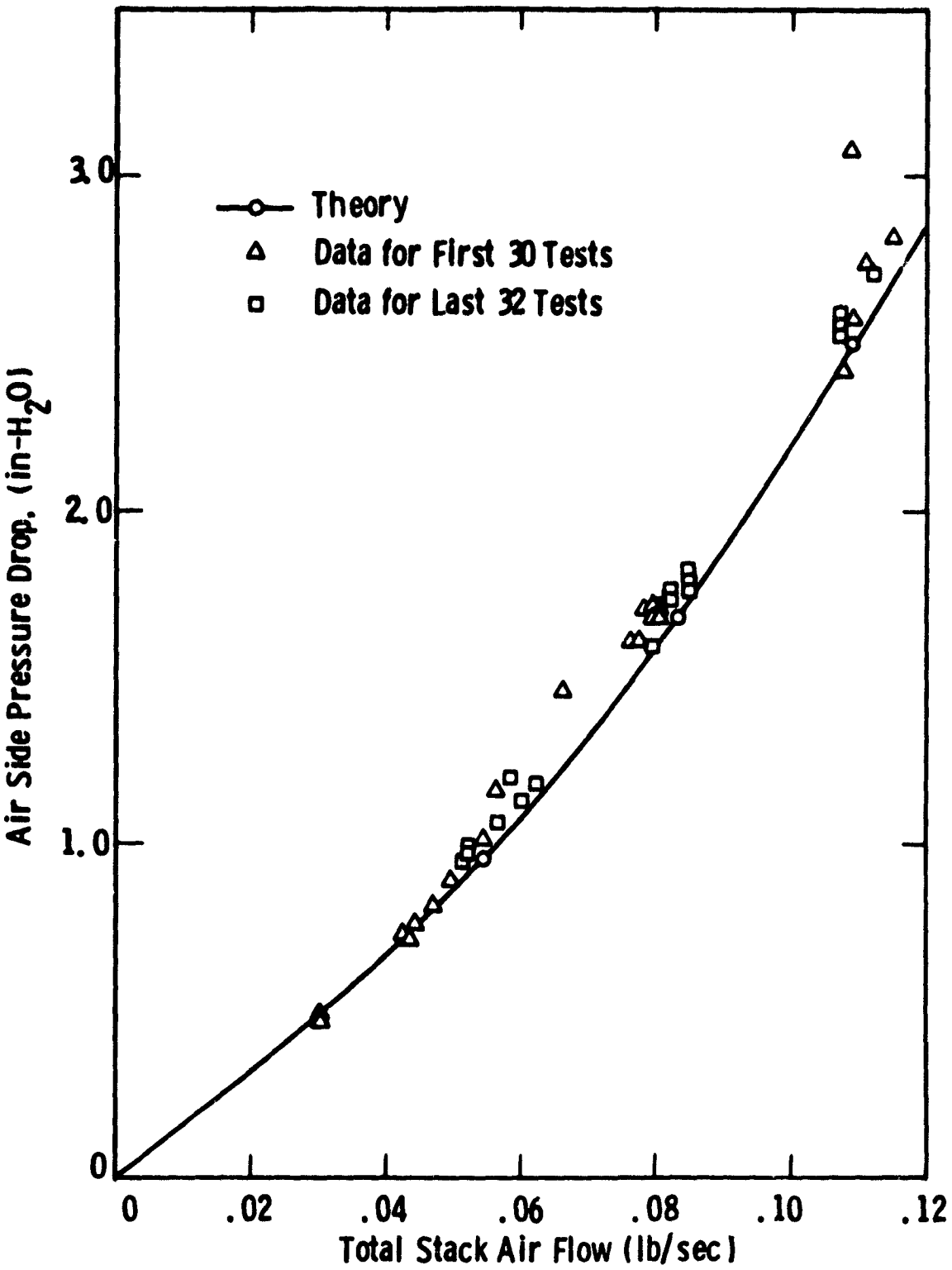

Fig. 30 — Pressure drop vs air flow rate for Stack #561

If the theory accurately predicts the cooling channel pressure drop, then the fact that measured pressure drop is higher than predicted indicates that process flow is less than predicted but the difference (5%) is too small to justify a definite conclusion.

Stack 562

Stack 562 is a 23-cell MK-2 stack (Z bipolar plate) with four cooling plates located after cells 4, 9, 14 and 19. The Z channel stack provides for separate cooling gas and process air flows. The stack includes heat treated bipolar and cooling plates and Mat-1 matrices. The active area after heat treatment is approximately 1030 cm^2. Each cooling plate has 31 equally spaced treed channels of the same design as stack 561. Cooling air enters and exits perpendicular to the 43.2 cm face of the stack. The 30.5 cm faces are manifolded in two equal sections with opposite faces each containing a process air and a fuel inlet/outlet manifold. In the 29 tests made to date, the process air and fuel inlets are near the cooling air inlet edge of the stack. Voltage instrumentation includes taps to measure voltage of each cell, drops across cooling plates and stack terminal voltage.

Thermocouple instrumentation is similar to that described for stack 561 except; 1) Rows 12 and 17 in cells 12 and 17, respectively, comprise five thermocouples 2) The first and last thermocouples in each row are located in the first and last process channel (air or fuel) at the edges of the active area in the cooling flow direction 3) The non-uniform spacing evident in the temperature distribution plots accommodate restrictions on insertion due to the Z channel configuration. The average temperature is calculated by averaging rows 11, 12 and 13. The row averages are obtained in this case by the trapezoidal rule to compensate for the non-uniform spacing.

Table XI presents a summary of test results and conditions for stack 562. Test 1, again is the pretest, and tests 2, 3 and 4 were made in the OS/IES loop without insulation for comparison with pretest results. Tests 5 to 10 were run to determine sensitivity to fuel utilization and

TABLE XI—SUMMARY OF TEST CONDITIONS AND TEST RESULTS FOR STACK 562

Test	Current Density mA/cm^2	Volts/Cell, V	Average Temperature, °C	Peak to Average Gradient, °C	Fuel Utilization	Dry H_2 Inlet Mole Fraction	Fuel Inlet Temperature, °C	Process Air, Stoichs	Process Air Inlet Temperature, °C	Cooling Air Flow g/sec	Cooling Air Inlet Temperature, °C	Cooling Air Temperature Rise, °C	Process Air Pressure Drop, in.H_2O	Cooling Air Pressure Drop, in.H_2O
1	144	.613	173	11.3	.77	.76	114	2.1	123	.055	122	38	3.70	1.73
2	146	.612	168	15.1	.60	.75	124	3.7	124	4.81	125	36	–	–
3	146	.614	171	13.1	.60	.75	125	3.7	155	3.4	124	39	–	–
4	146	.610	170	10.2	.60	.75	125	3.7	162	3.4	123	36	–	–
5	150	.585	170	18.4	.82	.75	126	2.0	160	3.7	109	52	–	2.25
6	150	.586	173	15.4	.82	.75	133	2.0	183	3.7	109	54	–	2.25
7	150	.586	173	15.4	.82	.75	133	2.0	187	3.7	109	54	–	2.25
8	150	.599	174	8.1	.72	.75	136	2.0	192	3.7	108	54	–	2.26
9	150	.601	173	9.7	.61	.75	139	2.0	175	3.86	108	54	3.35	2.29
10	150	.596	171	7.0	.71	.75	138	2.0	150	3.90	109	53	3.35	2.30
11	150	.607	172	8.4	.71	.75	135	3.0	150	3.90	114	50	4.74	2.30
12	150	.609	171	9.5	.71	.75	137	4.0	151	3.90	114	49	6.44	2.30
13	150	.601	175	7.1	.71	.75	135	2.2	148	3.90	114	51	3.20	2.30
14	150	.589	151	11.0	.70	.75	143	4.0	128	3.56	92	50	6.05	2.23
15	150	.598	156	11.5	.70	.75	141	4.0	128	3.81	98	49	6.10	2.24
16	150	.603	163	10.0	.70	.75	142	4.0	140	3.76	105	50	6.16	2.24
17	150	.610	177	9.4	.70	.75	147	4.0	154	3.76	118	49	6.26	2.26
18	100	.628	153	6.9	.71	.75	134	3.9	142	2.4	98	51	3.86	1.11
19	100	.632	158	7.1	.71	.75	134	3.9	148	2.4	105	50	3.89	1.12
20	100	.641	169	7.1	.71	.75	136	4.0	159	2.4	117	48	3.99	1.14
21	100	.648	179	7.6	.71	.75	137	3.9	166	2.4	128	47	4.10	1.17
22	200	.560	160	8.8	.71	.75	148	4.0	156	5.33	87	55	8.20	3.44
23	200	.568	166	10.1	.71	.75	151	3.9	156	5.29	96	54	8.20	3.44
24	200	.575	174	10.0	.71	.75	151	3.9	163	5.29	105	54	8.32	3.44
25	200	.547	151	11.3	.71	.75	149	3.9	139	5.61	78	56	7.97	3.59
26	50	.674	151	6.8	.71	.75	116	4.0	140	1.1	103	48	1.84	.40
27	50	.681	161	7.0	.71	.75	132	4.0	146	1.0	118	42	1.91	.39
28	50	.688	170	7.1	.71	.75	139	4.0	154	1.1	130	39	1.95	.40
29	50	.694	179	6.8	.71	.75	136	3.9	162	1.1	141	36	1.99	.41

the effect of process air inlet temperature on the temperature distribution. Tests 11 to 13 were made to determine the effect of process air stoichs on cell voltage. Tests 14 through 29 were conducted to obtain a performance map for current densities from 50 to 200 mA/cm^2 with average temperatures from 150 to 180°C with fuel utilization of 70% and process air flow of 4 stoichs for comparison with a similar map made for 561.

In all tests, except 1, the fuel was 75% H_2, 25% CO_2 humidified at room temperature.

Discussion of Results

Temperature Distribution in Stack 562

Tests 5, 6 and 7 were run with 150 mA/cm^2 at 82 percent fuel utilization and 2 stoich process air. The fuel exit edge of the stack (row 13) remained considerably lower in temperature than the center (row 12) or the fuel inlet edge (row 11) even when the process air temperature was increased to 14°C above the average stack temperature in test 7 as shown in Figure 31. Since it was suspected that fuel utilization was above the sensitivity point, the fuel flow was increased to reduce fuel utilization to 0.72 in test 8. The improved temperature distribution of test 8 is shown in Figure 32. The peak to average differential reduced from 15.4°C in test 7 to 8.1°C in test 8. Also the terminal voltage increased by 13 mV per cell. Test 9 had slightly reduced process air inlet temperature and fuel utilization of 0.61. The terminal voltage increased an additional 2 mV/cell. Test 10 was similar to test 8 with fuel utilization of 0.71 and process air inlet temperature reduced to 150°C. The results show excellent balance between rows 11, 12 and 13 and a peak to average temperature differential of only 7°C at a 53°C measured cooling air rise (Figure 33). Performance in test 10 was 3 mV below test 8 but this is largely due to the fact that the average temperature was 3°C lower than test 8 as discussed below. Figures 34 and 35 show the temperature distributions for 150 and 200 mA/cm^2 at 70 percent fuel utilization with 4 stoich process air. The higher process air flow in these tests results in a slightly larger peak to average temperature differential (10°C) and an apparent increase in

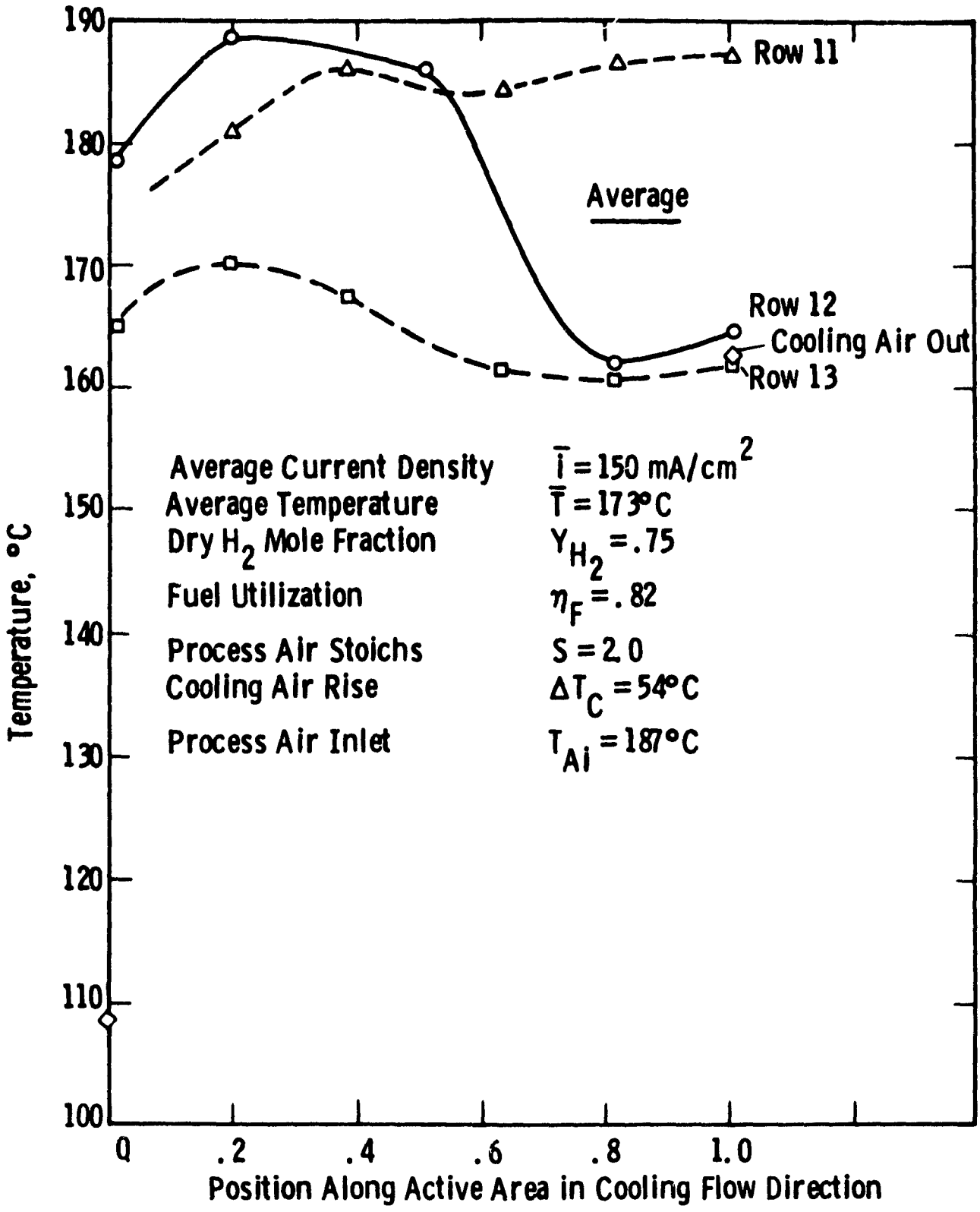

Fig. 31 – Temperature distribution in stack 562-Test 7

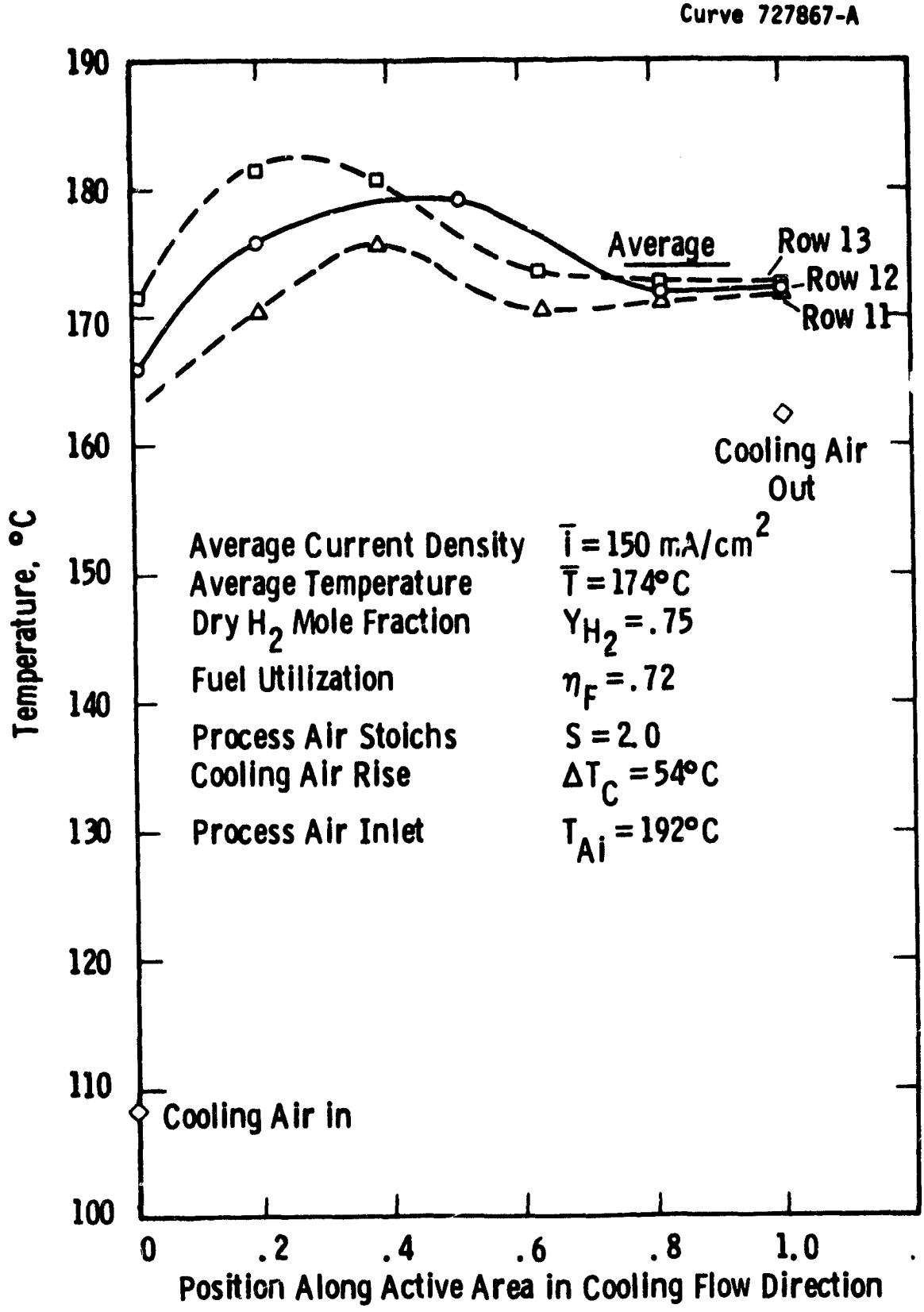

Fig. 32 – Temperature distribution in stack 562 - Test 8

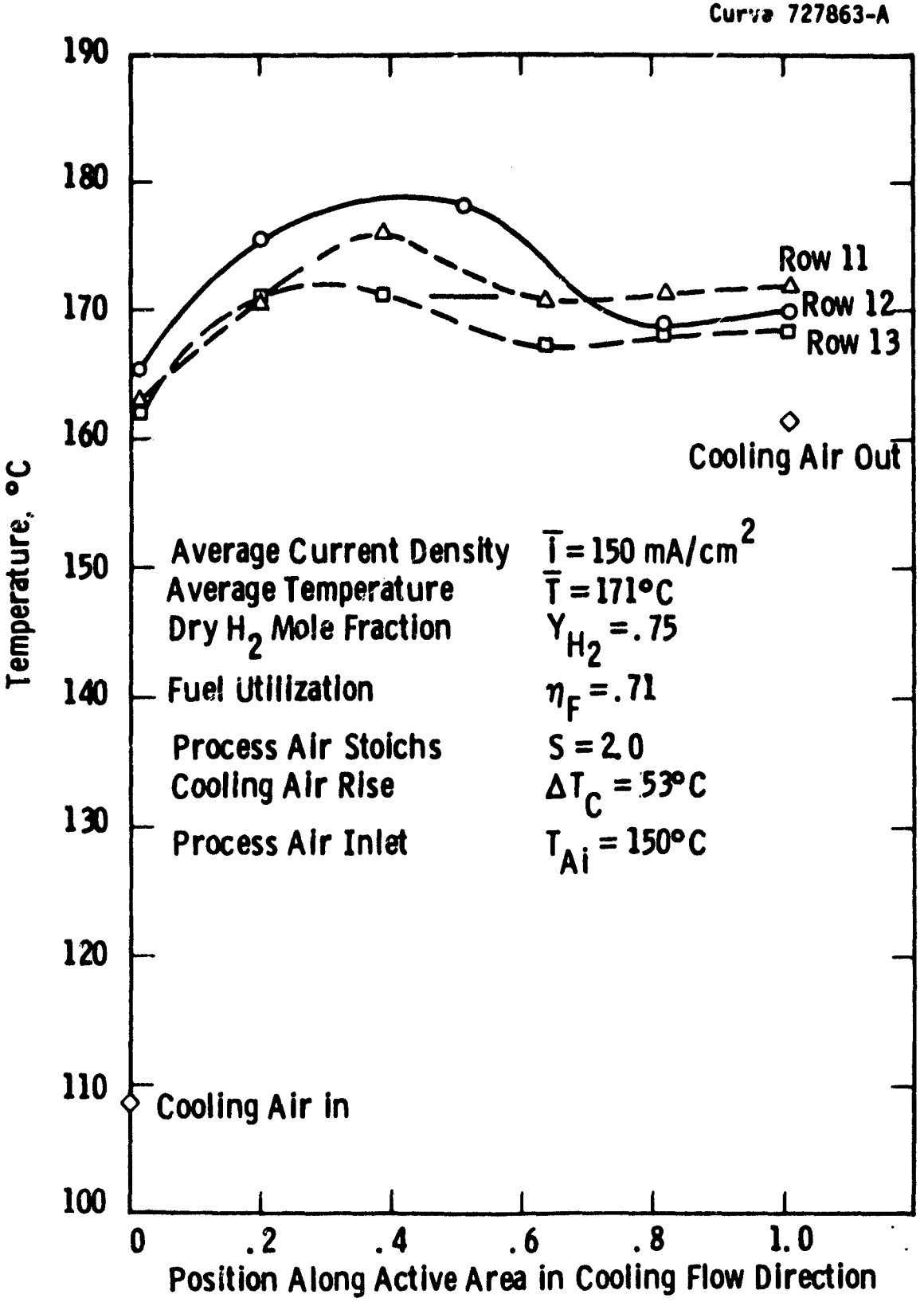

Fig. 33 – Temperature distribution in stack 562 - Test 10

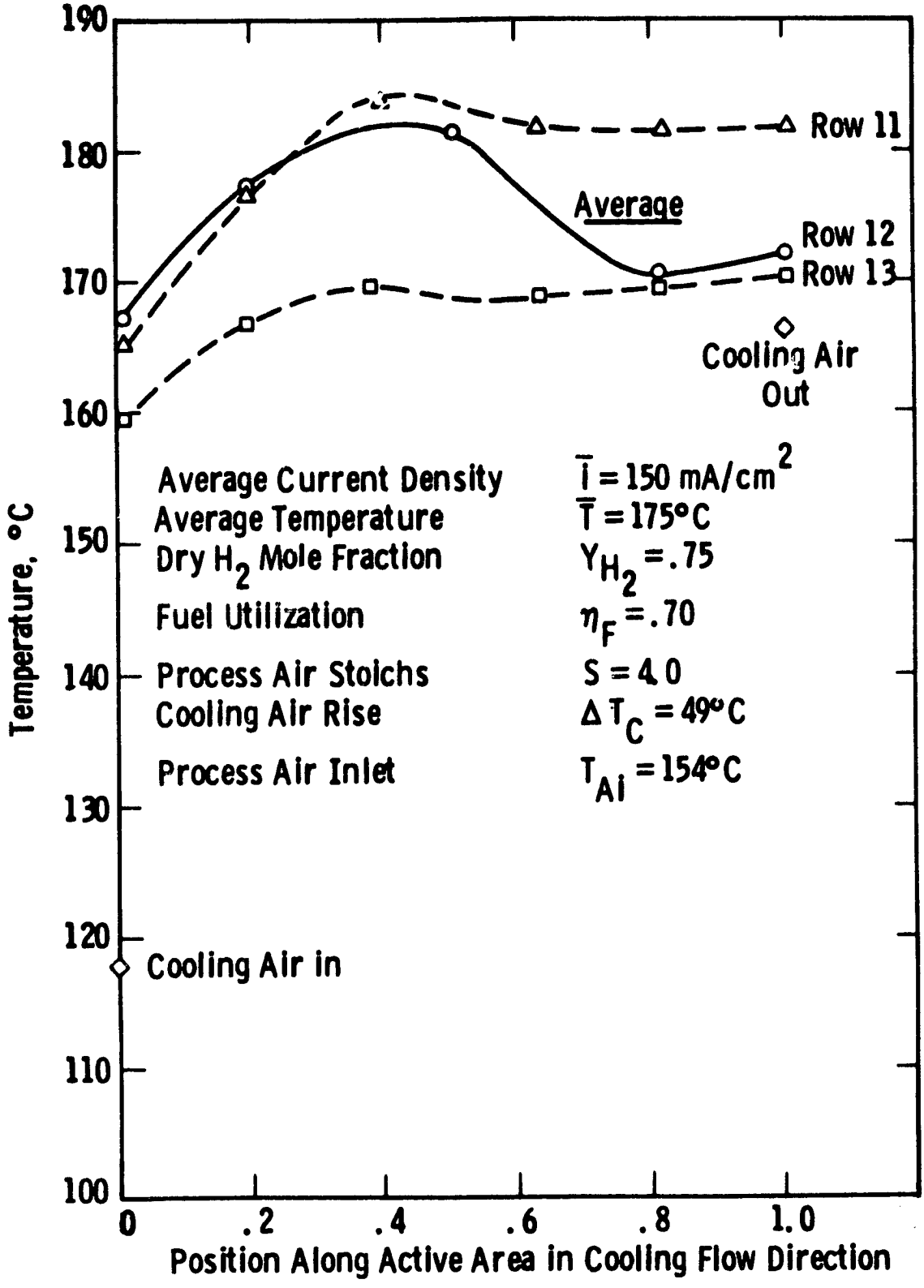

Fig. 34 – Temperature distribution in stack 562 - Test 17

Curve 727868-A

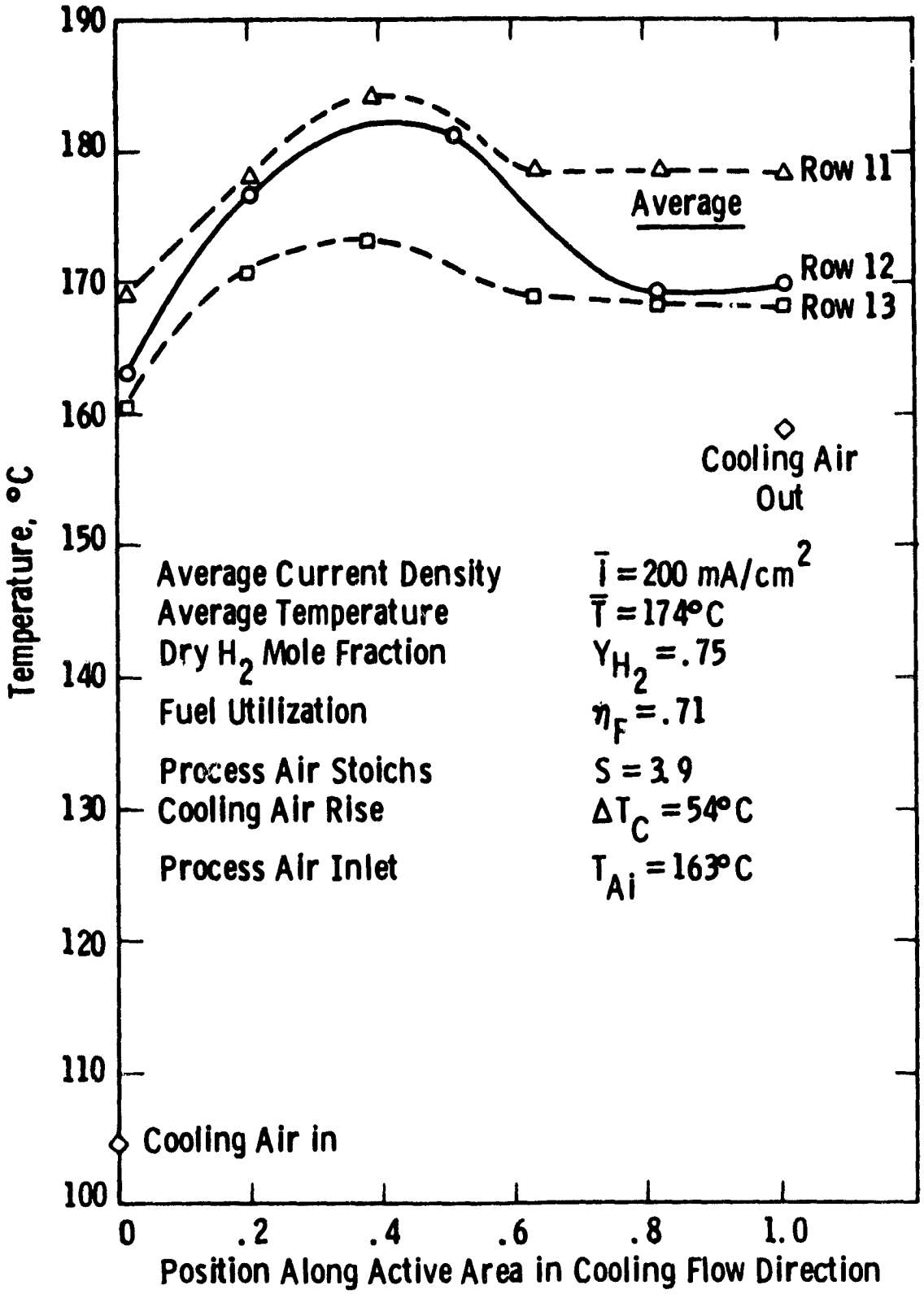

Fig. 35 — Temperature distribution in stack 562 - Test 24

current density near the hydrogen inlet edge of the stack as compared to 2 stoich air flow.

The temperature distributions obtained so far have shown that little improvement could be expected by redistributing cooling channels for 2 stoich process air. A redistribution could improve uniformity at higher process air flows and/or at higher fuel utilizations.

The Effect of Temperature on Performance

Figure 36 presents the average cell voltage for stack 562 as a function of average temperature for 4 current densities. The tests were run at nominal 4 stoich process air and 70 percent fuel utilization. Cooling air temperature rise varied between 48 and 56°C except in the final tests at 50 mA/cm^2. The temperature sensitivity ranges from 0.67 mV/°C at 50 mA/cm^2 to 1.09 mV/°C at 200 mA/cm^2. The data in Figure 36 was used to plot the polarization curves in Figure 37 as a function of average stack temperature.

Comparison of Stacks 561 and 562

The polarization curves of Figures 29 and 37 are plotted in Figure 38 for direct comparison for an average temperature of 180°C. The difference in average cell voltage ranges from 19 mV at 50 mA/cm^2 to 52 mV at 200 mA/cm^2. The theoretical O_2 gain of stack 562 over 561 due to separation of cooling and process air at 4 stoich process and 4 stoich makeup is 12 mV per cell. The additional gain observed must then be due to reduced polarization (e.g., resistance or higher catalyst utilization) or an H_2 gain associated with the observed reduction in water vapor in the anode exhaust of 562 or a statistical variation in cell performance between the two stacks.

The data analysis technique developed in Phase I was applied to the data of Figures 29 and 37 to obtain catalyst utilization and specific cell resistance for the two stacks assuming no H_2 gain. The results are compared in Figure 39. The catalyst utilizations determined this way are virtually identical for the two stacks. The specific

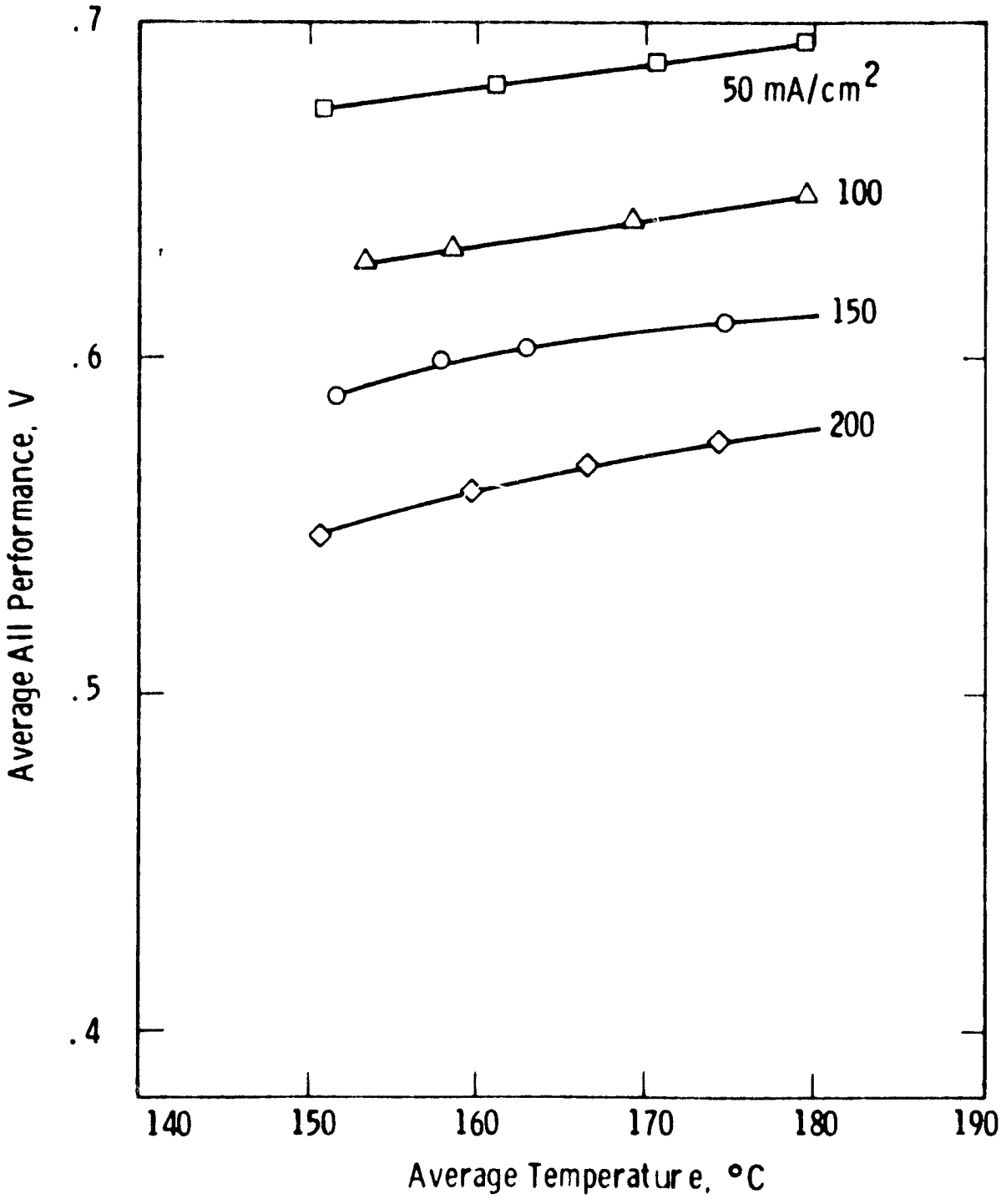

Fig. 36 – Performance of stack 562 as a function of temperature

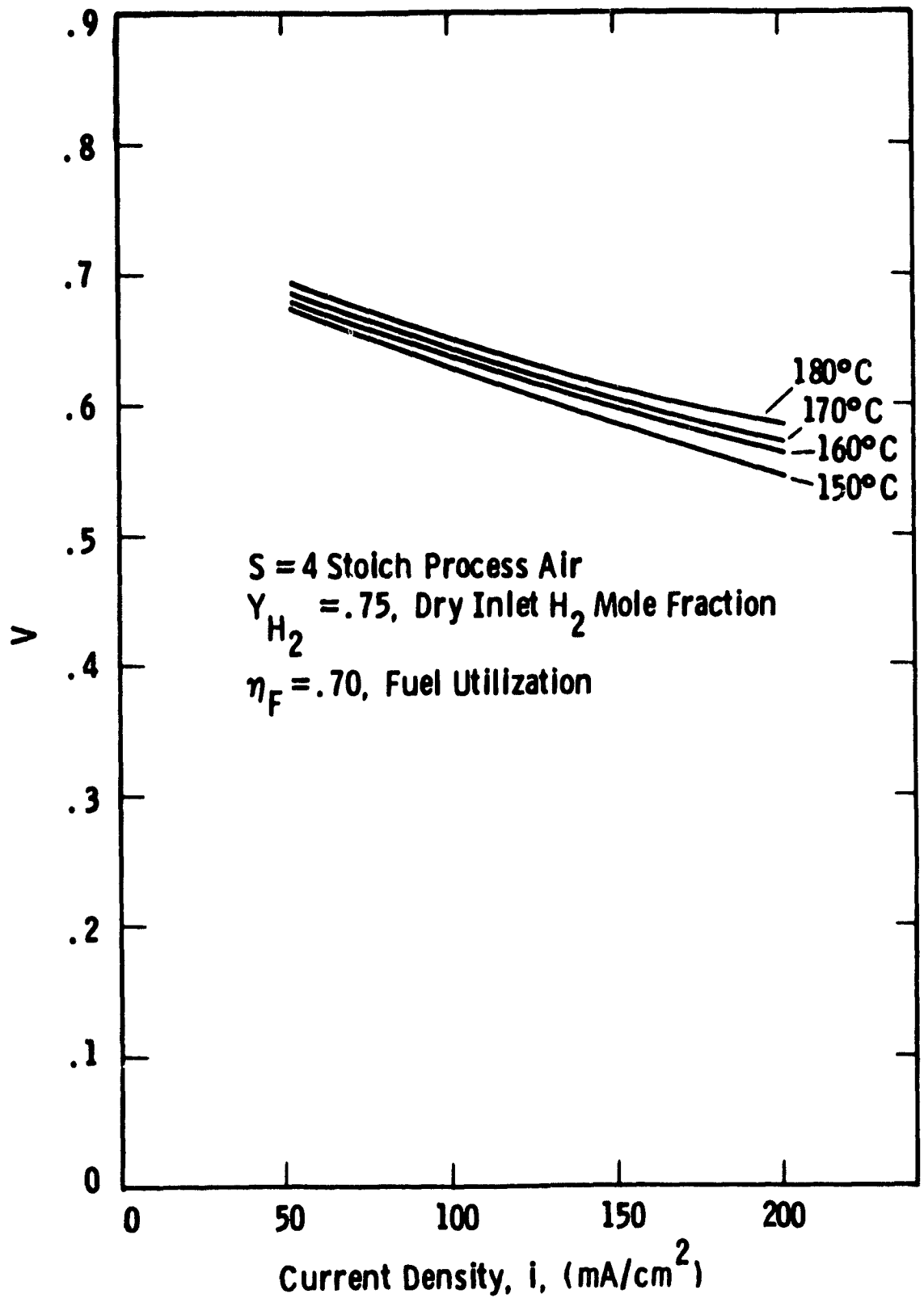

Fig. 37 – Polarization curves for stack 562 at various temperatures

Curve 727864-A

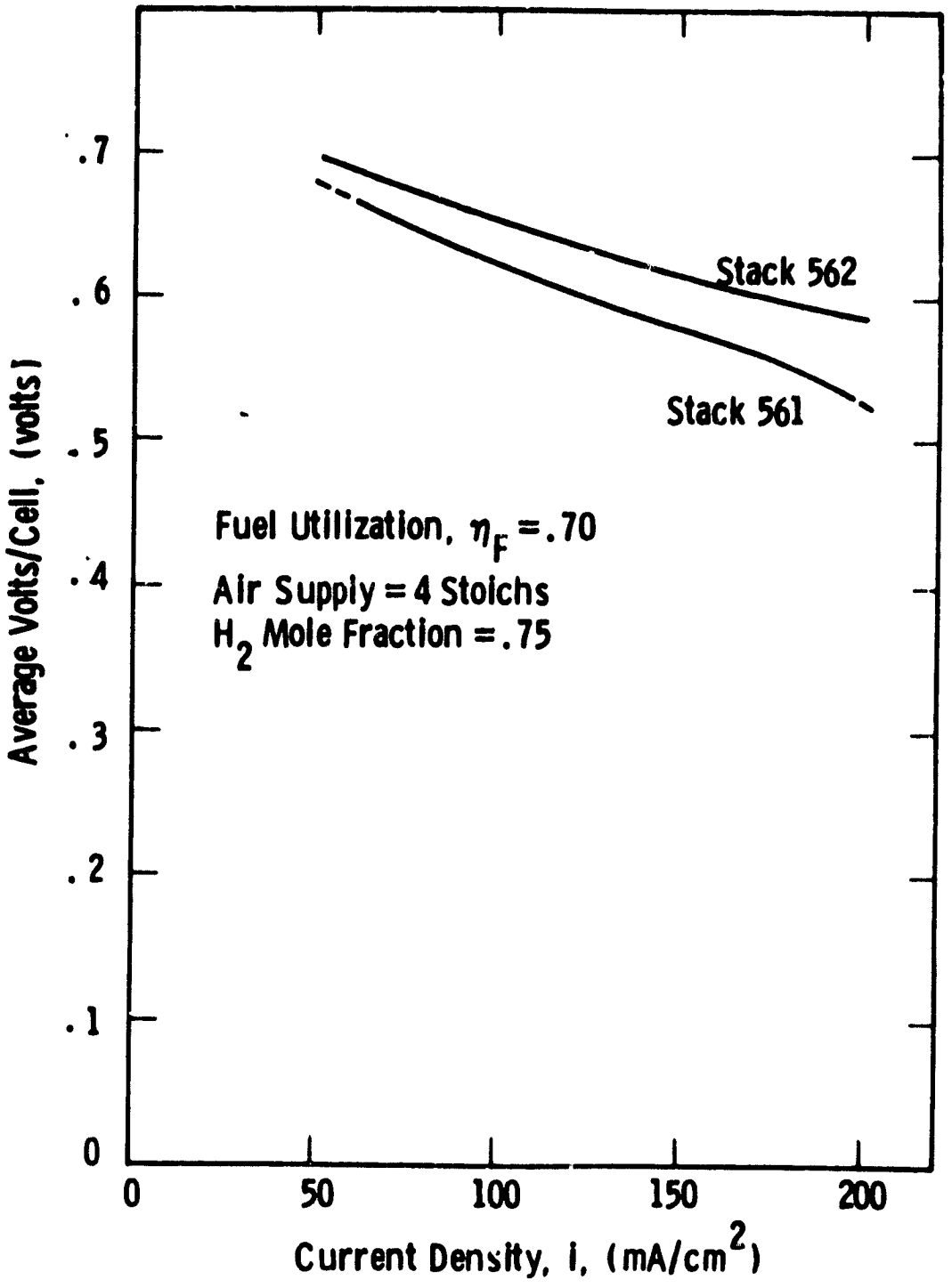

Fig. 38 — Polarization curves for stacks 561 and 562 at average temperature of 180°C

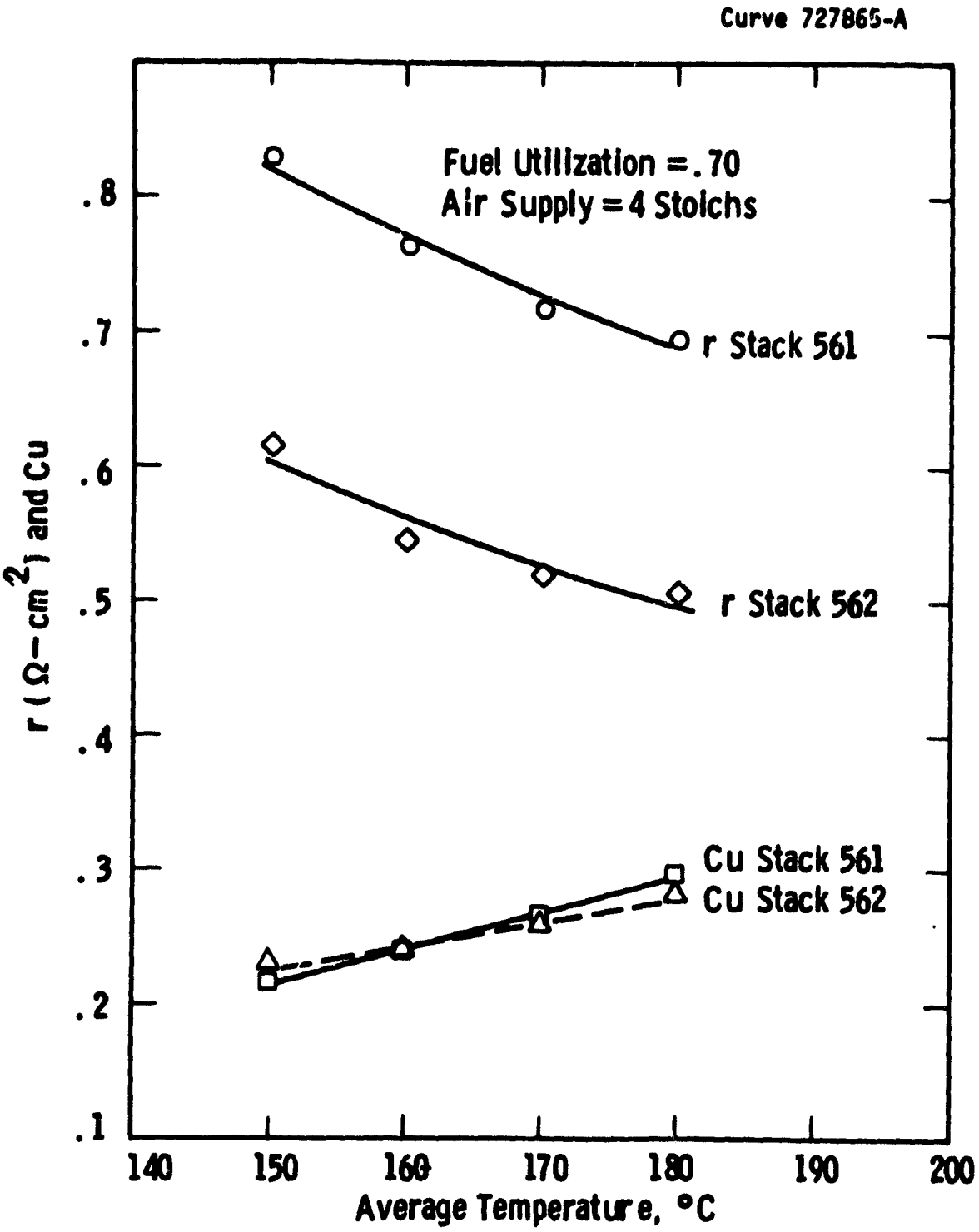

Fig. 39 — Specific cell resistance and catalyst utilization for stacks 561 and 562 vs temperature

resistance, however, is about 33 percent lower for stack 562 than for stack 561. This difference in resistance accounts for 38 mV at 200 mA/cm^2. Data on previous stacks indicated significant effect on resistance due to O_2 partial pressure or mole fraction but 38 mV appears too large to be due to a 4.6 percent difference in mean O_2 concentration (17.7 for 562 vs 13.1 for 561).

The cell to cell data for 561 showed five to seven cells significantly below the average cell voltage, while 562 showed only one cell having significantly lower than average performance. Comparison of the average of the best 18 cells in each stack shows a difference of about 25 mV per cell between 562 and 561 at 200 mA/cm^2. Thus, statistical variations in cell performance between the two stacks may account for a significant part of the performance difference but this may, in turn, be due to some unaccounted for effect of the design such as reduced moisture in the fuel stream reducing H_2 sensitivity of cells.

The temperature uniformity of stacks 561 and 562 were essentially the same when compared on the basis of peak to average temperature differential. Both stacks showed better uniformity at 2 stoichs than at 4. The profiles along the cooling direction are similar except 562 had peak temperatures nearer the cooling inlet. This was expected since the cooling effect of the process air is less in the MK-2 configuration and occurs in a different area. Data thus far indicates that the MK-2 design shows a performance gain greater than the theoretical O_2 gain of 28 mV/cell when both are operated with 2 stoichs of process/makeup air.

The power outputs of stacks 561 and 562 for similar operating conditions are plotted against stack terminal voltage and stack current in Figures 40 and 41. These are the formats which would be of most use to designers who must interface other equipment with the fuel cell or for systems analyst attempting to make tradeoff studies.

The curves in Figure 40 compare the stack power outputs for the same efficiency (voltage). They indicate a significantly greater output for stack 562 than for 561 for any terminal voltage. The percentage

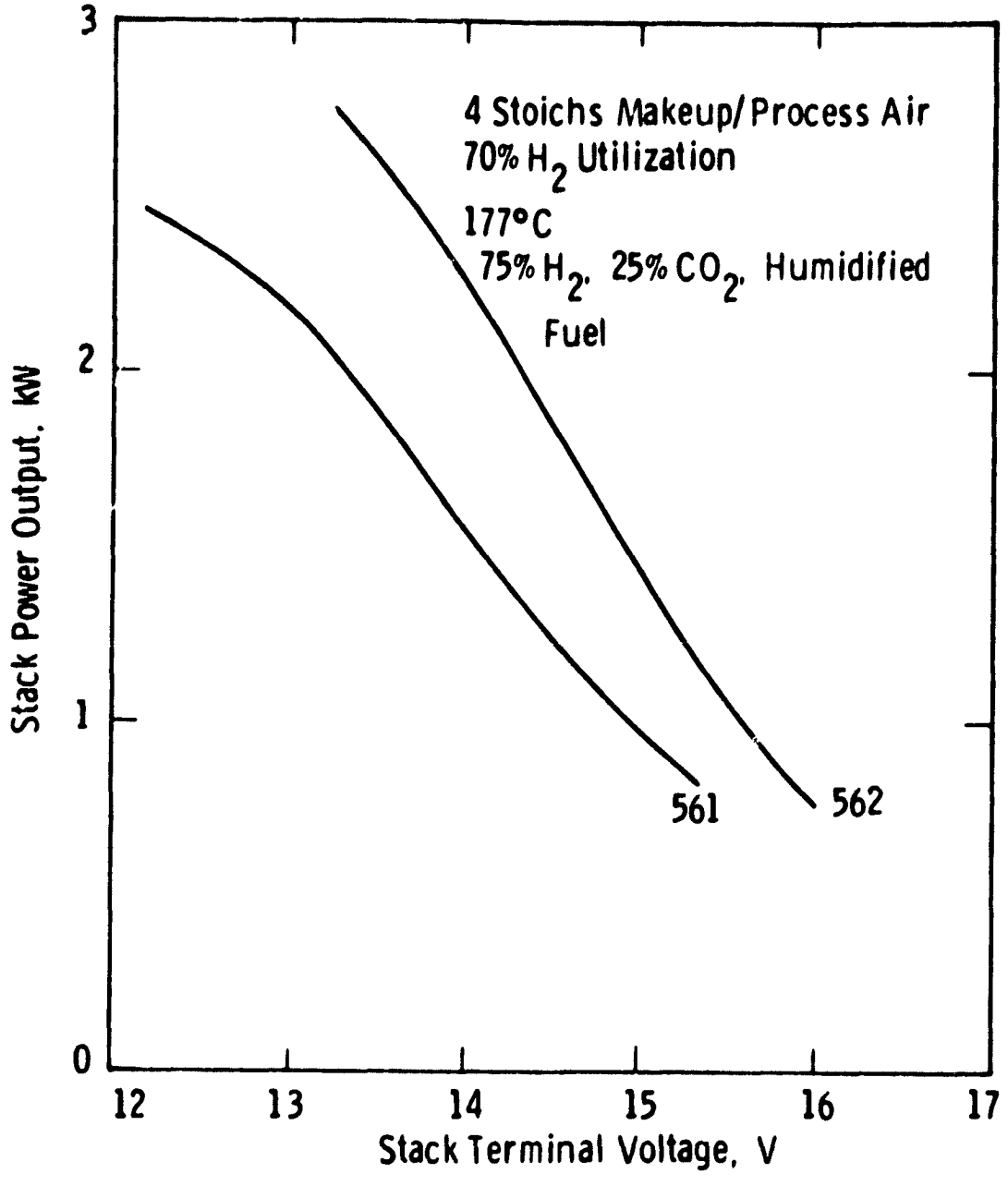

Fig. 40 – Comparison of power outputs vs terminal voltage for stacks 561 and 562

difference is highest at high efficiency (∿51% at 15.5V) but is significant at the lower values (∿38% at 13.5) corresponding to high power. This advantage would be more pronounced with lower makeup air flows than the four stoich conditions at which the data was taken. At the same power outputs, stack 562 has a higher efficiency than 561. For example, at the nominal rated power of 2 kW the 562's terminal voltage is 7.5% greater than 561's (14.3 vs 13.3V) corresponding to a 7.5% greater efficiency.

Since, unlike voltage, there is no direct relationship between current and efficiency, the greatest significance of Figure 41 may be the fact that the power output of these stacks is apparently well below their maximum value when operating at 200 mA/cm^2 at atmospheric pressure. Although no one can deny the importance of operating at high efficiency, the potential for reducing capital costs by operating at maximum power output should be carefully considered in cost/performance tradeoff studies.

Stack Resistance

The electrical resistances of the stacks 560, 561 and 562 were measured during the compression phase of the assembly operation. Figure 42 is a summary of the resistance vs stack compression with parameters of stack temperature shown on the curves. Since the deformations of cell components are apparently time and temperature dependent and the time required for the acid to fill the component pores is highly temperature dependent, the time-temperature history is important in interpreting the data.

The compressions were applied as follows:

Stack 561 - The compression was increased from 0 to 170 kPa at dry room temperature (∿40°C) and allowed to set overnight. The stack was then heated to 90°C and the compression was increased to 380 kPa in 2 hrs.

Curve 727869-A

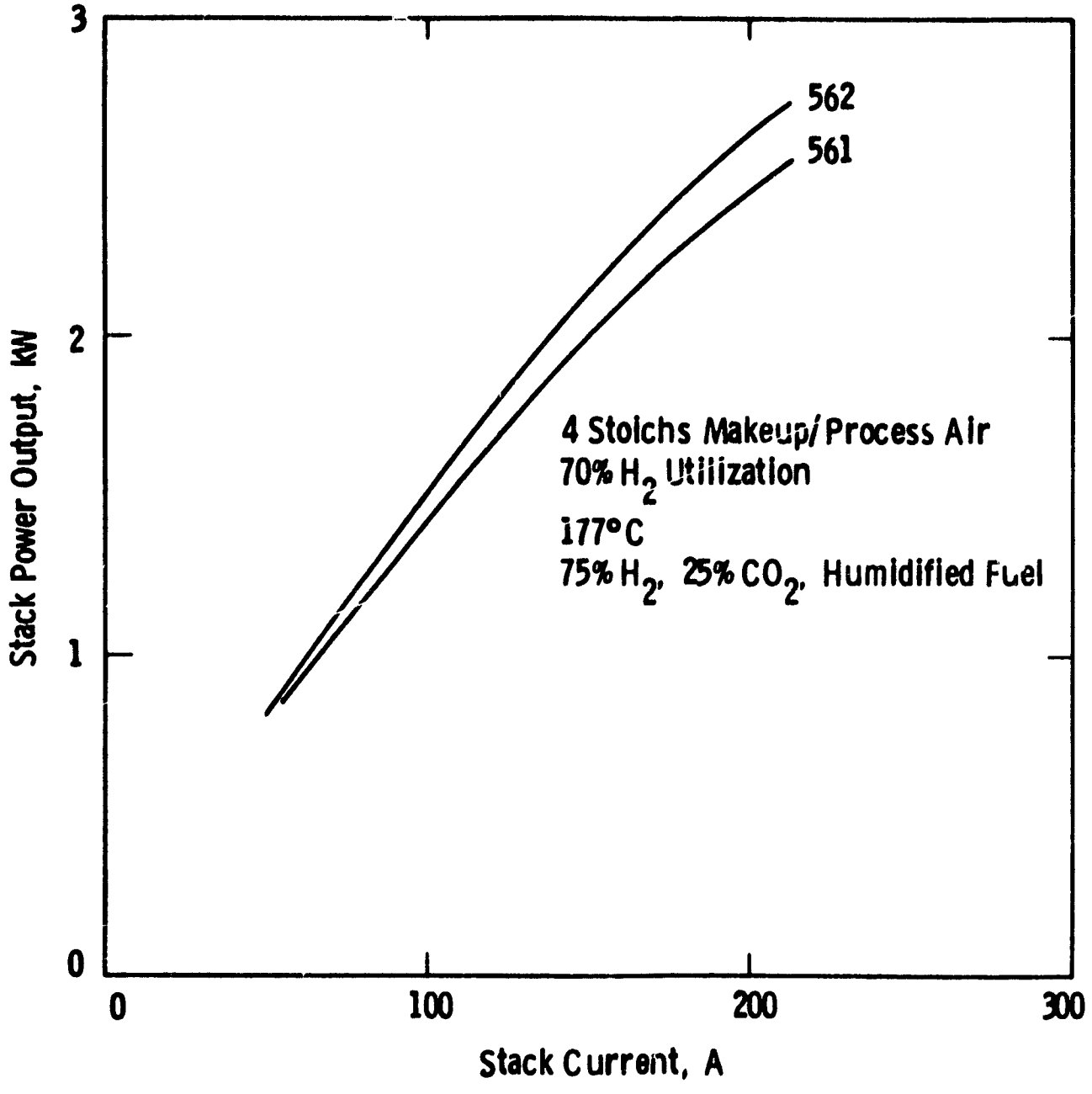

Fig. 41 — Comparison of power output vs current for stacks 561 and 562

Curve 727872-A

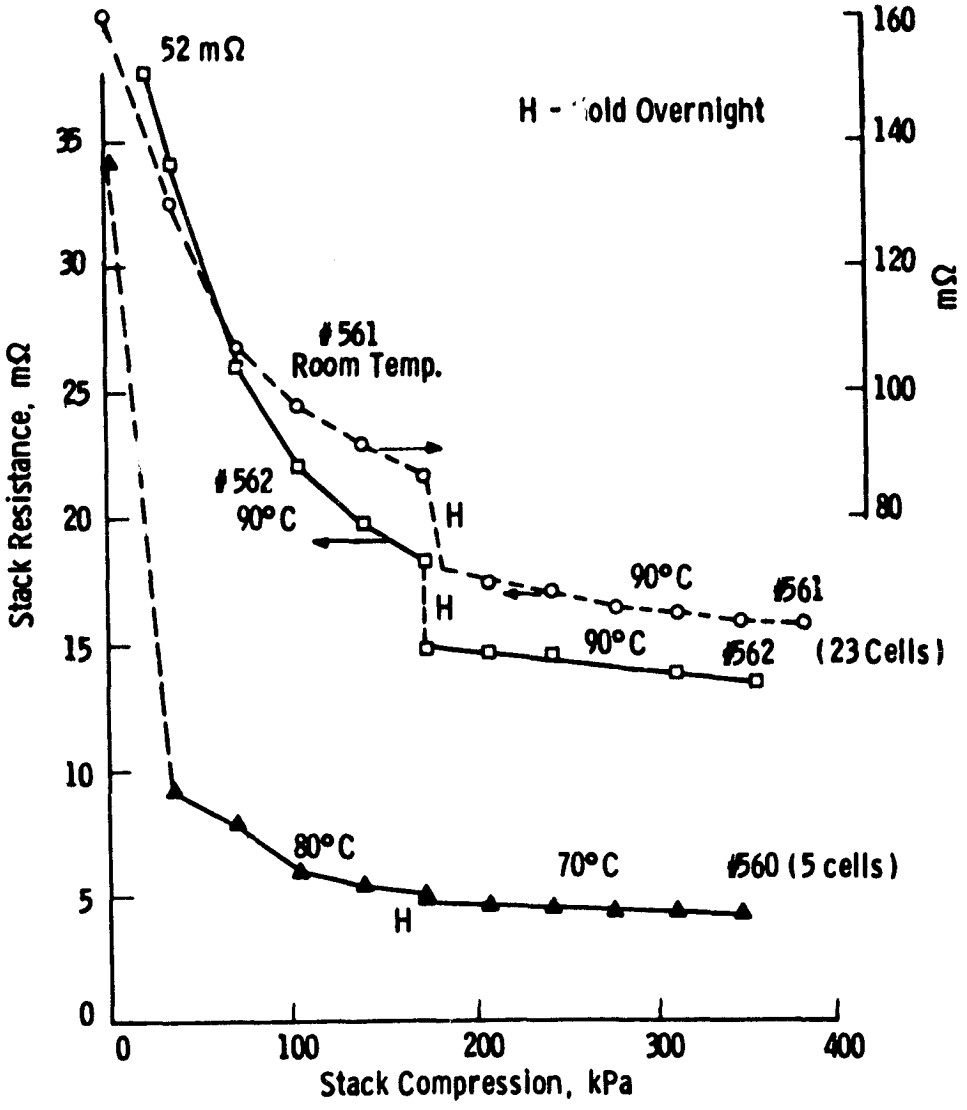

Fig. 42 – Change of electrical resistance during stack compression

Stacks 560 and 562 - The stacks were heated to ~90°C and held overnight with very little compression (<7 kPa). The compression was then increased to 170 kPa in 3 hours and held overnight. The compression was then increased to 340 kPa in 2 hours.

The procedure used for stacks 560 and 562 was intended to permit the acid to distribute itself uniformly in the component pores prior to compression of the stack. Observations during compression of previous stacks indicated that some acid could be squeezed through electrode wetproofing due to maldistribution.

3.4 8 kW Test Facility

Installation of all major components for the 8 kW test facility was completed, and the loop is being insulated. The anode preheaters were damaged during shipment; the replacement preheaters will be installed as soon as they are received. Preliminary dry runs indicated some leaks in the air loop which have subsequently been fixed. The data acquisition system trial program was run and revealed that I/O ROM had not been shipped by Hewlett-Packard. This caused a delay of about 6 weeks. The stack testing software is now expected to be ready by May.

Reference 4

1. T. G. Benjamin, et al. "Handbook of Fuel Cell Performance", Prepared for U. S. DOE, Project 61012, Institute of Gas Technology, May, 1980.

TASK 4: FUEL CONDITIONER DEVELOPMENT

4.1 Fuel and Water Definitions

The final technical consideration in water cleanup was a decision to discharge boiler blowdown containing less than 200 ppm of nontoxic salts to a sanitary sewer system at a rate not to exceed one liter/hr for a 120 kw dc OS/IES unit.

4.2 Operational Requirements

The P&I diagram, Figure 43, remains unchanged from that shown in the 5th Quarterly Report. However, the steam pressure available at the full load condition will not be capable of supplying the energy necessary to permit use of an eductor to boost natural gas to the pressure required by the system. Therefore, the boiler will be operated at constant temperature, and pressure (149°C and 460 kPa) and a natural gas compressor will be used to satisfy natural gas needs at all loads and for all projected OS/IES system pressure drops.

Preliminary start-up, load increase, load decrease, and shut-down procedures were developed for the system shown on the P&I diagram. When equipment selections are made from quotations being received, and the instrumentation modules to acquire data from and control the OS/IES are selected, these procedures will be revised and issued as part of the OS/IES prototype conceptual design.

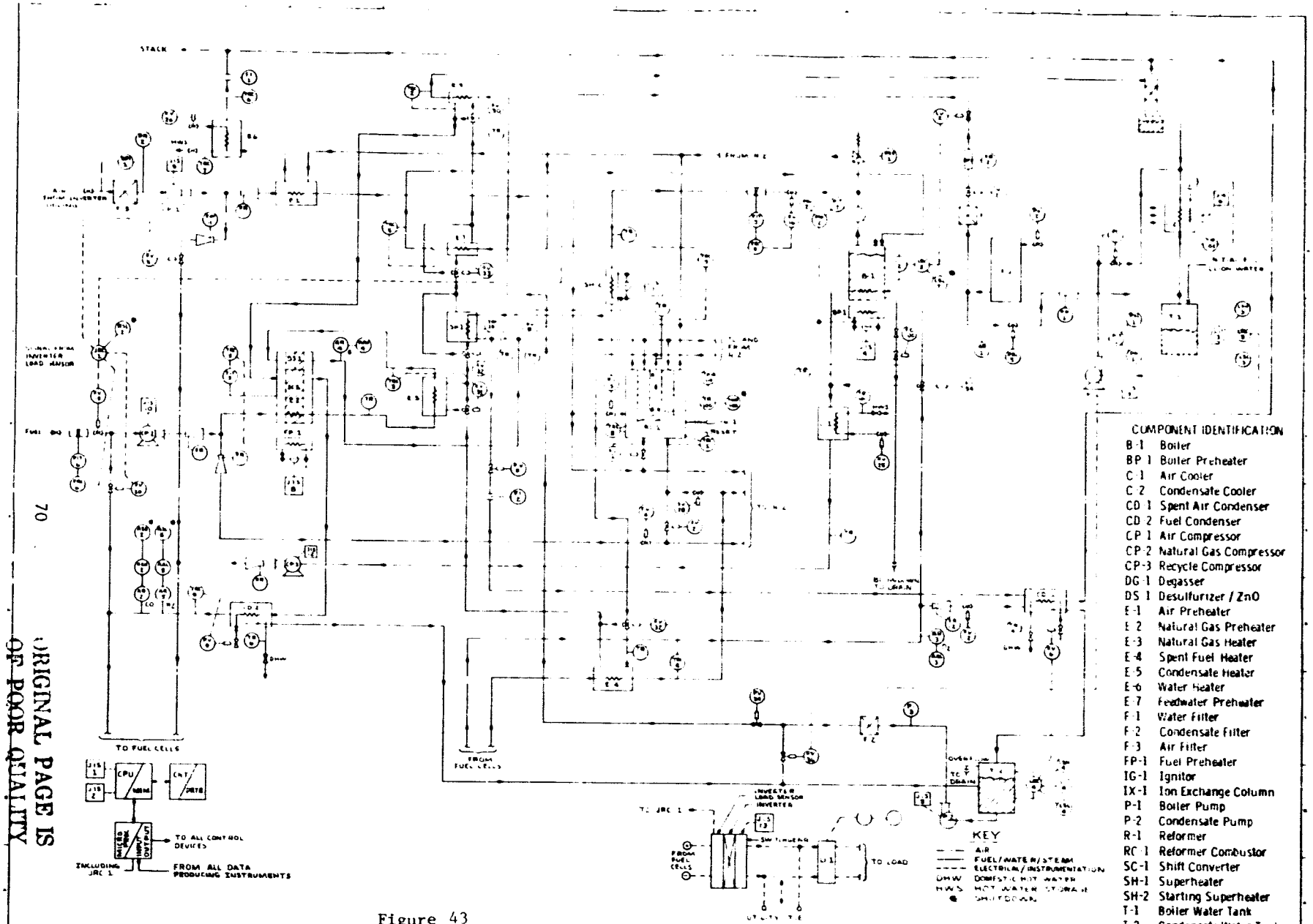

Figure 43

4.4 Ancillary Subsystem Data Base

Burner Development

Burner testing was essentially completed during this quarter. Two fuel gas compositions had been proposed for burner testing. One had a relatively low water vapor content for a system with the condenser upstream of the burner to recover water from the spent anode stream and one with a water vapor content near 25 vol. % for a system with the water recovery condenser in the supply line to the fuel cell anode. Tests were so successful on the high water vapor content fuel gas, an analysis for which is shown in Table XII, that no testing was required to demonstrate effective burner capability on the low water vapor content fuel. The tests were performed on the burner shown in Figure 44, which was described in previous reports. The combustion chamber was evaluated for turndown or lean limit blowout range at atmospheric pressure over the following ranges:

Air Flow	0.32 to 0.80 normal* m^3/minute
Fuel Flow	0.008 to 0.08 normal m^3/minute
Air Temp	93 to 315°C
Fuel Temp	115 to 415°C

The method of determining the lean blowout limit was to establish the air flow rate (nominally 0.32 m^3/min for 30 kw operation and 0.67 m^3/min for 60 kw operation) and a nitrogen flow rate of approximately 0.13 m^3/min through the fuel system. Heaters were brought on-line and the air and fuel systems were preheated to the test conditions prior to ignition, conserving the expensive fuel. When burner inlet conditions are attained, the fuel gas was substituted for the nitrogen and the burner lit. Fuel flow was rapidly decreased until an air equivalence ratio [actual fuel/air ratio divided by stoichiometric fuel/air ratio] of about 20 was reached, at which time the fuel rate was reduced in 10% increments until blowout occurred. In Figure 45, the last combustion points prior to blowout are shown in terms of the correlating variables. The region below the line represents the area of stable combustion.

---

* at 0°C and 101.3 kPa, 1 normal m^3 = 37.3 standard ft^3

TABLE XII

NOMINAL FUEL CELL EFFLUENT GAS COMPOSITION

SPECIE	MOLE PERCENT "WET"	MOLE PERCENT "DRY"
CH_4	2.87	3.78
CO	2.35	3.10
H_2	32.21	42.41
CO_2	38.50	50.71
H_2O	24.07	0.00

Dwg. 7742A62

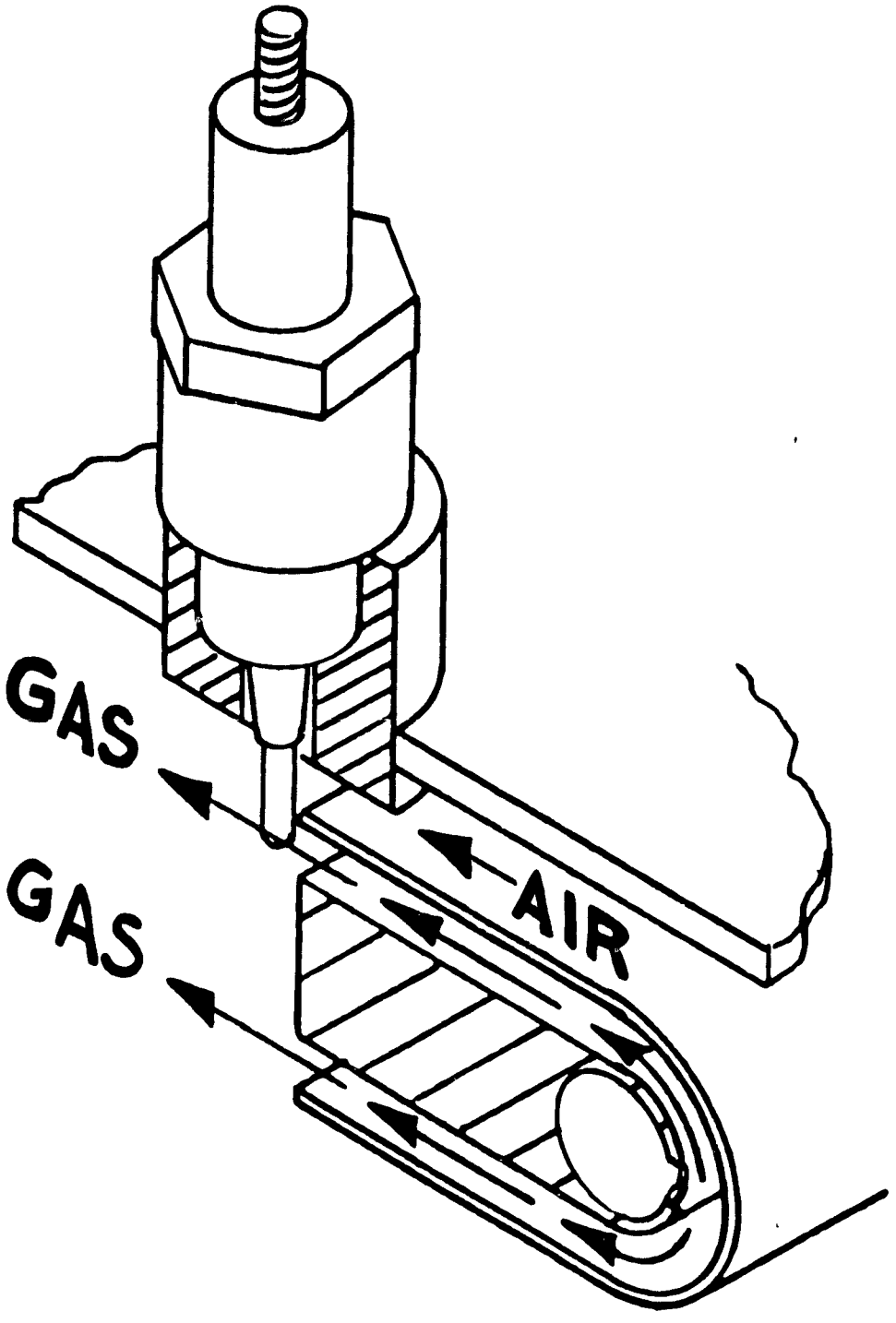

Fig. 44—Cross section schematic of fuel cell reformer burner

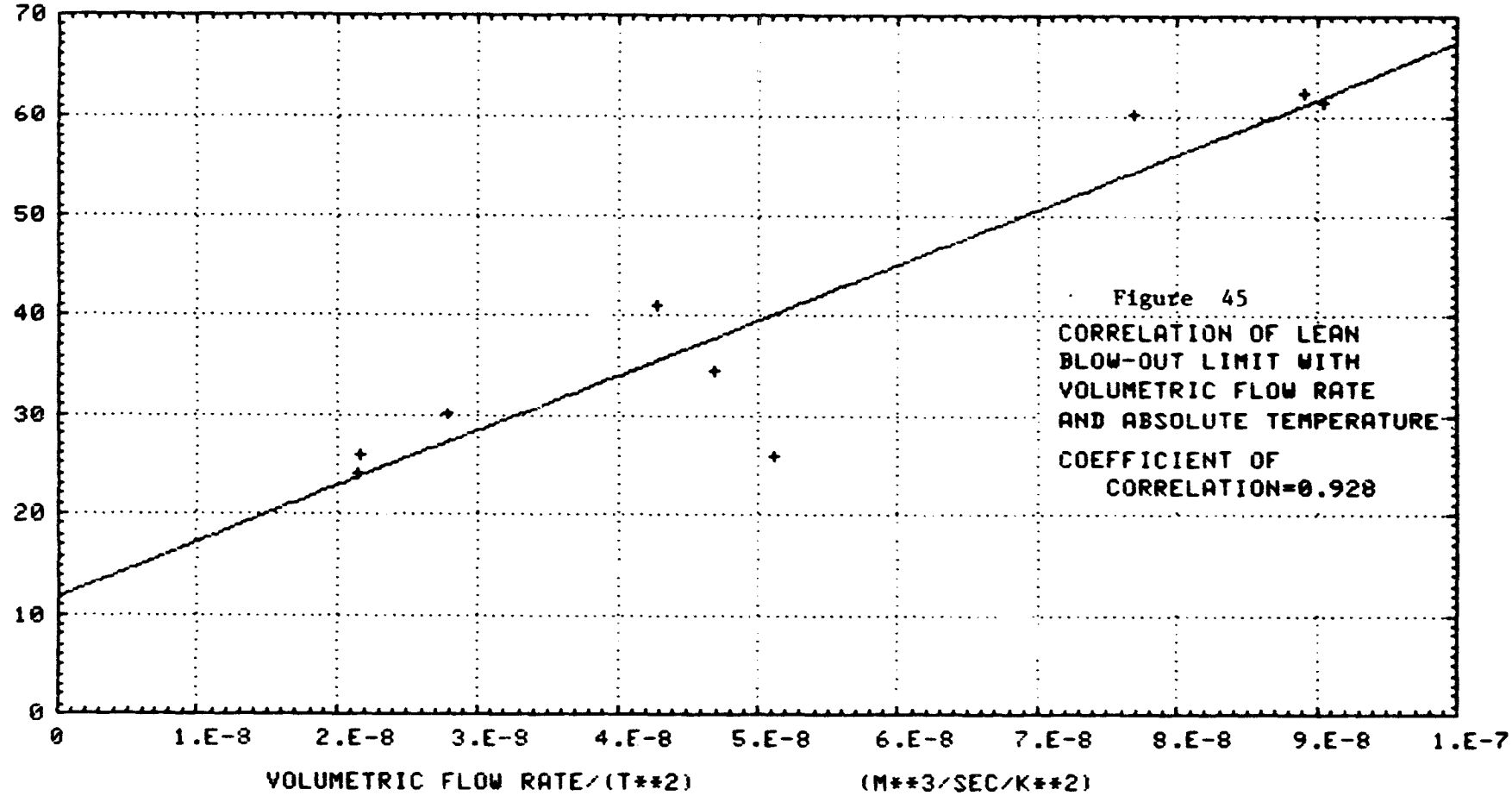

Figure 45
CORRELATION OF LEAN BLOW-OUT LIMIT WITH VOLUMETRIC FLOW RATE AND ABSOLUTE TEMPERATURE

COEFFICIENT OF CORRELATION=0.928

The correlating variables are the air equivalence ratio, volumetric flow rate (Q), and the volumetric weighted temperature of fuel and air (T). The correlation parameter Q/T^2 is based on the Longwell[1] parameter $M^2/V \cdot P^2$ (mass flow/reactor volume pressure^2) with the second order temperature effect included as suggested by Hottel.[2] While the correlation of the limits of flammability with the correlation parameter is good (correlation coefficient = 0.928), the trend of increasingly lean combustion, as the severity of the conditions increases with higher flows or lower inlet temperature, was contrary to expectations and the general behavior of combustion systems (References 3, 4, and 5). This may be due to the heat loss of the flame to the environment in the water cooled flame duct. At low flows and high inlet temperatures, the value of Q/T^2 would be the smallest while the heat losses would be the greatest resulting in rapid quenching and requiring a relatively higher chemical energy release or lower air/fuel ratio than at the higher flows and lower inlet temperatures.

The burner demonstrated excellent performance levels at the high turndown conditions (>20) where flameout occurred. The temperature rise across the burner prior to blowout was as low as 30°C. NO_x emissions were less than 2 ppm at all conditions, but improvements are needed in the CO and unburned hydrocarbon emissions which at the 30 kw condition approached values of 1400 ppm and 400 ppm, respectively, for the most adverse conditions. A minor improvement in air/fuel mixing in the prototype burner could provide satisfactory part load CO and hydrocarbons. This burner in its present configuration can provide a thermal source for evaluating the heat transfer elements of the reformer and serve as a design basis for an integrated burner-reformer unit.

Heat Exchanger Data

During this quarter, performance specifications previously prepared for the 12 heat exchangers used in the fuel conditioner subsystem of the OS/IES were sent to 13 potential vendors. Of these, three were provided with duplicate replacements of specifications they claim

not to have received, six indicated they would not bid, two have not responded in any way, and two vendors (The Heat Transfer Division, American-Standard Co., Buffalo, NY and The Harrison Radiator Division of General Motors Corporation, Lockport, NY) presented preliminary responses at meetings held at Westinghouse R&D. American-Standard proposed using both shell and tube type and coil type heat exchangers. Harrison proposed the use of plate type, round tube and fin type and flat tube and fin type heat exchangers. Preliminary costs were provided by American-Standard for all units except the boiler. Harrison requested some supplemental information before they could quote. This information has been provided and their quotes are expected shortly. Preliminary cost, configuration and technical design information from both suppliers are based on full power normal duty operation, with the understanding that at part load, the exchangers will achieve closer approaches of cooled fluid exit temperature to cooling fluid temperature.

Compressor Data

Performance specifications for the three compressors of the fuel conditioner subsystem were sent to nine potential vendors. These vendors indicated they would not bid due to the items being outside their product line. Telephone contacts were then made with a number of additional suppliers to identify those with applicable equipment lines. These can be categorized as:

1. Suppliers of low flow high pressure blowers
2. Suppliers of turbo compressors or low flow multi-stage blowers
3. Suppliers of rotary positive displacement blowers

Specifications, including an alternate specification for the recycle compressor (CP-3) for a lower static discharge pressure, were sent to six additional vendors. The alternate specification for CP-3 resulted from an indication of reduced gas pressure drop across boiler B-1 provided by one of the heat exchanger suppliers. This decreased pressure drop will decrease the amount of parasitic energy required.

To date, responses have been received for all three compressors from the Roots-Dresser Industrial Products Division of Dresser Industries and for two of the compressors from Westinghouse, Sturtevant Division. One of the Westinghouse proposals involves a tandem arrangement of two turbo blowers, with the discharge of one turbo blower feeding to the suction of the second turbo blower, to achieve the required static discharge pressure.

Pump Data

Performance specifications for the two pumps used in the fuel conditioner subsystem were sent to three potential vendors. Responses were received from two of these vendors. One proposed a turbine type pump for the recirculation and boiler feed pump (P-1) and declined to bid on the condensate pump (P-2). The other vendor proposed a reciprocating pump for P-1, which might produce considerable pulsation in the system piping. These proposed pumps are being evaluated for their intended applications. A number of additional pump suppliers have been contacted for information. Catalog information received from one of these (Procon Products, Murfreesboro, Tennessee) indicates their rotary vane positive displacement pumps may be suitable for the intended applications. These pumps are being further evaluated.

Preliminary Sizing of OS/IES Piping

Lines shown on the OS/IES Process and Instrumentation Diagram (Figure 43) were sized on a preliminary basis. Gas line sizes were established, generally, by setting velocity limits between 3 and 30 m/sec and friction losses at 1-10 kPa/100 m of line. Water lines were established on the basis of setting the smallest line at a nominal 1.2 cm ID. Steam lines were calculated to be one inch schedule 40 pipe (2.6 cm ID). The largest gas line was the air line to and from the fuel cell. Its size is 36 cm ID with a velocity of 31 m/sec and a friction loss of 3.5 kPa/100 m. This line carries 7,782 kg/hr of air at 177°C.

Controls and Instrumentation Data

Information was obtained from several valve suppliers and a meeting was held with a representative of Delta Equipment, a supplier of programmable Jamesbury valves. They will supply further information on operation and this application has been discussed with representatives of Hewlett Packard. Their "stepper" control will handle Jamesbury valves. John Fluke was also contacted, but, to date, has not responded.

Six computer control systems quoted by various suppliers were discussed with the Manager of Digital products of Consolidated Controls Corporation. Their earlier response to the specification had said that "the required system would be best implemented by using several commercially available instruments, interconnected and programmed by an independent systems house." Accordingly a P&ID and all quotations received were sent to CONDEC, which is an independent systems house, for review. Unfortunately, CONDEC declined to supply this service for the prototype since it would require development which they could not afford to do for a single system. However, they could perform this function for production assemblies in the future. CONDEC expressed no strong preference for any of the quotations but favored Hewlett Packard (one of the expensive quotations) and the DIGITEC Datalogger Microprocessor system quoted by COMTEL (one of the least expensive).

4.6 10 kw Reformer

Test Stand Design

The design of a 10 kW fuel conditioner system was completed. Approval to begin construction of the test stand was obtained from the NASA Project Manager based on a preliminary test plan and schedule which were sent to NASA and JPL for review. Construction of the stand began in March.

The flow and instrumentation diagram for the system is shown in Figure 46 and layout elevation and plan views are shown in Figures 47 and 48. As shown, the metered CO, CO_2 and H_2 gases are mixed with

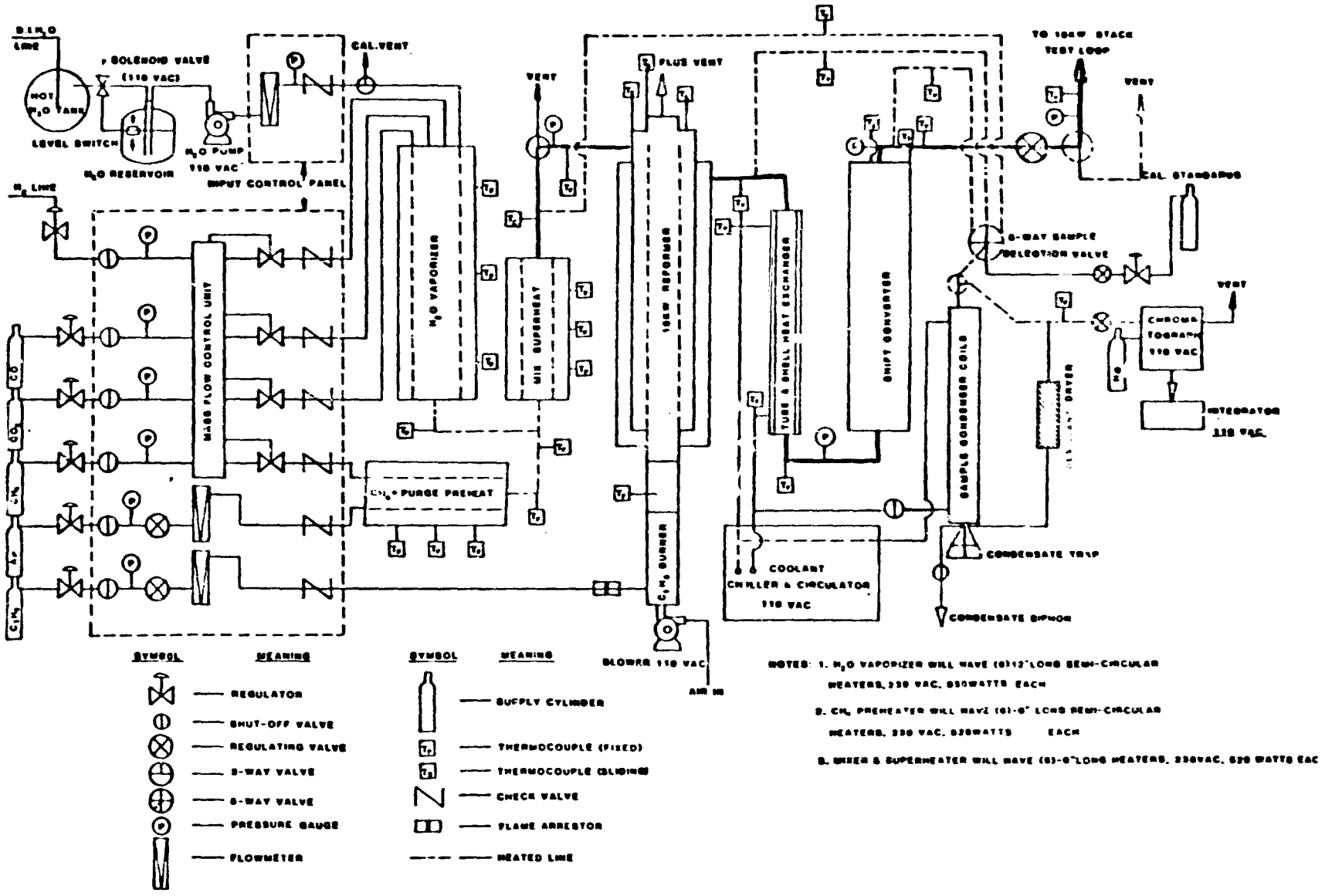

FIGURE 46 FLOW DIAGRAM FOR 10 kW METHANE/STEAM REFORMER

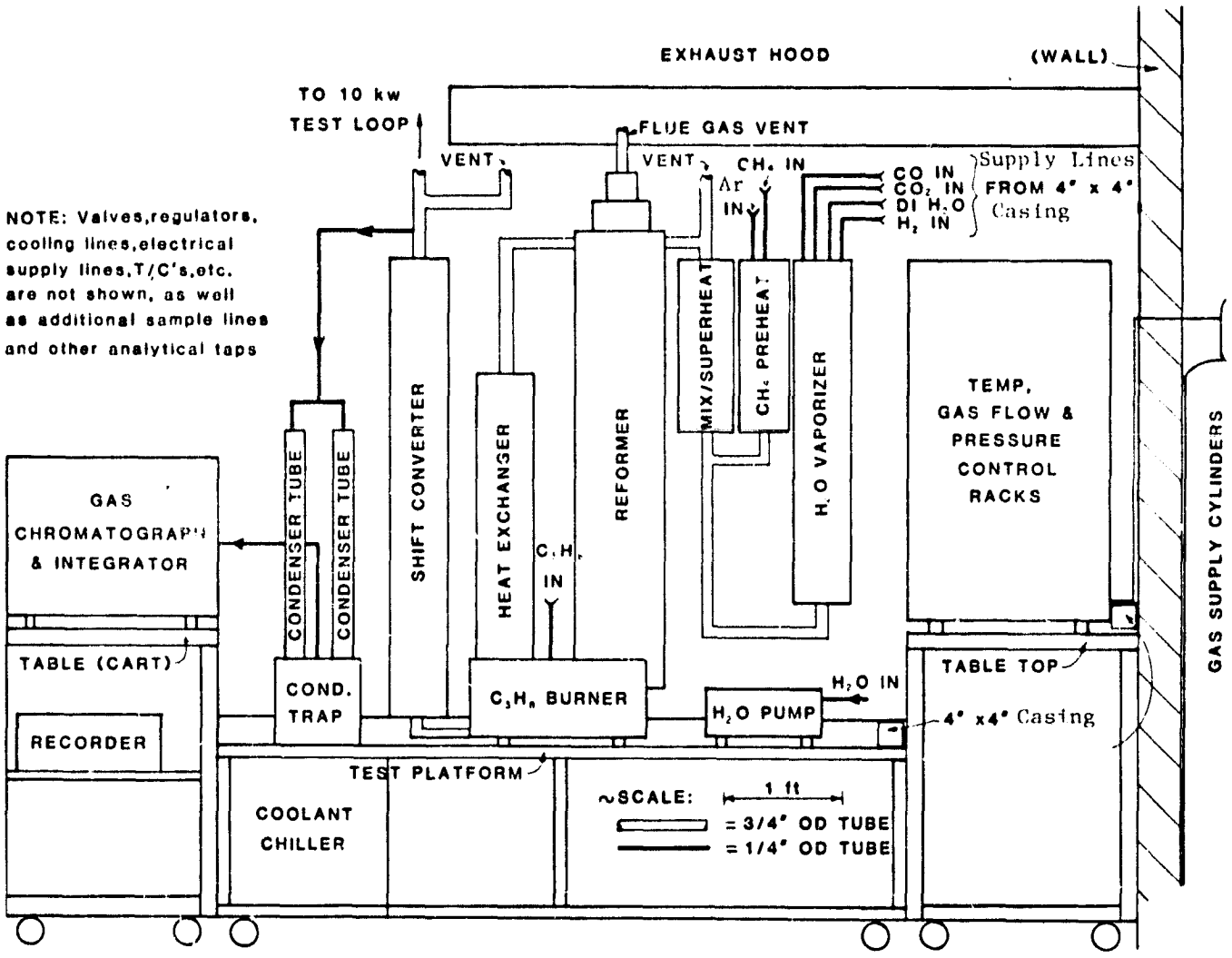

FIGURE 47 - LAYOUT ELEVATION FOR 10 kW METHANE/STEAM REFORMER

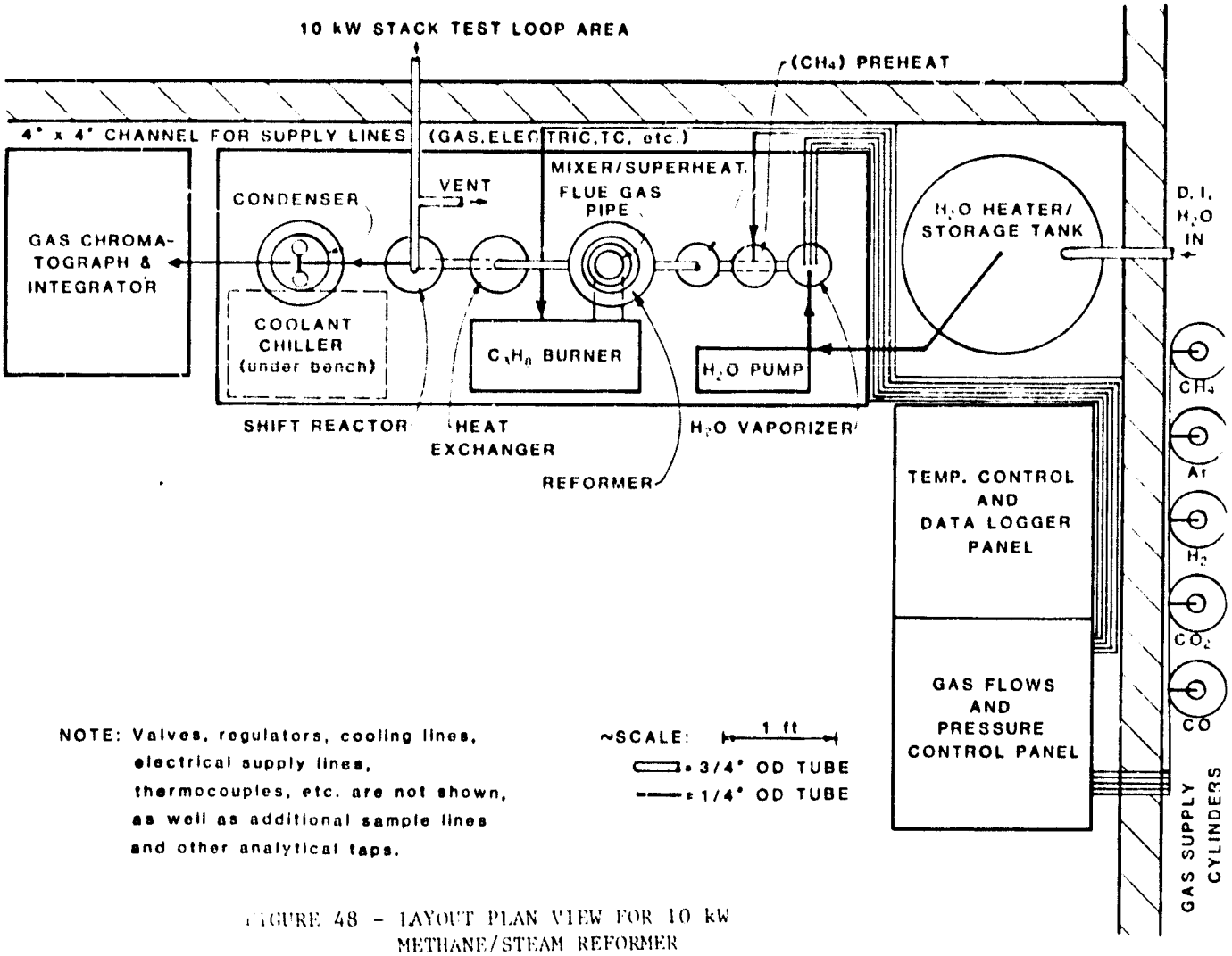

FIGURE 48 - LAYOUT PLAN VIEW FOR 10 kW METHANE/STEAM REFORMER

deionized water in the vaporizer. They are then mixed with the preheated methane upstream of the mixer/superheater and then enter the reformer at the top of the bed.

The reformed products pass through a tube-and-shell heat exchanger and then enter the bottom of the shift converter. The shift converter will not be included in the test system initially. If added later, the hydrogen-rich product gases leaving the shift converter will be sent either to the cell stack test loop or to the gas chromatograph for analysis.

The countercurrent, regenerative reformer tube for the system is shown in Figure 49. The reactor includes an annular reaction chamber which is heated along its inner wall by burner flue gases. The reaction chamber is also heated along its outer wall by the reaction products which leave the bottom of the annular chamber and flow upward.

An existing burner (previously used in MHD tests) has been tested on propane and the compressed air supply available to the test stand. Performance was excellent over the range of conditions anticipated and we plan to use this as the heat source for the reformer. The burner gases will flow upward through the inner tube which is filled with a packing material such as stainless steel spheres or a tapered mandril for better heat transfer. The packing particles or mandril increase the heat transfer coefficient in a bed to several times that of an empty tube at the same gas flow rate. The tapered mandril will be movable so that the distribution of heat transfer coefficient to the wall can be varied by changing the velocity distribution in the tube. The mandril will also increase heat transfer by radiating to the tube wall.

Energy Balance Calculation

The energy balance calculations for the reformer, the burner, the heat exchanger and the shift converter are given in Table XIII. For the 10 kW reformer, the total heat of reaction of methane with steam is 5514 kcal/hr (21881 Btu/hr) and the total sensible heat required for the fuels is about 2520 kcal/hr (10000 Btu/hr) for a total of 8034 kcal/hr

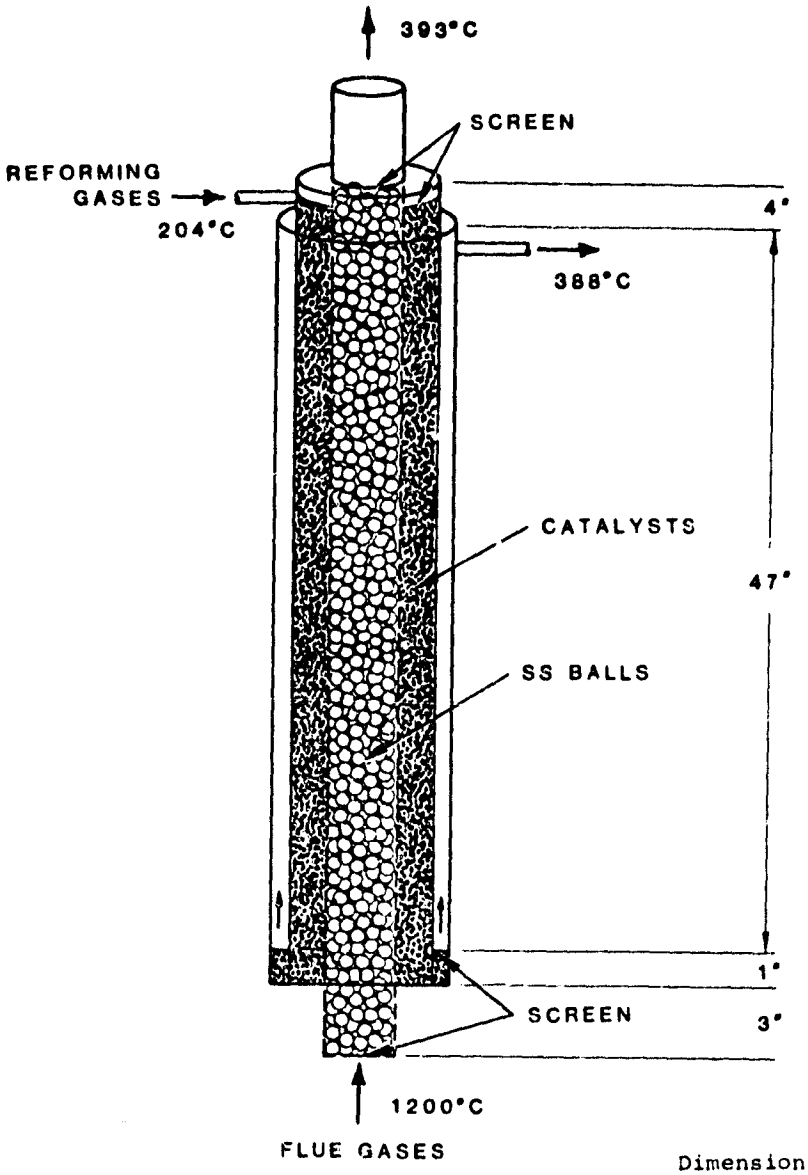

Dimensions not in proportion.

Tube	Type	Dimensions, in. OD	Wall Thickness
Inner	SS316	2.0	0.065
Middle	SS316	3.25	0.065
Outer	SS316	4.25	0.237

FIGURE 49 - 10 kW REFORMER SCHEMATIC

TABLE XIII

ENERGY BALANCE CALCULATIONS FOR A 10 KW DOUBLE COUNTERFLOW REFORMER

Reformer

$$CH_4 + 2H_2O \rightleftharpoons CO_2 + 4H_2$$

$\Delta H600°C = 44.76$ kcal/gmol

Methane Flow Rate: 123.2 gmol/hr

	ΔT_{LM}, °C	U, kcal/m²-hr-°C	A, m²	Q_T, kcal/hr
Furnace Gases	317	73	.200	4637
Regenerative Gases	56	49	.316	857

Total Heat of Reaction = 123.2 x 44.76 = 5514.1 kcal/hr (21881 Btu/hr)
Total Heating Value Fuels Required ≈10000 kcal/hr
Total Heat transfer to Reactor Bed = 4637 + 857 = 5494 kcal/hr

Burner

Fuel = Propane

$$C_3H_8 + 5O_2 \longrightarrow 3CO_2 + 4H_2O\ (\ell)$$

$\Delta H25°C = 530.6$ kcal/gmol

1 gmol C_3H_8 + 23.8 gmol Air $\longrightarrow$ 3 gmol CO_2 +
4 gmol H_2O + 18.8 gmol N_2

Burner Gases - Flow Rate = 24 kg/hr
Temperature = 1200°C

Fuels Required for Burner:

Propane = 16.51 gmol/hr (0.218 SCFM)
Combustion Air = 393.0 gmol/hr (5.184 SCFM)
Excess Air = 409.5 gmol/hr (5.402 SCFM)

Total Heat of Combustion = 16.51 x 530.4 = 8762 kcal/hr (34080 Btu/hr)

Heat Exchanger

Tube side: Temperature In = 388°C
Temperature Out = 177°C

Component	Flow Rate, gmol/hr	C_p, cal/gmol °C
CH_4	8.20	11.0
H_2O	197.8	8.4
H_2	431.7	7.0
CO	79.29	7.2
CO_2	51.59	10.4

Total Heat Loss = 1241 kcal/hr (4925 Btu/hr)

Shift Converter

$$CO + H_2O \rightleftharpoons CO_2 + H_2$$

$\Delta H200°C = 9.57$ kcal/gmol

Component	Flow Rate In, gmol/hr	Flow Rate Out, gmol/hr
CH_4	8.20	8.46
H_2O	197.8	126.1
H_2	431.7	502.5
CO	79.29	6.92
CO_2	51.59	123.8

Total Heat of Reaction = -692.6 kcal/hr (-2748 Btu/hr)

(31881 Btu/hr). Such heat is supplied by the heat transferred through the walls from the burner flue gases and the regenerative gases.

For a total of 8034 kcal/hr (31881 Btu/hr) heat transfer in the reformer shown in Figure 49, the overall heat transfer coefficient should be 3.16×10^{-3} cal/sec-cm^2-k (23.2 Btu/ft^2-hr-°F) for the furnace gases side.

For the propane burner, the flue gases entering the reforming inner tube have a flow rate of 24 kg/hr and a temperature of 1200°C. The propane fuel required is 16.5 gmol/hr, and the combustion and dilution air are 393.0 and 490.5 gmol/hr, respectively.

The heat capacity for the heat exchanger is 1241 kcal/hr (4925 Btu/hr). The total heat of reaction for the shift converter is approximately -693 kcal/hr (-2748 Btu/hr) on the basis of 200°C average reaction temperature.

Hardware Procurement

Hardware procurement for the 10 kW reformer system was started in March. Most of the major components (such as temperature controller, mass flow controller and data logger) are on order. The estimated delivery date of this hardware is the middle of May. The construction of the test setup will be started when the necessary hardware is received.

Properties of Combustion Products of Propane

Some concern was expressed that the use of propane rather than spent anode fuel in the 10 kw test would confound evaluation of the catalyst performance. Analysis shows that the combustion product is similar in either case. Its molecular weight of the propane product is 28.696 compared to 28.644 for spent fuel. Because of its higher water and CO_2 content, the spent fuel product specific heat will be 0.316 compared to 0.292 for propane. For a given heat release, this requires a propane product flow of 26.4 kg/hr compared to 24.4 kg/hr for spent fuel. As a result, the Reynolds Number would increase by about 8% for a

fixed flow area. If it is desired to maintain the Reynolds Number, the open area should be decreased for propane product. If a mandril is used in the tube, its diameter will be 0.5 mm larger for propane product than for spent fuel.

Reformer Heat Transfer Analysis

Several of the relations offered in Perry's Handbook of Chemical Engineering for heat transfer from gas streams to walls were used to estimate h_c for the 10 kw test. The results indicated an impossibly high coefficient. It was necessary to go back to several of the original references. One of the best (JACOB - Heat Transfer) offered examples approximating the 10 kw facility and showed h_c = 164 $w/m^{2\circ}C$ for a packed bed of 13 mm spheres in a 5 cm tube. It was also calculated that the maximum h_c occurred with 7.9 mm spheres (171 $w/m^{2\circ}C$), dropping off to 70.7 for 2.5 cm spheres and 22.7 for an open tube This suggested an open tube at the bottom where the gas temperature is the highest, 7.9 mm spheres in the middle third where nearly 90% of the total heat is absorbed in the reaction, and perhaps 2.5 cm spheres or the equivalent in the top third where the reactants are heated sensibly. For preliminary tests, a tapered mandril appears preferable for determining the required heat flux distributions. The mandril has the advantage that it can be moved to adjust the transfer coefficient without shutting down.

Reformer Tube Material

Alternate alloys (for 316 SS) were considered. The Westinghouse R&D Metallurgy Department made a brief survey and determined that no alternate exceeded the combined mechanical, environmental and economic properties of 316 SS. However, 309 SS and 310 SS have better oxidation resistance than 316 SS and are only slightly more expensive. The biggest problem with the 300 series alloys will be embrittlement due to carbide formation at the grain boundaries caused by thermal cycling over the range of 640-750°C. Stabilized stainless steel would be recommended. There

are other alloys that have better creep strength and fatigue resistance than 316 SS at 980°C but they are considerably more expensive. Aluminizing shows great promise in preventing both oxidation and carburization. For example, commercial "ALON" processing reduces the depth of penetration of carburization at 920°C for 309 SS from 2.5 m in 1000 hours to less than 0.25 mm.

4.8 Development of Computer Model

Tubular and flat slab geometry double counter-current flow computer models was initiated. The double counter-current flow model contains six basic equations. The equations derived for a tubular geometry case (Figure 50) are:

1. Kinetic mass balance: This is the same as in the REPENT/BOLTAR models, and gives X1.

$$\frac{dX1}{dZ} = \frac{e_B P k_o e^{-E_{A/RT}}}{u_o c_o} \left[\frac{F1(1-X1)}{F+2(X1)F1} - \frac{F1(1-XE)}{F+2(XE)F1} \right]$$

2. Demethanation reaction equilibrium: again, the same as before, and gives XE.

$$K_{E1} = \frac{Y_{CO_2} Y_{H_2}^4}{Y_{CO}\, Y_{H_2O}^2} P^2$$

3. Water gas shift equilibrium: again the same as before, gives XE2.

$$K_{E2} = \frac{Y_{CO_2} Y_{H_2}}{Y_{CO} Y_{H_2O}}$$

Only the energy balances change.

4. **Reformer gas energy balance:**
gives TC

$$(\Sigma FACPA)\, dTC = UI\, (TH-TC)_{avg}\, \Pi(D2)dz +$$

$$UO'\, (TR-TC)_{avg}\, \Pi(D1)dz +$$

$$\Sigma F(-\Delta H)dx$$

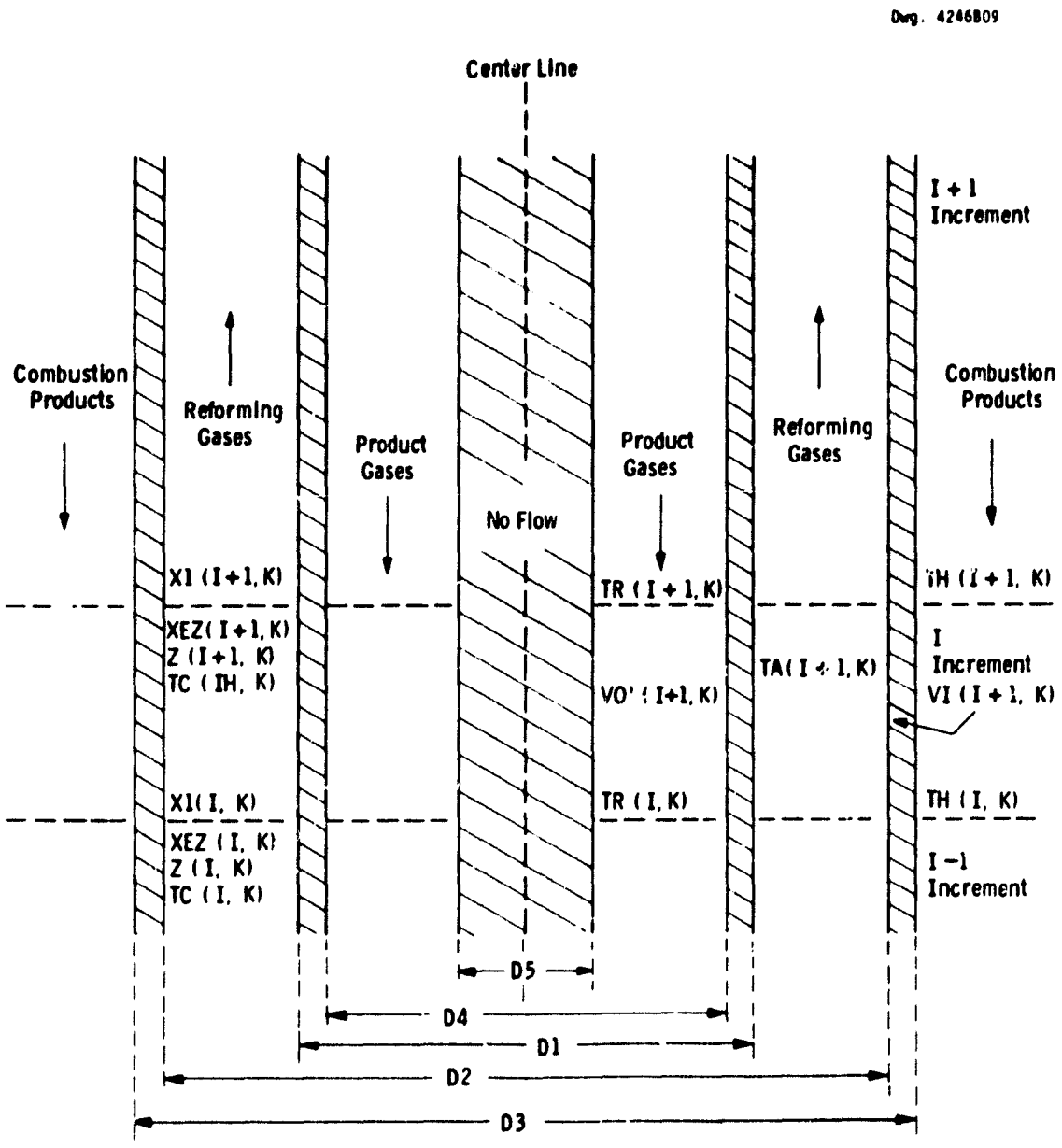

Fig. 50—Double counter-current flow, tubular geometry reformer model (regenerative gases flow on the inside)

5. Combustion gas energy balance. gives TH

$$(MH)(CH)dTH = UI(TH-TC)_{avg}\,\Pi(D2)dz$$

6. Product gas energy balance: gives TR

$$(MR)(CR)dTR = UO'(TR-TC)_{avg}\,\Pi(D1)dz$$

UO' is the product gas side overall heat transfer coefficient

TR is the product gas temperature

MR is the product gas molar flow rate

CR is the product gas heat capacity

All other variables are as defined in the BOLTAR report.

Thus, it can be seen that an extra independent variable (TR) is introduced, along with an extra equation to describe it (equation 6). Therefore, there are six equations with six unknown variables, and the system is completely defined. The product gas flow rate (MR) and composition do not constitute independent variables, as they are determined by X1 and XE2 at the top of the reformer, but they complicate the model programming.

Comparison with the REPENT/BOLTAR system of equations indicates that the energy balances require an iterative rather than an analytical solution, due to the complexity of equations 4 to 6. Only if an exterior tube wall temperature profile is used can analytical solutions be obtained. Changes in flow arrangement or geometry can be accommodated by adjusting the flow and heat transfer areas.

Equations 1 through 6 have been put into finite difference forms, and, using the arithmetic mean temperature difference, solved for the pertinent variables. These calculations and models have been added to the previous BOLTAR program. Thus, given the proper choice of routing variables, the new BOLTAR program can perform the calculations for both the earlier models and the newly derived ones. These new, double countercurrent flow models are:

1. Tubular geometry, product gases flow on the inside (Figure 50).
2. Tubular geometry, product gases flow on the outside.
3. Flat slab geometry, product gases flow on the inside
4. Flat slab geometry, product gases flow on the outside.
5. Exterior tube wall temperature profile in place of combustion gas information for any of the above models.

These models, program choices, and use will be detailed in the next quarterly report.

As of the end of this report period, the program was running for the two tubular models with minimal problems. No definitive predictions were obtained. However, preliminary results on the UTC 40 kW reformer design, using best guess input data and optimistic heat transfer assumptions, indicate an actual hydrogen gas output equivalent to 7-9 kW. This design and our 10 kW reformer will be evaluated further in the next quarter.

We were concerned about convergence problems and long (>1 min) computer run times on the double counter-current flow models. To date, simple secant convergence techniques have produced run times ranging between 20 and 40 seconds. Some convergence problems have been encountered on low feed temperatures, and these have been circumvented by closing both product and combustion gas temperature loops simultaneously. Present work will continue to involve program debugging.

REFERENCES

1. J. P. Longwell, "Flame Stabilization by Bluff Bodies and Turbulent Flames in Ducts," Fourth Symposium (International) on Combustion, The Williams and Wilkins Co., 1952.

2. H. C. Hottel, G. C. Williams, W. P. Jensen, A. C. Tohey, and P. M. Burrage, "Modeling Studies of Baffle-Type Combustors," Ninth Symposium (International) on Combustion, Academic Press, 1962.

3. J. P. Longwell, W. W. Chenevey, W. W. Clark, and E. E. Frost, "Flame Stabilization by Baffles in High Velocity Gas Streams," Third Symposium on Combustion, Flame, and Explosion Phenomena, The Williams and Wilkens Co., 1949.

4. E. A. DeZubay, "Characteristics of Disk Controlled Flames," Aero, Digest, 61 (1950).

5. M. Barrere and A. Mestre, "Stabilization des Flammes par des Obstacles," Selected Combustion Problems (ARARD), Butterworth Scientific Publications (1954).

TASK 5: MANAGEMENT REPORTING AND DOCUMENTATION

5.1 Supervision and Coordination

Four meetings of key personnel of the fuel cell development (Tasks 1, 2 and 3) and management tasks of this project, the parallel ERC technology program (DEN3-205), the NASA program team, and representatives of the Westinghouse Advanced Energy Systems Division were held to plan and coordinate the on-going fuel cell development work and the pending Electric Utility program. The meetings focused on redirecting the work to obtain maximum benefit from and synergism of the remaining efforts with the Electric Utility program. As a result of these meetings, the NASA Project Manager approved the appointment of a Technical Integrator (the designated Electric Utility Program Manager) to ensure a continuing coordination effort of these projects and the pressurized stack design, fabrication and testing being done under contract DEN3-201. A revised plan for this program was submitted to the NASA Program Manager.

A meeting of division and department level managers of Westinghouse R&D, Westinghouse AESD and the NASA fuel cell project office was held to define the Westinghouse strategy for development of appropriate power plants for the OS/IES and Electric Utility applications.

5.2 Documentation and Reporting

The Fifth Quarterly Report and the Technical Status Reports for January and February were submitted for NASA patent approval. Patent approvals for the Technical Status Reports for October, November, and January and the Fourth and Fifth Quarterly Reports were received and they were distributed in accordance with the NASA supplied lists. The management reports (533M and 533P) for December, January and February, along with additional cost and manhour graphs, and the financial plan for the Seventh Quarter (533Q) was prepared and submitted to the NASA Project Manager.

The Fabrication and Assembly Procedures document was expanded to include Stacks 563 and 564 and is in the final stages of preparation for submittal.

Technical highlights were reported on a weekly basis to the NASA Project Manager by telephone and monthly summaries were reported by letter or telephone.

A review of progress to date and demonstration of the OS/IES simulation loop and burner test rig were presented to the DOE Phosphoric Acid Fuel Cell Program Managers.

C-2

III. PROBLEMS

While they are necessary and productive, the planning of program changes has a substantial impact on on-going work. Developing plans to accommodate these changes requires time and manpower which further reduces the limited resources available for achieving the projects technical goals. Once the extent of funding level changes are identified, every effort will be made to identify logical goals, but some work will inevitably be left hanging.

Fuel cell design fabrication and testing are behind schedule for the reasons discussed in previous reports.

IV. PLANS

TASK 1: DESIGN OF LARGE CELL STACKS

Development of detailed analytic model for the MK-2 bipolar plate configuration will be continued. The correlations used in the detailed analytic model and the lumped parameter model will be modified to reflect the information obtained from the stack being tested as part of Task 3.

The cooling plate configuration for stack 564 will be designed, based on results of stack 562 tests, during the next quarter.

The analysis of the distribution of compression forces among active area, seals and shims and the effective compression on bipolar plate ribs will be continued during the next quarter.

The evaluation of manifold materials and the design of stack compression hardware is continuing.

TASK 2: STACK FABRICATION

Heat treatment of plates for 563 will be completed and assembly of the stack is scheduled for the first month of the next quarter. This assembly will be preceded by the disassembly and post test analysis of

stack 561, so that the assembly will have the benefit of any knowledge acquired during post test analysis.

The plates for 564 are being molded and will be machined when the cooling channel configuration is finalized. The plates will then be heat treated and assembled. Assembly is scheduled for the next quarter.

Fabrication of components for the 5-cell modules is underway. Tests of the methods for assembly of the stacks, based on concepts described separately to the NASA Project Manager, will start in the next quarter.

TASK 3: STACK TESTING

Endurance testing of stack 560 will continue through the next quarter.

OS/IES loop testing of stack 562 will continue according to the plan submitted to the NASA Project Manager. The data will be analyzed to provide a foundation for the design of cooling plates for 564.

Pretesting of stacks 563 and 564 will be initiated when assembly is complete and then the testing of each will be initiated.

The 8 kW test stand work will be completed next quarter.

TASK 4: FUEL CONDITIONER DEVELOPMENT

Construction of the 10 kW test stand will be completed during the next quarter. Analysis of the heat transfer to the catalyst bed will continue and the design of the first test configuration will be finalized.

Acquisition and evaluation of vendor design and cost data for the prototype components will be continued and the results factored into the P&I diagram and the system conceptual design.

Debugging of the modifications of the computer model should be completed next quarter and parametric studies to guide the 10 kW design and experiments will be made.

TASK 5: MANAGEMENT AND DOCUMENTATION

Coordination of efforts among the task leaders and between ERC and Westinghouse will be continued.

The increased effort on coordinating this project with DEN3-201, DEN3-205 and the pending Electric Utility Program will be continued and will be primarily the responsibility of the Technical Integrator. The Inter Works Requisition (IWR) to support the Technical Integrator will be executed in the first month of the next quarter. Meetings will be held, as required, to effect this coordinating effort.

Technical review meetings will be held at the convenience of the NASA Project Manager and presentations to and meetings with DOE personnel will be scheduled as requested.

The task leaders' inputs to the Technical Status Reports and Quarterly Reports will be edited and the reports will be submitted to the NASA Project Manager for patent approval. The management reports will also be prepared and submitted to the NASA Project Manager. Technical highlights will be transmitted to the NASA Project Manager on a weekly and monthly basis.

The Monthly Technical Progress Narrative and Quarterly Reports will be distributed in accordance with the list provided by NASA as patent approvals are received.

The Fabrication and Assembly Procedures document will be submitted to the NASA Project Manager early in the next quarter.